

1984

Water Diffusion Rates Through Serpentinized Peridotites: Implications For Reaction Induced Dynamic And Chemical Effects In Ultramafic Rocks

Andrew Harrington Macdonald

Follow this and additional works at: <https://ir.lib.uwo.ca/digitizedtheses>

Recommended Citation

Macdonald, Andrew Harrington, "Water Diffusion Rates Through Serpentinized Peridotites: Implications For Reaction Induced Dynamic And Chemical Effects In Ultramafic Rocks" (1984). *Digitized Theses*. 1376.
<https://ir.lib.uwo.ca/digitizedtheses/1376>

The author of this thesis has granted The University of Western Ontario a non-exclusive license to reproduce and distribute copies of this thesis to users of Western Libraries. Copyright remains with the author.

Electronic theses and dissertations available in The University of Western Ontario's institutional repository (Scholarship@Western) are solely for the purpose of private study and research. They may not be copied or reproduced, except as permitted by copyright laws, without written authority of the copyright owner. Any commercial use or publication is strictly prohibited.

The original copyright license attesting to these terms and signed by the author of this thesis may be found in the original print version of the thesis, held by Western Libraries.

The thesis approval page signed by the examining committee may also be found in the original print version of the thesis held in Western Libraries.

Please contact Western Libraries for further information:

E-mail: libadmin@uwo.ca

Telephone: (519) 661-2111 Ext. 84796

Web site: <http://www.lib.uwo.ca/>

CANADIAN THESES ON MICROFICHE

I.S.B.N.

THESES CANADIENNES SUR MICROFICHE



National Library of Canada
Collections Development Branch

Canadian Theses on
Microfiche Service

Ottawa, Canada
K1A 0N4

Bibliothèque nationale du Canada
Direction du développement des collections

Service des thèses canadiennes
sur microfiche

NOTICE

The quality of this microfiche is heavily dependent upon the quality of the original thesis submitted for microfilming. Every effort has been made to ensure the highest quality of reproduction possible.

If pages are missing, contact the university which granted the degree.

Some pages may have indistinct print especially if the original pages were typed with a poor typewriter ribbon or if the university sent us a poor photocopy.

Previously copyrighted materials (journal articles, published tests, etc.) are not filmed.

Reproduction in full or in part of this film is governed by the Canadian Copyright Act, R.S.C. 1970, c. C-30. Please read the authorization forms which accompany this thesis.

THIS DISSERTATION
HAS BEEN MICROFILMED
EXACTLY AS RECEIVED

AVIS

La qualité de cette microfiche dépend grandement de la qualité de la thèse soumise au microfilmage. Nous avons tout fait pour assurer une qualité supérieure de reproduction.

S'il manque des pages, veuillez communiquer avec l'université qui a conféré le grade.

La qualité d'impression de certaines pages peut laisser à désirer, surtout si les pages originales ont été dactylographiées à l'aide d'un ruban usé ou si l'université nous a fait parvenir une photocopie de mauvaise qualité.

Les documents qui font déjà l'objet d'un droit d'auteur (articles de revue, examens publiés, etc.) ne sont pas microfilmés.

La reproduction, même partielle, de ce microfilm est soumise à la Loi canadienne sur le droit d'auteur, SRC 1970, c. C-30. Veuillez prendre connaissance des formules d'autorisation qui accompagnent cette thèse.

LA THÈSE A ÉTÉ
MICROFILMÉE TELLE QUE
NOUS L'AVONS REÇUE

WATER DIFFUSION RATES THROUGH SERPENTINIZED PERIDOTITES,
IMPLICATIONS FOR REACTION INDUCED DYNAMIC
AND CHEMICAL EFFECTS IN ULTRAMAFIC ROCKS

by

Andrew H. Macdonald

Department of Geology

Submitted in partial fulfillment
of the requirements for the degree of
Doctor of Philosophy

Faculty of Graduate Studies
The University of Western Ontario
London, Ontario
September, 1984

ABSTRACT

The serpentinization-reaction is characterized by reactions of the type: $Mg_2SiO_4 + MgSiO_3 + 2H_2O \rightarrow Mg_3Si_4O_5(OH)_4$, involving a 40% volume expansion and considerable heat generation. At all temperatures between 100°C and 400°C rates of serpentinization are geologically rapid and are controlled by the rate at which water is supplied to the reaction interface (surfaces). Therefore, once serpentine begins to form, any further reaction will depend on the rate of water penetration through an existing layer of serpentine. Defects 100-1000 Å wide produced by the buckling of the platy serpentine mineral, lizardite, provide the permeability necessary for the transport of water into fresh peridotites and hence continuous reaction. If flow rates are slow, water will be consumed at the reaction interface as fast as it arrives, leading to irreversible volume expansion stress and strain. This is strongly supported by the major element chemistry.

An experimental study, at room temperatures (250°C-400°C), has shown that a thin (3-4 mm) slice of serpentinized peridotite placed in a diffusion cell exhibits a

significant permeability to water, while behaving semi-permeably to salt. Diffusion coefficients of water at 340°C range from 10^{-7} to $10^{-8} \text{ cm}^2 \text{ sec}^{-1}$, whereas using a modified Darcy equation intrinsic permeability coefficients of 10^{-11} to 10^{-12} darcys are obtained. Similar transport coefficients have been measured for zeolites and compressed clays, respectively. The results suggest also that serpentinization can produce high salinity fluids.

At typical serpentinization temperatures (e.g. 200-300°C) D_{H_2O} is estimated to be on the order of 10^{-4} to $10^{-5} \text{ cm}^2 \text{ sec}^{-1}$. Using the simplified parabolic rate law, $x = (2Dt)^{1/2}$, such coefficients imply a mean penetration distance, x , through serpentinized peridotites in the range of $1-80 \text{ cm a}^{-1}$. It thus appears that in deep (i.e. $>5 \text{ km}$) groundwater or marine environments, water will penetrate massive serpentinite at an appreciable rate and hence will lead to moderately rapid reaction rates. Given the large P_{H_2O} gradient produced by the reaction (i.e. P_{H_2O} external - P_{H_2O} reaction interface), the process will cause large volume strains coupled to flow and reaction rates. As the swelling pressure (stresses) of the reaction are on the order of $\pm 1 \text{ kb}$, refracturing will be a continuous process. Microstructures, ubiquitous to all serpentinized peridotites, show that microfracturing has occurred on all scales and is in accord with high local volume strains. In such environments, therefore, serpentinization should be a

continuous process, controlled only by water access to ultramafic rocks through their cover.

Ultramafic rocks represent a major component of the earth's crust, with special dynamic and chemical effects as a result of both the serpentinization and the deserpentinization reaction.

ACKNOWLEDGEMENTS

I would like first to express my very sincere thanks to W.S. Fyfe, for providing not only the necessary financial support, but a dynamic scientific atmosphere in which to work during the course of this investigation.

W.S. Fyfe suggested the research topic and Z. Haq conducted the first experiments. Z. Haq deserves special thanks for the time he spent explaining the fundamentals of diffusion. I would like, also, to thank my colleagues at the Department of Geology for valuable criticism and discussion during this project; especially A. Kishida, M. Ferriera and F. Barriga on hydrothermal convection and metamorphism; R. Tronnes and W.R. Church on the processes of formation of ocean crust and H. Koral on the physics of crack growth. F. Wicks of the Royal Ontario Museum is thanked for his guidance in the use of the microbeam camera, his continued interest in this study, and many helpful discussions on both serpentine mineralogy and serpentinization itself.

My field work in the Philippines would not have been possible without the support of A.F. Faretta, Executive Vice President and Development Benguet Consolidated Mines, and E. Quimson, Controller, of the Acohe Mining Company. I am indebted to F. Ignacio, chief geologist at Acohe, and especially to S. dela Cruz, senior geologist at Coto, who contributed significantly to my knowledge of the geology of

the Zambales ultramafic complex; as well as to the other geological staff of both the mines who contributed to making my research a success.

Special mention must also go to W. Chauvin of the Surface Science Laboratory (UWO) for showing me how to operate the SEM, to T. Wu for patiently explaining to me both how to run the XRF and what little I know about computers; to B. Harwood for making the glass diffusion cells used in the experiments; to J. Forth, who prepared all the thin sections, and to A. Noon for the photographic work. Grace McIntyre is gratefully acknowledged for the superb typing of the manuscript and tables.

Finally, to Midge Hamill for her continual support and inexhaustable patience, and to my parents, who have always been an unfailing source of encouragement, I express my deepest appreciation.

TABLE OF CONTENTS

	Page
CERTIFICATE OF EXAMINATION	ii
ABSTRACT	iii
ACKNOWLEDGEMENTS	vi
TABLE OF CONTENTS	viii
LIST OF PHOTOGRAPHIC PLATES	xi
LIST OF TABLES	xiii
LIST OF FIGURES	xiv
 CHAPTER 1 - AN INTRODUCTION INTO THE SERPENTINIZATION PROBLEM	
1.1 The Peridotite-Serpentine Association	1
1.2 Occurrences of Peridotites and Serpentinized Peridotites	3
1.3 Evidence for the Hydration of the Ocean Crust and Mantle	5
1.4 Problems	7
1.4.1 The Emplacement of Serpentinized Peridotites into Upper Levels of the Crust	7
1.4.2 Subduction of Oceanic Serpentinites	9
1.4.3 How does Serpentine Form?	10
1.4.4 Constant Volume Replacement: Yes or No?	11
1.4.5 Thermal Effects	14
1.4.6 Volume (Strain) Effects	15
1.4.7 Timing of Serpentinization	16
1.5 Conclusions	17
1.6 Emphasis and Scope of this Study	17
 CHAPTER 2 - THE GEOCHEMISTRY AND STRUCTURE OF THE SERPENTINE MINERALS: A REVIEW	
2.1 The Structure and Crystal Chemistry of the Serpentine Minerals	19
2.1.1 1:1 Layer Type Silicates	22
2.1.2 Chemical Differences Among the Serpentine Minerals	24
2.1.3 Misfit Relief and Interlayer Bonding ..	25
2.2 Serpentine Phase Equilibria	27
2.3 Summary	31
 CHAPTER 3 - GEOCHEMISTRY AND STRUCTURE OF SERPENTINIZED PERIDOTITES AND SERPENTINITES FROM THE ZAMBALES ULTRAMAFIC COMPLEX, PHILIPPINES	
3.1 Introduction: Tectonic Setting	33
3.2 Regional Geology	38

	Page
3.3 Tectonic and Geochemical History	44
3.4 Island or Ophiolite?	45
3.5 Serpentinization	48
3.5.1 Location and Extent of Serpentinization	48
3.5.2 Serpentine Textures and Mineralogy	51
3.5.3 P-T Conditions of Serpentinization	56
3.6 Strain Fabrics in Serpentinized Peridotites: Including Samples from Italy and Newfoundland	61
3.6.1 Microstructures in Massive Serpentinized Peridotites and Serpentinites	61
3.6.2 Scanning Electron Micrographs of Serpentine Structures	71
3.6.3 Crack Growth in Rocks in the Presence of Moisture	74
3.6.4 Swelling Pressure (Stress) of the Reaction	76
3.7 Mineral and Whole Rock Chemistry	78
3.7.1 The Mobility of Mg, Si, Ca, Na, Fe, and H ₂ O	80
3.7.2 The Oxidation of Fe	85
3.8 Vein and Crack Formation During Serpentinization	88
3.8.1 Reaction Induced Volume Strains	88
3.8.2 Serpentine Veins	92
3.9 Conclusions	93
 CHAPTER 4 - SOME MEASUREMENTS OF WATER AND SALT TRANSFER THROUGH SERPENTINIZED PERIDOTITES	
4.1 Purpose of Study	96
4.2 Transfer Processes in Open Systems	97
4.2.1 Transport Equations for Diffusive Flow	98
4.2.2 Osmotic Flow	103
4.3 Experimental Methods	106
4.3.1 Samples	106
4.3.2 The Diffusion Cell	107
4.3.3 Measurement of Sodium Chloride and Water Fluxes	110
4.3.4 Determination of the Diffusion Coefficients of Sodium Chloride and Water	113
4.4 The Results of the Diffusion Experiments	114
4.4.1 Fluxes of Water and Sodium Chloride in Response to a 6 Molal Sodium Chloride Concentration Difference at 340°C	114
4.4.2 Diffusion Coefficients of Water and Sodium Chloride	122

4.4.3	Discussion of Results	125
a)	Fluxes and Diffusivities	125
b)	Salt Filtration	135
c)	Temperature Dependence of D	137
d)	Transport Coefficients of H ₂ O	142
4.5	Summary and Conclusions	151
CHAPTER 5 - THE DRIVING FORCE FOR SERPENTINIZATION ..		154
5.1	The Serpentine-Peridotite Interface	154
5.2	A Semi-Quantitative Analysis of the Forces and Fluxes Coupled to Serpentization	168
5.3	Limits on the Depth of Serpentinization in the Crust	174
5.3.1	The Lower Boundary	174
5.3.2	The Upper Boundary	175
5.4	Summary and Conclusions	176
CHAPTER 6 - SUMMARY AND CONCLUSIONS		181
* * * *		
APPENDIX I. Summary of Analytical Techniques		187
APPENDIX II. Thermodynamic Calculations and Concentrative Properties of Aqueous Solutions		191
APPENDIX III. Representative Microprobe Analyses of Peridotites from the Philippines ..		195
APPENDIX IV. Representative Whole Rock Analyses of Peridotites from the Philippines ..		211
APPENDIX V. Physical and Chemical Properties of the Solutions and Specimens Used in the Experiments		216
APPENDIX VI. Additional Fluxes and Diffusion Coefficients of Salt and Water		220
APPENDIX VII. Representative Total Water Volume Flow vs Time Plots		223
APPENDIX VIII. Mineralogy and Textures of the E. Ligurian (Italy) and Bay of Islands (Newfoundland) Serpentinites		235
REFERENCES		238
VITA		266

LIST OF PHOTOGRAPHIC PLATES

Plate	Description	Page
1A	Morphology of the serpentine mineral lizardite	21
1B	Povlen-type serpentine structure	21
1C	Sectioned image of chrysotile	21
2	Landsat image of the Zambales Range, Luzon, Philippines	35
3A	Diabase dykes in ultramafic rocks at Coto, Zambales, Philippines	50
3B	Fractures in the diabase dykes (Coto)	50
3C	Sheared serpentine zone (Coto)	50
4	Serpentine textures (Philippines)	55
4A	Mesh textured serpentine	55
4B	Fine-grained serpentine in mesh centers	55
4C	Hourglass textured serpentine	55
4D	Ribbon textured serpentine	55
4E	Lizardite bastite after pyroxene	55
4F	Non-pseudomorphic (recrystallized) serpentine	55
5	Reaction induced strain fabrics on the hand specimen scale	64
5A	Transgranular serpentine-filled fracture, Acohe, Philippines	64
5B	Typical fracture distribution in serpentinite, Bay of Islands, Newfoundland ..	64
5C	Typical fracture distribution in serpentinite, Coto, Philippines	64
5D	Close-up of fractures seen above	64
6	Microscopic strain fabrics in serpentinized peridotites (Philippines, Newfoundland and Italy)	67
6A	Typical "cubic" microstructures in olivine ..	67
6B	Close-up of microstructures in olivine	67
6C	Cataclastic fabric structures in olivine	67
6D	Complex banded transgranular microstructure	67
6E	Ribbon textured microstructures	67
6F	Transgranular microstructure in completely serpentinized peridotite	67

Plate	Description	Page
7	Syntectonic serpentinization fractures	69
7A	Conjugate shear fracture in dunite	69
7B	Close-up of conjugate shear fractures	69
7C	En-echelon shear fractures in thin section ..	69
7D	Chrysotile asbestos in shear fractures	69
8	SEM photomicrographs of microstructures in serpentine and peridotites	73
8A	Typical microfracture in olivine, Philippines	73
8B	Typical serpentine (lizardite) structures in microfracture, Philippines	73
8C	Lizardite showing trigonal structures, Philippines	73
8D	Crenulated lizardite plates in serpentinite, E. Liguria, Italy	73
9A	A typical experimental diffusion slice	119
9B	Iron staining on surface of diffusion slice imbibed in de-ionized water	119
9C	Surface of diffusion slice imbibed in the salt solution	119
9D	Iron oxyhydroxides coating lizardite plates	119
9E	Iron (oxidation) staining as seen in thin section	119
9F	Close-up of iron oxidation along serpentine mesh rims	119
10	The serpentine diffusion slices (cont.)	121
10A	Iron staining in cross-cutting veins (Newfoundland)	121
10B	Same as above (Philippines)	121
10C	Iron oxidation along mesh rim veinlets	121
10D	Alteration in a non-experimental diffusion slice	121

LIST OF TABLES

Table	Description	Page
1.1	Scale of serpentinization in some selected land-based ophiolites	4
2.1	Classification of the serpentine minerals	23
3.1	Metamorphic minerals and textures of mafic and ultramafic rocks from the Zambales Complex, Philippines	57
3.2	Typical swelling pressures generated by a serpentinization reaction	77
4.1	Measured fluxes of water and salt through completely serpentinized peridotites at 340°C	115
4.2	Measured fluxes of water and salt through partially serpentinized peridotites at 340°C	116
4.3	Calculated diffusion coefficients of water and salt in partially serpentinized peridotites	123
4.4	Calculated diffusivities of water and salt in completely serpentinized peridotites	124
4.5	Intrinsic permeabilities of partially serpentinized peridotites	144
4.6	Intrinsic permeabilities of completely serpentinized peridotites	145
4.7	Transport coefficients of water and ions in other low permeability materials	149
4.8	Permeability coefficients in some unfractured porous media (including serpentinized peridotites)	150
5.1	Typical serpentinization rates at moderate temperatures	167

LIST OF FIGURES

Figure	Description	Page
1.1	Olivine expansion cracks in plagioclase	13
2.1	Pressure-temperature diagram for the serpentine minerals	30
3.1	Tectonic and location map of the Philippine island arc	37
3.2	Geologic map of the Zambales Range, Philippines	40
3.3	Magnetite concentration versus degree of serpentinization	87
4.1	Schematic diagram of the diffusion cell	109
4.2a,b	Concentration profiles of Na ⁺ and Cl ⁻ across the diffusion slice	132-133
4.3	Arrhenius plot for water and salt in serpentinized peridotites	139
4.4	Estimated diffusion coefficients of water at higher temperatures	141
4.5	Measured transport coefficients of water through serpentinized peridotites as a function of rock density	148
5.1	Reaction environment along the margins of a crack in a peridotite	156
5.2	Corrected P-T diagram for the reaction serpentine + brucite = forsterite + water	159
5.3	The rate of advance of the reaction front as a function of time	166
5.4	Schematic relations between serpentinization stress, cracking, and permeability	179

CHAPTER 1

AN INTRODUCTION INTO THE SERPENTINIZATION PROBLEM

1.1 The Peridotite-Serpentine Association

Steinmann (1927) was one of the first geologists to recognize the association, in alpine-type orogenic systems, of serpentized peridotites,¹ pelagic cherts (radiolarites), and spinelites ("Steinmann's trinity"), along with subordinate gabbro, diabase, their metamorphic equivalents, and related sedimentary rocks. Benson (1926) emphasized the worldwide nature of this association. Grouped together these rocks are called ophiolites, which has its origin in the Greek word "ophi", meaning snake or serpent, because of the mottled or greenish appearance of sheared serpentinite (Brogniant, 1827 from Coleman, 1977).

In 1955, the late Professor Harry Hess published a paper entitled "Serpentinites, Orogeny, and Epeirogeny", in which he suggested that the common presence of serpentinites in all modern island arcs (e.g. Cuba, Philippines, New Caledonia) is compelling evidence that island arcs

¹The rock name serpentinite will be reserved for peridotites containing more than 50% serpentine-group minerals (Coleman, 1971).

represent an initial stage in the development of an alpine-type mountain system, and hence (Wilson, 1949; Hess, 1954) argue for the growth of continents by both vertical and horizontal accretion along their margins. Seismic studies by Ewing, Rait and others (see Rait, 1956), and observations on samples of serpentinized peridotites dredged from fault scars on the ocean floor (Shand, 1949; Ross, Foster and Myers, 1954), had by this time shown that the Mohorovicic discontinuity is the boundary between basaltic rocks and mantle peridotite (P-wave velocity changes from ≈ 6.7 km/sec to ≈ 8.1 km/sec). Hess (1955) went on to say that layer 3 of the ocean crust might be composed of serpentinized peridotites, formed as fluids ascending with the rising limb of a mantle convection cell at mid-ocean ridges cross the 500°C isotherm (Bowen and Tuttle, 1949) and react with dry peridotite: the Moho is thus a hydration boundary, separating serpentinized from un-serpentinized peridotites.

And then in his classic paper of 1962, "History of the Ocean Basins", Hess proposed the modern theory of sea floor spreading (see discussion by Wyllie, 1971, pp. 298-305; Dietz, 1961; Bullard, Maxwell and Revelle, 1956 on heat flow measurements; Vine and Mathews, 1963 on the linear magnetic anomalies), in which he concluded that alpine ophiolites represent allochthonous slices of ocean crust and mantle (Dietz, 1963; Gass and Masson-Smith, 1963). The

3

characteristics of ultramafic rocks (peridotites), usually serpentinized, gabbros and basalts dredged from the sea floor near midoceanic ridges (Quon and Ehlers, 1963; Melson et al., 1967; Bonatti, 1968; Miyashiro, 1969; Aumento, 1969; Melson and Thompson, 1971), from trench walls (Bowin et al., 1966), and those exposed in Alpine complexes from various parts of the world (Gass, 1968; Thayer, 1967, 1969; Bonatti et al., 1970; Moores and Vine, 1971), are so similar as to imply a common origin.

1.2 Occurrences of Peridotites and Serpentinized

Peridotites

The major occurrences of massive alpine peridotite bodies (slabs) are listed in Table 1.1, along with their sizes, and the extent of serpentinization. Associated with these more massive peridotites are semi-continuous belts, up to 200 km², of sheared-sedimentary and brecciated (Lockwood, 1971) serpentinite (usually 100% serpentinized) melanges (e.g. Big Blue Formation, California 20 km³, Oriete, Cuba, 4 km³; E. Papua (Musa Valley) 200 km³, Green, 1961).

The largest occurrence of peridotite is found, however, at the base of the ocean crust. The total area of all the ocean basins is 3.62×10^8 km² (Pacific - 1.65×10^8 km², Atlantic - 0.82×10^8 km², Indian - $.75 \times 10^8$ km², Arctic - 0.14×10^8 km², the rest $.28 \times 10^8$ km²; Elder,

Table 1.1. The scale of serpentization in some selected land-based ophiolite complexes.

Ophiolite	Degree of Serpentization %	Approximate Dimensions of Serpentized Rock (area x thickness) ¹⁾ . km ² x km	Reference
Iroodos, Cyprus (Xeros-Olympos)	15-50 (up to 80)	72 x 2	Wilson et al. (1959)
Vourinos	0-50	4 x (0.7)	Moores (1969)
Oman	60-80	400 x 9(?)	Boulder and Coleman (1981)
New Caledonia (Lelebaghi Massif)	15-30!	160 x (1-2)	Rodgers (1975), Moutte (1979)
Papua, New Guinea	20!	6000 x (4-6)	Rodgers (1975)
Burro Mt., Calif.	30-100	2 km diameter	Coleman and Kleth (1971)
Hettford, Quebec	50-100	1-4 km ² thick	
Bay of Islands			
- upper unit (2)		400 x (3-4)	Riccio (1976)
- lower unit (1)		400 x (0.2-0.5)	
Philippines, Zambales Complex			
- Acote Mine Area	20-100	25 x (0.5)	This study
- Cojo Mine Area	80-100	25 x (0.5)	

1) Serpentization is always greater along the borders of the massif and along faults, and major fractures. In New Caledonia (Moutte, 1979) sheared serpentinite, up to 100 meters thick, is present along the basal contacts.

1978). Let us assume, as a conservative estimate, that only 20% of the total ocean basin crust is underlain by a layer of serpentinized peridotite 1 km thick. If serpentinization is complete (100%), then the density will be 2.55 g/cm^3 and the amount of hydrated peridotite will be $7.24 \times 10^7 \text{ km}^3$ ($\approx 18 \times 10^{22} \text{ g}$). As a completely serpentinized peridotite contains ≈ 15 wt. % H_2O , at least 2% of the total ocean mass = $1.4 \times 10^{24} \text{ g}$ may be tied up in serpentine minerals in the lower ocean crust. Observations of peridotites - dominantly lherzolites and harzburgites (tectonites) - dredged from fracture zones on the ocean floor show that serpentinization ranges from 20-100% (Bonatti and Hamlyn, 1981; and references above). The recovered specimens include both reworked ultramafics (brecciated and sedimentary serpentinites) and massive serpentinized peridotite 'intrusions' up to 4 km thick (bodies 40 km (length) \times 10 km (wide) have been observed).

1.3 Evidence for the Hydration of the Ocean Mantle

Based on his water-assisted thermal cracking model, Lister (1974) concluded that convective fluid penetration to depths close to the Moho (≈ 10 km) is likely to be obtained (see also Strauss and Schubert, 1977; Ribando, 1976; Lister, 1981a and b). Oxygen isotope studies of the Oman ophiolite by Gregory and Taylor (1981) have demonstrated that in the cooling process, seawater has circulated to at least the base of the gabbroic layer (i.e. ≈ 7 km)

in the Oman ophiolite. Vibetti (personal communication, 1984) has found extensive veining and alteration in the gabbros from the Troodos complex (Cyprus) to depths 2 km below the sheeted dyke complex.

A synthesis of seismic refraction data from the Pacific suggests that the lower oceanic crust thickens by about 2 km with age, until it is about 40 Ma years old (Goslin et al., 1972; Christensen and Salisbury, 1975; Bottingha and Steinmetz, 1980). Lewis and Snydman (1980) studied similar data from the North Cocos Plate, and have suggested that a low velocity zone (<6.8 km/sec; i.e. >50% serpentinization, Fig. 17 in Christensen and Salisbury, 1975), develops at the base of layer 3 as a result of the gradual hydration of upper mantle material by serpentinization (see discussion in Christensen and Salisbury, 1975). Based on a comparison of synthetic seismograms from ophiolites and actual marine refraction data, Kempner and Gettrust (1983) presented, at the recent Geodynamics Symposium on the Oceanic Lithosphere (1983), an aging model for the lower ocean crust which includes a 1 km thick layer of serpentinized peridotite. At the same conference, Mutter et al. (1983) reported on double reflectors near the Moho, with a 2 km separation in very old ocean crust. Purdy (see Fyfe and Macdonald, 1984) emphasized, however, that "the scale upon which the experiments were carried out was almost always inappropriate to the processes that

determine velocity structure."

De Beer et al. (1983, Gough, 1981; De Beer and Gough, 1980) measured high magnetic and electrical conductivity anomalies in the Southern Cape Fold Belt of Africa, which they interpret as resulting from mineral conduction in magnetite formed during the serpentinization of marine rocks, that have been partially subducted (underthrust) beneath the continent during an Andean-type collision.

Recent measurements of the magnetic intensity of sea-floor rocks, synthesized by Harrison (1981; Cande and Kent, 1976), suggest that a significant fraction of the magnetic anomalies ("magnetic stripes"), observed in ocean floor crust must come from layer 3 (cf. Watkins and Pastor, 1971).

1.4 Problems

1.4.1 The Emplacement of Serpentinized Peridotites into Upper Levels of the Crust.

According to the model envisioned by Raleigh and Patterson (1965) and others, the partial (i.e. along its margins) dehydration of a serpentinite body may generate high local pore fluid pressures (P_{H_2O}), thus substantially weakening the rock (Hubbert and Rubbey, 1959) and hence facilitating its movement by brittle fracture in discrete fault zones. Evidence for dehydration appears to be lack-

ing, however, (see below), as shown by the observations of Hess (1955), Jahns (1967) and others; instead alpine peridotite bodies are characteristically surrounded by a plastic (slickensided) zone of intensely sheared (schistose) serpentine, often on the order of 5 meters thick, which grades into an intermediate zone composed of shear (cyclopean) polyhedrons and finally (depending on the size of the body) more massively serpentinized peridotite (e.g. Burro Mtn., California; Loney et al., 1970; Coleman and Kiełk, 1971). This is consistent with the experimentally observed transition from brittle to ductile behavior shown by mesh-textured serpentinites at confining pressures greater than 2 kb ($T < 500^{\circ}\text{C}$; Raleigh and Patterson, 1965).

The processes leading to the emplacement of an ophiolite massif or melange are poorly understood. Ben-Avraham and Nur (1982) have suggested that for a thick piece of ocean crust to be obducted it must be light and buoyant, and have some topographic relief (e.g. oceanic plateaus, seamounts, island arcs, old hot spot traces). While tectonic forces must certainly be important, the contribution that serpentinization may make to the process has been largely ignored. As a result of the serpentinization reaction peridotites develop, if completely serpentinized, two very special dynamic properties: (1) a peridotite's density drops from 3.25 g/cm^3 to $\leq 2.55 \text{ g/cm}^3$, and (2) when compressed (i.e. squeezed) it deforms ductilly, in

9

a manner similar to a shale (Handin, 1964).

Gass (1976) has suggested that diapirism accompanying large scale serpentization of mantle peridotite may be significant in the obduction of the lesser deformed ophiolites (e.g. Troodos, Cyprus). Serpentinized ultramafic protrusions, exposed in fracture zones on the sea floor, are believed to be examples of lower crustal material which has risen diapirically because of its lower density (Aumento et al., 1971; Bonatti, 1978).

In ophiolites showing evidence of extensive tectonic stacking (e.g. Oman), due to gravity sliding and/or tectonic pushing (i.e. collision), sheared serpentinite at the base of the thrust sheet may reduce the frictional stresses necessary for obduction. When temperatures rise above the upper stability of serpentine (i.e. > 500°C), the partial deserpentinization of a peridotite may also contribute to its tectonic emplacement (see ref. above: Lockwood, 1972).

1.4.2 Subduction of Oceanic Serpentinites

Ocean crust is being subducted at an annual rate of 2.995 km² (Parson, 1981). If 20% of the ocean crust being subducted is underlain by a layer of serpentinite 1 km. thick - containing ~15 wt. % H₂O when totally hydrated - the amount of water subducted yearly will be on the order 2 x 10¹⁴ g, as compared to (Itô et al., 1983) the 8.8 ± 2.9 x 10¹⁴ g of water estimated to be tied-up in a (overlying)

6.5 km thick slab of altered oceanic crust.

Water released during the deserpentinization of entrained hydrated peridotites (harzburgite) may be important in the melting of island arc magmas, and in the transport of incompatible trace and minor elements found in these rocks (e.g. boninites; Green, 1984; Ringwood, 1982), as well as in the hydration of the overlying mantle wedge (i.e. which is part of Gass's model, section 1.4.2).

1.4.3 How does Serpentine Form?

Once serpentine begins to form, the serpentinization reaction involves the penetration of water into peridotites. The process then involves the transport of water through a product interface. Basic reactions are,



water + pyroxene + olivine serpentine.

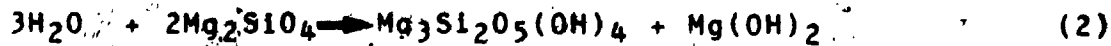
$$\Delta V_{\text{solids}} = +33 \text{ cm}^3 \text{ or } 40\%$$

$$\Delta H^\circ = -16 \text{ k cal mol}^{-1}$$

$$\Delta G^\circ = -15,109 \text{ cal mol}^{-1}$$

$$\Delta S^\circ = -91.958 \text{ cal mol}^{-1} (\text{°K})^{-1}$$

or



water + olivine serpentine + brucite

$$\Delta V_{\text{solids}} = +45 \text{ cm}^3 \text{ or } 50\%$$

$$\Delta H^\circ = -19.5 \text{ k cal mol}^{-1}$$

$$\Delta G^\circ = -17,492 \text{ cal mol}^{-1}$$

$$\Delta S^\circ = -312.472 \text{ cal mol}^{-1} (\text{OK})^{-1}$$

(Fyfe and Lonsdale, 1981).

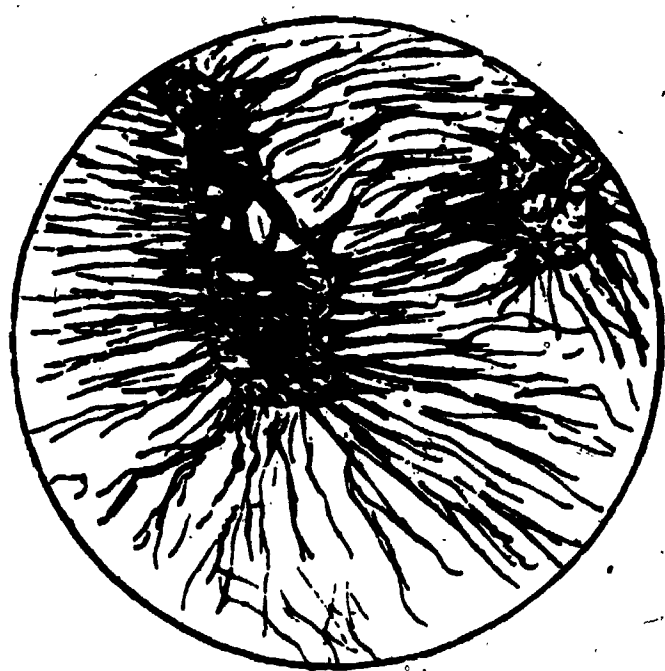
An experimental study on the kinetics of the hydration of forsterite and enstatite has shown that given fluid at the reaction interface, rates of serpentinization are geologically rapid between 1000°C and 4000°C (Martin and Fyfe, 1970). This study concluded that in natural systems, the diffusion of water to the reaction interface through a serpentine reaction layer will be rate limiting.

1.4.4 Constant Volume Replacement: Yes or No?

Most of the whole-rock geochemical studies have shown that, except for the introduction of water, serpentinization has occurred with minimal changes in the original chemical composition of the rock (i.e. also the petrographic study of Clark and Greenwood, 1972; Hess and Otárlora, 1964, 1976; Green, 1964; Hostettler et al., 1966; Condie and Madison, 1969; Page, 1967, 1968; Coleman and Kieth, 1971). And yet the myth of constant volume replacement remains, as is seen in this statement by Hawkins and Evans (1983, p. 104): "The olivine has been replaced by an anastomosing networks of serpentine, which give the grains an 'exploded' appearance; but the grain shape has been retained. There is little or no evidence for volume change and no evidence for penetrative deformation."

Figure 1.1

The large volume expansion associated with the nearly complete serpentinization of olivine in a troctolite has caused radial fractures to develop in the surrounding labradorite plagioclase (white) (from Harker, 1935, Fig. 24).



deformation."

If fluid flow is slow, then serpentinization may occur as fast as H_2O arrives at the reaction interface, since the process appears to be controlled by diffusion and not by reaction chemistry. Until serpentinization is complete, fluid flow must be essentially unidirectional! Thus arguments of constant volume replacement by the removal of large amounts of Mg and Si (30%, Thayer, 1966; Turner and Verhoogen, 1960) in solution can hardly be relevant in most (any?) serpentinized peridotites. Therefore, this process must involve significant volume expansion.

1.4.5 Thermal Effects

Fyfe (1973) has calculated that the heat evolved in completely serpentinizing 1 cubic kilometer of peridotite (3.2×10^{15} g) will be on the order of 2×10^{17} calories. For such a hydration reaction to make a significant contribution to the heat flux flow rates must be slow, relative to hydration rates, the water/rock ratio low (Fyfe and Lonsdale, 1981) and large volumes of peridotite must be serpentinized moderately rapidly; in which case the permeability of both the overlying basaltic crust and the serpentine layer must be appropriate (cf. Martin, 1968).

The failure of the $age^{1/2}$ law (based on the semi-infinite slab model of Parker and Oldenburg, 1973; Parson and Slater, 1977) to account for the observed mean heat

flow values (values $>\approx 1.5$ HFU) in old ocean crust (Anderson and Skilbeck, 1981), and in extinct plateaus, (Matsubayashi, 1983) suggests that an additional heat source is necessary.

1.4.6 Volume (Strain) Effects

Serpentine minerals produced during the hydration of a peridotite will rapidly reduce the porosity and seal cracks, but if there is any further reaction volume strains may be generated and the rock will continue to fracture. Microstructures, as shown by the extensive veining ubiquitous to all serpentinites and partially serpentinized peridotites (cf., Coleman and Kieth, 1971), suggest that volume strain rates were locally high, and is in accord with rather rapid diffusion rates. And is in agreement with the large volume increases predicted by equations (1) and (2).

If cracks propagate at high velocities (i.e. fast unstable fracturing), the process may be accompanied by focussed microseismic activity (cf. Francis, 1981; Prothero and Reid, 1982).

Serpentinization, and deserpentinization of hydrated peridotite in the ocean crust (Hess, 1955) by renewed igneous activity or later during subduction, may cause large changes in surface (seafloor or continental) topography.

1.4.7 Timing of Serpentinization

Wenner and Taylor (1973, see also Magaritz and Taylor, 1974; Wenner, 1979) studied the oxygen and hydrogen isotope compositions of serpentinized peridotites from ophiolite complexes and the seafloor, and concluded that most Alpine peridotites have been serpentinized by meteoric water (dominantly) during a late stage in their emplacement history, at temperatures $>1000^{\circ}\text{C}$. Sakai and Tsutsumi (1978) showed, however, that the fractionation of hydrogen isotopes during serpentinization, which forms the basis for the conclusion above, reflects kinetic rather than equilibrium processes. These authors also suggest that the source of water for submarine serpentinization has been two-fold: a seawater and magmatic or upper mantle derived component (e.g. subducted peridotite?).

Considering the dynamic nature of obduction, and the low concentration of hydrogen in unaltered rocks, extensive hydrogen isotope re-equilibration (and to a lesser extent oxygen) is likely to occur, especially at high water/rock ratios. If serpentinized peridotites behave as semi-permeable membranes, additional kinetic isotope fractionation is possible (Graf et al., 1965; Coplen and Hanshaw, 1973).

Nicolás et al. (1981) have used intrusive relationships among the diabase sills and gabbro dikes in the Xigaze ophiolite (Tibet) to show that the peridotites were

serpentinized near the spreading ridge itself.

1.5 Conclusions

Peridotites are a major component of the ocean crust, with very special dynamic effects (properties) as (1) volatile acceptors, during serpentinization and as (2) volatile releasers when dehydrated.

1.6 Emphasis and Scope of this Study

According to Lister (1977, 1981a) active cracking and fluid penetration ceases when the descending plume of seawater encounters a peridotite layer, since the serpentinization reaction(s) with its attendant volume expansion must significantly reduce the permeability and be self-throttling. The ultimate problem involves, therefore, the permeability of serpentized material.

In Part I of this study, the thermodynamically calculated swelling pressures produced by a serpentinization reaction are used, in combination with a textural and mineralogical investigation of serpentine microstructures from the Zambales Ultramafic Complex in the Philippines, to explain the development of microstructures in massively serpentinized peridotites worldwide.

In Part II of this thesis, the emphasis is on the experimental determination of the mechanism and rates of water transport through serpentized peridotites at

temperatures between 250°C and 400°C. Some preliminary work is also presented on serpentinization by saline fluids where membrane filtration may occur. The results are compared with transport coefficients obtained in other porous materials.

The experimentally obtained permeabilities are then used to estimate possible serpentinization rates in natural geothermal systems, and to predict (semi-quantitatively) what effect the associated flows of heat and pressure have on the reaction rate.

CHAPTER 2

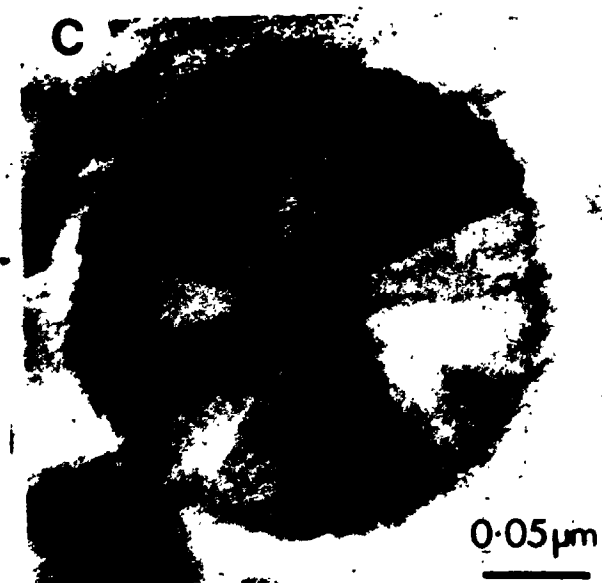
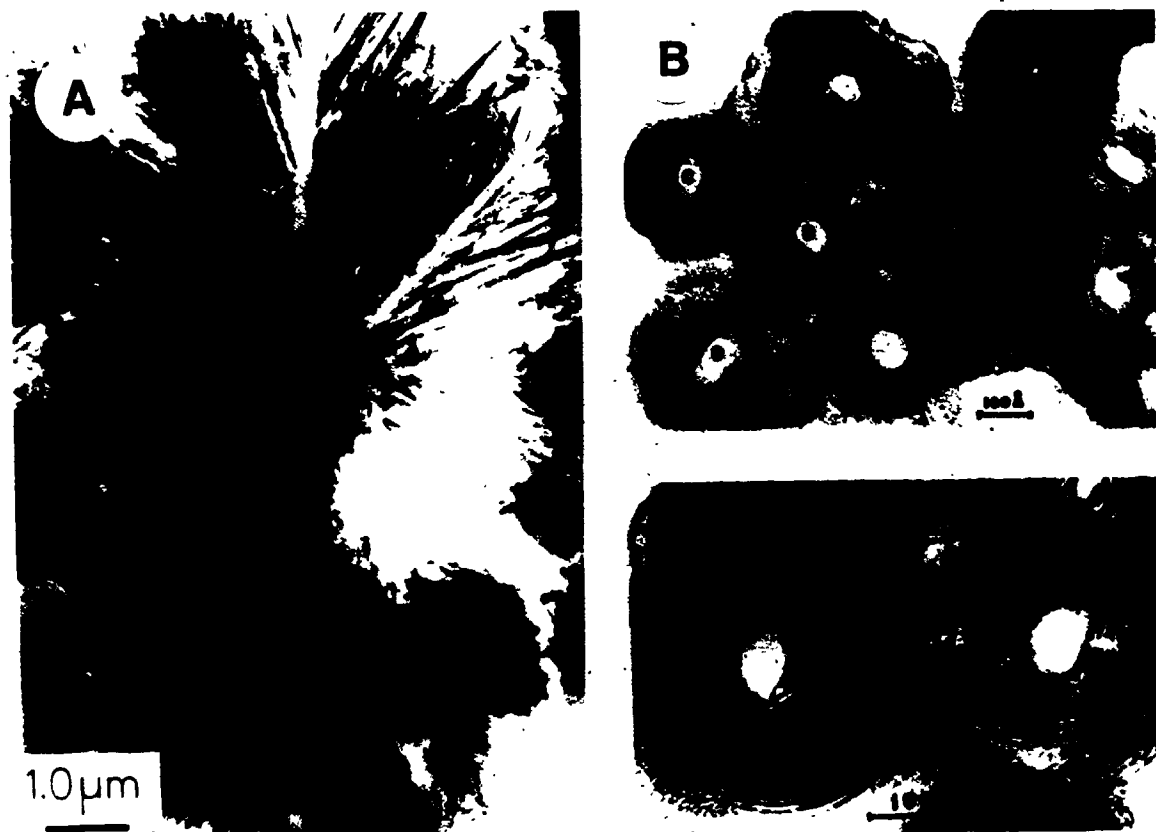
THE GEOCHEMISTRY AND STRUCTURES OF THE SERPENTINE MINERALS: A REVIEW

2.1 The Structure and Crystal Chemistry of the Serpentine Minerals

The serpentine minerals are essentially hydrated magnesium silicates with orthorombic (pseudo-trigonal) symmetry. On structural grounds, the serpentine minerals have been divided into lizardite with a planar structure (Plate 1A), chrysotile with a cylindrical structure (Plate 1B), and antigorite with an alternating wave or corrugated structure (Whittaker and Zussman, 1956; Kunze, 1956; Wicks and Whittaker, 1975). Chrysotile also forms an intermediate planar structural form called Povlen-type chrysotile, composed of polygonal serpentine fibers arranged concentrically around a more normal tubular core (Plate 1C; Middleton and Whittaker, 1976). Lizardite and chrysotile - though not antigorite - form a variety of polytypes based

Plate 1

- A. The serpentine polymorph lizardite seen in this transmission electron photomicrograph (TEM) displays its characteristic blade-like morphology. Specimen is from the margin of a complexly banded vein (from Cressy, 1979).
- B. High resolution electron micrographs of the cylindrical serpentine mineral of chrysotile (i.e. asbestos) observed parallel to the sectioned fiber axis. Curling of the serpentine layers has produced a tubular structure with an open circular core (from Yada, 1967).
- C. Povlen-type serpentine seen in cross-section under the TEM. The cylindrical chrysotile-like core is surrounded by a shell or polygonally arranged flat layers similar to lizardite (from Cressy and Zussman, 1976).



on different stacking sequences. Table 2.1 provides a brief summary of this classification.

2.1.1 1:1 Layer Type Silicates

Structures that combine a gibbsite (Al hydroxide) or brucite (Mg hydroxide) sheet with a Si-O sheet are designated as 1:1 layer types. The serpentine group minerals belong to the same structural category of clay minerals as the kaolinite group (Bailey, 1969; Brindley, 1967). As both of these phyllosilicates consist of layers that are electrically neutral and are without interlayer cations, they don't normally show interlayer swelling (Brindley, 1981). Clay minerals containing a brucite sheet are trioctahedral, while those with a gibbsite sheet are dioctahedral.

Although chemically less complex than the amphibole group, 1:1 layer silicates exhibit a complex variety of morphologies (Wicks, 1979). Bailey (1969) has suggested that the relative structural stabilities of tricotahedral 1:1 layer polytypes can be predicted by considering the following factors (listed in order of importance):

- (1) The relative amounts of attraction and repulsion between tetrahedral and octahedral cations.
- (2) The effect (i.e. repulsion or attraction) of tetrahedral rotation on basal oxygens as a result of tetrahedral-octahedral misfit.

Table 2.1

Classification of Serpentine Minerals

chrysotile	chrysotile-2M _{cl} * chrysotile-20T _{cl} chrysotile-1M _{cl}
parachrysotile*	
lizardite	lizardite-LT lizardite-2H ⁺ lizardite of various multi-layer polytypes
antigorite	various superlattices

* May occur in cylindrical or polygonal Povlen-type structures.
+ May occur with cylindrical chrysotile-20T_{cl} in a Povlen-type structure.

(from Wicks, 1979)

(3). Repulsion or attraction between cations of adjacent layers.

Bailey (1969) concluded that the order of stability is $2T > 1T > 2H_2 > 2H_1 > 1M = 2M_1 > 2M_2 = 2O_R = 6H$. Bates

(1959) suggested that morphology and chemistry are interrelated as a result of the following: (1) misfit of the octahedral and tetrahedral sheets; and (2) strength of the interlayer bonding.

Less attention has been given to the effect of inter-layer bonding on morphology. In contrast to 2:1 phyllosilicates, the bonding in 1:1 layer structures has been thought to be primarily of the hydrogen bond type, which develops between the basal oxygen of one layer and the outer hydroxyls of another layer. More recent modelling by Giese (1973, 1980) has shown that the orientation of the hydroxyl groups in amesite, serpentine and kaolinite determines the strength of the interlayer hydrogen bonds. Bonding forces between layers may be significantly strengthened if ionic substitution, for example the substitution of Al^{3+} in both the octahedral and tetrahedral sites (eg. amesite; Giese, 1980), leads to the development of a dipolar layer charged based on hydrogen (electrostatic) bonds (cf. Cruz et al., 1972).

2.1.2 Chemical Differences Among the Serpentine Minerals

Wicks (1979) and Whittaker and Wicks (1970) have

summarized the general compositional differences, i.e.

(1) Antigorites have a higher SiO_2 , and lower MgO and H_2O^+ content than chrysotile or lizardite. Fe^{2+} seems to dominate over Fe^{3+} .

(2) Chrysotile and lizardite have overlapping MgO and SiO_2 contents, and an excess of H_2O^+ .

(3) Fe^{3+} greater than Fe^{2+} in lizardite.

(4) The total Fe content of chrysotile is lower than that of either lizardite or antigorite.

Wicks and Whittaker (1975) argue that chrysotile and lizardite are polymorphs, and not simply polytypes, even though they may have different ranges of composition. As a consequence of its slightly different composition antigorite is not considered a polymorph of the other serpentine minerals.

2.1.3 Misfit Relief and Interlayer Bonding

The development of a particular serpentine structure (i.e. planar, curved, curved-wave) has been attributed, in part, to the mismatch in the dimensions of the larger octahedral and smaller tetrahedral sheets (Wicks and Whittaker, 1975; Wicks; 1979). In planar structures, such as lizardite, the mismatch is partly accommodated by a buckling of the Mg plane (and thus a thinning of the tetrahedral sheet) due to the repulsive forces between cations (see factor #1 and #3 above; Bailey, 1969; Radoslovich, 1962). The misfit

in curved structures, such as chrysotile, is only partially relieved by curvature; in fact, a significant amount of mismatch between the two sheets is necessary if rolled structures are to develop. The greater thickness of the octahedral sheet of chrysotile appears to be an important difference between it and lizardite. Antigorite, with its curved wave-like structure, behaves in a similar manner. The substitution of Al^{3+} and Fe^{3+} ($\pm \text{Ni}^{2+}$, Cr^{2+}) in sites in the octahedral sheet and Al^{3+} ($\pm \text{Fe}^{3+}$) in the octahedral sites reduces the misfit necessary if planar structures are to form; whereas in curved structures there is a limitation to the amount of substitution possible.

The weakness of this model lies in its failure to take fully into account the charge distribution, arising from ion substitution, within layers and between successive layers (cf. Gillery, 1959; Chernosky, 1975). Mellini (1982) has suggested that the substitution of trivalent ions in both the octahedral and tetrahedral sheets will tend to produce an excess of positive and negative charges on the two sheets, respectively. If this extra charge is localized on the hydroxyl groups and the tetrahedral oxygens, stronger hydrogen bonds may be formed. Consequently, the sheets are less likely to curl into tubes, and the development of planar structures, such as lizardite, will be favoured.

It is difficult to apply this model to antigorite.

Systematic hydrogen bonding is lacking - as it is in chrysotile - because of the curvature of its wave-like structure. Compositional limitations are similar, though they are not as rigorous as they are for chrysotile; the increased substitution of Fe^{2+} increases even further the amount of Al^{3+} and Fe^{3+} that can be incorporated into the structure and the misfit between the octahedral and tetrahedral sheets (Wicks, 1979). The very long Mg-(O,OH) bonds observed may develop as a result of the substitution of Fe^{2+} for Mg in the octahedral sheet which, because it has a greater electronegativity than Mg (see Fyfe, 1964), may produce weaker hydrogen bonds. This effect, as well as the large bond angles at shared octahedral edges, may be partly responsible for the development of a wave-like structure, in which the octahedral sheet is linked in an alternating manner to one set of Si-O tetrahedral, either above or below the Mg-OH sheet (see figure 1.26, Wicks, 1979). The final structure thus seems to be a balance between weak interlayer forces that encourage the structure to curve, and yet are strong enough to link some of the units together (see also discussion in Wicks and Whittaker, 1975).

2.2 Serpentine Phase Equilibria

Pertinent phase relations in the system $\text{MgO-SiO}_2\text{-H}_2\text{O}$ (+ Al_2O_3) under conditions where $\text{P H}_2\text{O} = \text{P}_{\text{total}}$, and the

$a_{H_2O} = 1$ are summarized in Figure 2.1.

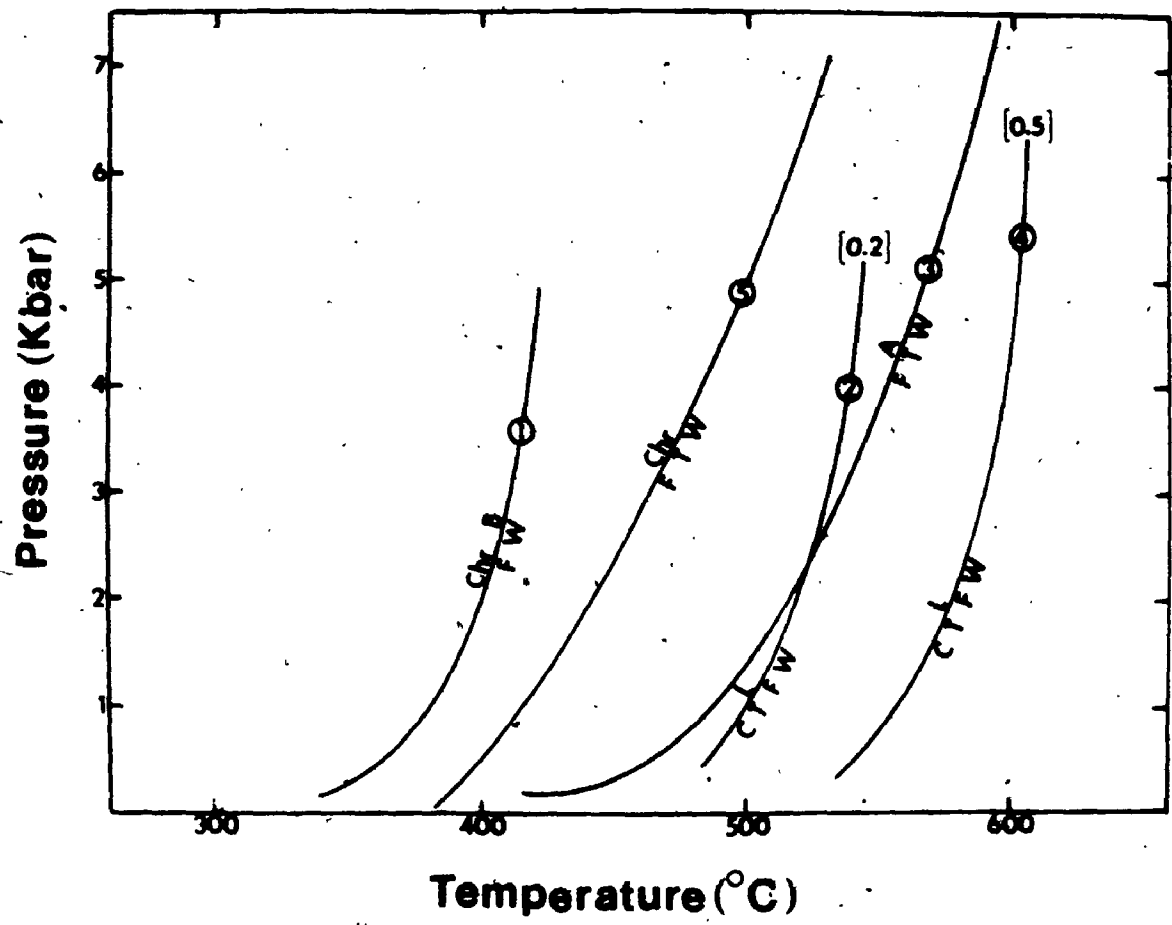
Lizardite (usually 1T) and chrysotile have been produced simultaneously in experimental runs containing Fe and/or Al (Chernosky, 1975; Moody, 1976), and appear to co-exist stably in serpentized peridotites (Coleman and Keith, 1971; Wicks and Plant, 1979). SEM studies by Pritchard (1979) show clearly that lizardite is the dominant serpentine mineral, but that the amount of chrysotile increases slightly with the degree of serpentization (i.e. but is less than 5%). However, in the pure MgO-SiO₂-H₂O system chrysotile is the only serpentine mineral that has been synthesized stably (Gillary, 1959; Roy and Roy, 1954; Yoder, 1952; Chernosky, 1975). Iishi and Saito (1973) have shown that the formation of antigorite is promoted by higher temperatures and pressures, the limited availability of water, and Mg/Si less than 3:2.

Experimental studies in the system MgO-SiO₂-Al₂O₃-H₂O by Yoder (1952), Gillery (1959), Chernosky (1975) and Caruso and Chernosky (1979) suggest that the upper stability limit of lizardite (and probably antigorite) increases as the Al content increases, while at lower temperatures it may form a solid solution series with amesite (Roy and Roy, 1954; Nelson and Roy, 1958). The introduction of iron into the system appears to have the opposite effect (Moody, 1976).

Activity diagrams have been employed by Pfeifer

Figure 2.1

Pressure-temperature diagram ($P_{H_2O} = P_{total}$) for serpentine minerals in the system $MgO-SiO_2-H_2O + Al_2O_3$ ($X = [0.2] = 4$ wt. % Al_2O_3 ; $X = [0.5] = 9.25$ wt. % Al_2O_3). Chr = chrysotile, B = brucite, L = lizardite, A = antigorite, F = forsterite, T = talc, W = water, and C = clinochlore (after Caruso et al., 1979).



(1977), Hemley et al. (1977), Nesbitt and Bricker (1978) and more recently Brennan (1983) to model the possible reaction paths and hence sequence of alteration minerals (i.e. brucite, talc and serpentine) that might form during the hydration of an ultramafic body.

2.3 Summary

The transition from chrysotile/lizardite to antigorite during the progressive metamorphism of serpentized peridotites occurs near where the prehnite-pumpellyite facies gives way to the greenschist facies assemblage, actinolite + epidote + H_2O (Trommsdorff and Evans, 1974; Scarfe and Wyllie, 1967; Chidester, 1962). Nitsch (1971) showed experimentally that the lower limit of this boundary is about $3500^{\circ}C$ ($\pm 250^{\circ}C$) if $P_{fluid} = P_{total}$, and the $aH_2O = 1$. By the middle of the amphibolite facies ($5000^{\circ}C$) antigorite has been completely replaced by newly formed olivine + talc \pm tremolite (see also O'Hara, 1967; Vance and Dungan, 1977).

Retrograde serpentine assemblages are composed of lizardite 1T + minor chrysotile + magnetite \pm brucite. The presence of brucite clearly indicates that the reaction took place at temperatures below curve (1); however, its absence may indicate higher temperatures (i.e. below curve (2)) or that the $aSiO_2$ is high (Brennan, 1983). The studies of Martin and Fyfe (1970) show that at temperatures

between 400°C and 1000°C, that hydration rates are rapid. At lower temperatures the dissolution of anhydrous phases appears to proceed at a faster rate than the precipitation of the hydrous serpentine minerals (Nesbitt and Bricker, 1978).

Retrograde antigorite is very rare (eg. Wicks and Plant, 1979), and hence probably doesn't form easily unless temperatures remain fairly high (cf. Evans et al., 1976; Evans, 1977).

The growth of planar (buckled) or rolled structures is apparently compositionally (via isomorphous substitution)-controlled. Given the composition of the phases being replaced, and the temperature interval over which hydration is rapid, it is not surprising that lizardite + brucite + minor chrysotile (plus magnetite) is the most commonly observed retrograde serpentine assemblage seen in ophiolites. The less extensive development of brucite in serpentine samples dredged from the ocean floor (Bonatti and Hamlyn, 1981) may reflect a slightly higher temperature of formation.

CHAPTER 3

GEOCHEMISTRY AND STRUCTURE OF SERPENTINIZED PERIDOTITES AND SERPENTINITES FROM THE ZAMBALES ULTRAMAFIC COMPLEX, PHILIPPINES

3.1 Introduction: Tectonic Setting

The Philippines are an archipelago of over 1,000 islands situated in the western margin of the Philippine Sea between 5° and 15°N. Separating the Philippine Sea basin from the South China, Subu, and Celebes seas marginal basins, the Philippines are in a zone of convergence between the Eurasian and Philippine Sea plates (see Fig. 3.1 and Plate 2). Active, near vertical, east-dipping subduction is marked by a belt (arc) of Quaternary volcanoes of South China Sea lithosphere associated with the Manila Trench (Hamburger et al., 1983; Cardwell et al., 1980). Present volcanism and earthquake activity along the western margins of the archipelago suggests that westward (shallow)

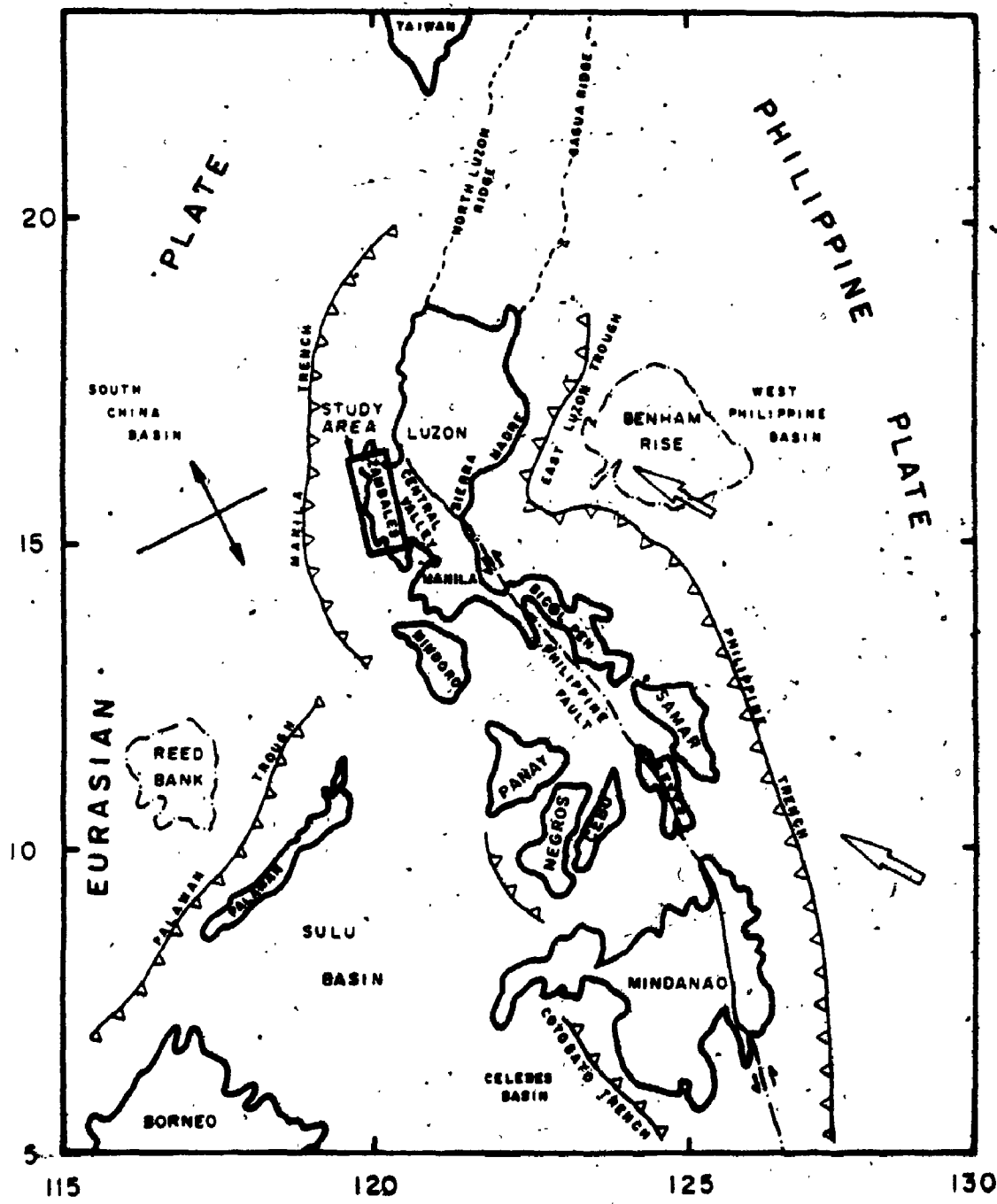
Plate 2

Landsat photo of the Zambales Range, Luzon, Philippines, showing the South China Sea (bluish black) to the west and the Central Valley (greyish-white area) to the east. A part of the Central Cordillera is exposed in the upper right hand corner of the photo. Red color is produced by vegetation, the light blue colors are rivers, and the white patches are clouds (MSS bands 4, 6, and 7; Feb. 26, 1976).



Figure 3.1

Map showing the tectonic setting and location of the Philippine island arc (after Hamburger et al., 1983; Weiszel, 1980). Present spreading centers are marked by solid lines with the sense of motion indicated by the solid arrows. Convergent plate boundaries are denoted by sawtooth lines, with the sawteeth on the overriding plate. Open arrows indicate the direction of predicted plate motion. Dashed line denote strike slip zones, with the sense of motion defined by the arrows.



subduction of Philippine Sea crust may be beginning at the Philippine Trench. The geology of the Philippines records, in a broad sense, the complex history of a mobile region squeezed between two major plates (above; Fuller et al., 1983).

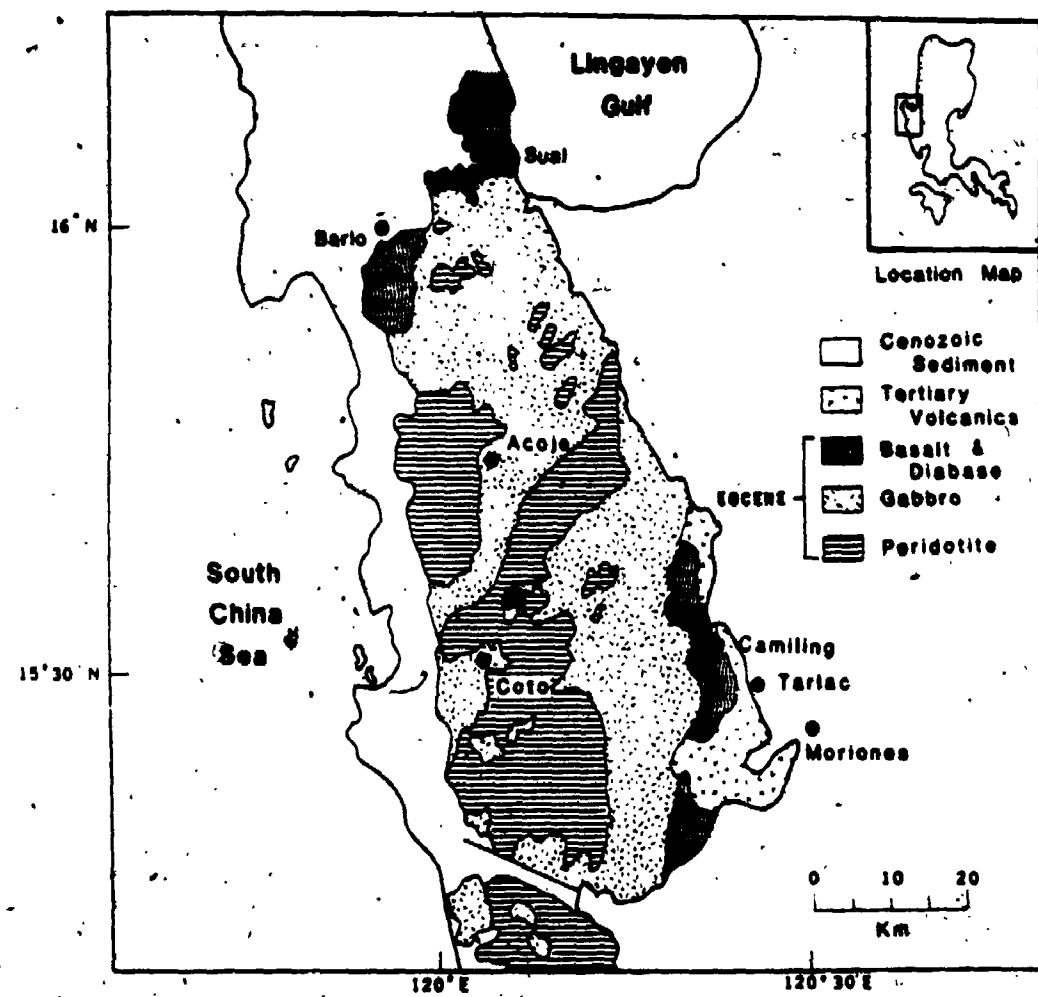
3.2 Regional Geology

The Zambales Range, outcropping over 2300 km² (i.e. 110 x 30 km) is located in the west-central portion of the island of Luzon, between the South China Sea Basin and the east-dipping Manila Trench to the west, and the Central Luzon Valley to the east (Fig. 3.1 and Plate 2). Four provinces are covered by this rugged mountain range, which has an average relief of about 1600 m: Zambales, Pangasinan, Tarlac, and Bataan.

The range (see map, Fig. 3.2) is composed dominantly of peridotites and gabbros, which have been sub-divided into three to four fault bounded massifs (belts; Fernandez, 1960) and collectively called the Zambales Ultramafic Complex (Rossman, 1964). The peridotite sequence is composed of harzburgites (locally called saxonite, En₇₅₋₉₅), dunites (Fo_{88-91.5}), and pyroxenites (Rossman, 1964). Massive podiform chromite deposits, typical of alpine type complexes (Thayer, 1960, 1964), are found throughout the Zambales range, as irregular lenses or pods within the harzburgite, often near the gabbro (either

Figure 3.2.

Generalized geologic map of the Zambales Range, Luzon, Philippines, showing the location of the Acohe and Coto mines (from Fuller et al., 1983).



olivine gabbro or norite) contact (Stoll, 1952; Rossman, 1964; Bacuta, 1978). Two grades of chromite ore are mined; a metallurgical grade (high chromium) from the Acoje Mine (operated by the Acoje Mining Co.) and a refractory grade (high Al) from the Coto Mine (Benguet Mining Co.; see Figure 3.2). Note: these mines appear on the map to be located in the gabbro as the peridotites in the mine area are covered by a layer of gabbroic rocks. The combined production from these two mines places the Philippines in about seventh place as a world supplier of chromite (Federal Institute for Geosciences and Raw Materials, 1978).

The contacts between the various rock units are generally faulted and/or masked by lateritic soils; when they can be observed, however, it appears that olivine-gabbro grades into norite, which grades into a diabase dyke (or sill) swarm, which in turn grades into basic volcanic rocks (Rossman, 1964). Complex intrusive relationships are often observed at contacts (e.g. gabbro-peridotite contact; Thayer, 1967); for example, at the gabbro-peridotite contact along the South Lewis River, 1-2 km east of the Coto Mine, breccias consisting of slabs of peridotite and gabbro in a matrix of mafic gabbro, as well as xenoliths of recrystallized gabbro enclosed in massive peridotite, are observed (Thayer, 1967; see below also). A basaltic-andesite dyke swarm (not sheeted dykes), with a diabasic

texture (Hawkins and Evans, 1983) and chilled margins (Hawkins, 1979; Stoll, 1952; this study) is highly visible at the Coto Mine, where it is seen intruding both the peridotites and gabbros (Plate 2). According to S. dela Cruz (personal communication, 1981), senior geologist at Coto, similar dykes are present throughout the central portion of the Zambales Range.

To the west the complex is overlain by Lower Miocene to Pliocene sedimentary rocks consisting of conglomerates of serpentinized dunites and harzburgites, shale, sandstone, limestone, and recent deposits. On-going erosion has produced deeply incised streams that are filled with enormous peridotite boulders. Along the more gentle slopes lateritic soils, which are often high in chromium, are accumulating. Once covered by a dense tropical forest, the area has suffered, as has most of the Philippines, from intense logging and a lack of any proper conservation management.

The complex (at least locally along its northern flanks) has been tilted down to the northeast (Hawkins and Evans, 1983). Because of erosion on the tilted block the most complete stratigraphic sections are located along the ranges eastern, northeastern, and southeastern flanks. The Geologic Map of the Philippines (1967) indicates dacitic-andesitic flows in this area. Reconnaissance work by A. Macdonald and W.S. Fyfe in 1981 confirmed the existence of

easterly dipping massive flows, sills(?), and pillowd flows, all extensively subaerially weathered. Their contact and relationship to the mafic-ultramafic sequence is not clear. Along some of the river valleys which extend into the foot-hills of the complex, massive basalt flows (Cretaceous-Paleogene(?) in age), often with an upper layer of spilitic pillow basalts, basalt rubble, and associated manganeseiferous cherts and metallic sulfides, as well as dykes and sills that appear to be feeders to them, are observed (Bryner, 1967; Hawkins and Evans, 1983). At the Barlo Mine in Dasol, Pangasinan, this assemblage is underlain by silicified gabbroic and dioritic rocks (Hawkins, 1979).

Along the upper stretches of the North Balincaguin River, east of Barlo (see map Fig. 3.2), massive and brecciated basalts were observed unconformably covering bodies of dunites and pyroxenites (personal observation). Sporadic occurrences of sill-like bodies of plutonic (tonalitic to trondhjemitic) rocks, which show mutually intrusive contact relations with the upper-level gabbros and diabases (c.f. Hawkins and Evans, 1983), were also seen. Some of the coarse grained basalts seen in the same area may actually be gabbroic rocks that were able to reach the surface as small intrusions (Macdonald and Fye, personal observation, 1983). This sequence is conformably overlain by the upper Eocene Askitero Formation, which is

composed of both volcaniclastic turbidites and pelagic limestones (Schweller et al., 1983). It is covered unconformably by the upper-middle Miocene clastic sediments (includes serpentinized peridotite fragments) of the Moriones Formation (Amato, 1965; Villones, 1980). This suggests that sometime after the late Eocene volcanic activity ceased, and that by early Miocene erosion and uplift(?) of the complex began (Schweller et al., 1983).

3.3 Tectonic and Geochemical History

A geochemical and petrological study by Hawkins and Evans (1983) suggests that the Zambales Range ophiolite resembles, at least in part, a poorly evolved island arc-tholeiite series that formed within an interoceanic island arc (eg. Marianas Arc). The geochemical data indicates that the diabase dykes that cut the peridotites in the Coto Mine area (elsewhere?), and most of the basaltic rocks, are genetically related. Additional evidence suggests that some of the Bario series basalts may be chemically related to boninites, while the associated trondhjemites are apparently petrologically similar to the so-called plagiogranites of Coleman and Peterman (1975). However, some of the basaltic rocks along the eastern edges appear chemically more similar to those generated in back-arc basins (or deep ocean basins). The ultramafic rocks that form the root of the complex include an unusually

(compared to back arc basin or deep sea ocean floor crust?) thick (.7 - 1.3 km) sequence of cumulate ultramafic rocks and shows signs of extensive partial melting, especially in the Acohe belt.

Paleotectonic reconstructions (Hawkins and Evans, 1983; Fuller et al., 1983; Taylor and Hayes, 1983) suggest that the Zambales Range existed as an east-west trending Eocene arc-back arc basin complex behind a West Philippine Sea spreading center. Counterclockwise rotation by as much as 90°, and westward migration in the upper Eocene, formed the Manila Trench and led to subsequent obduction, essentially *in situ*, of the arc. Seafloor spreading in the South China Sea Basin began in the middle Oligocene to early Miocene and (Taylor and Hayes, 1983), thus it is probably not the source for this piece of obducted oceanic lithosphere.

3.4 Island or Ophiolite?

It has been widely accepted, until only very recently, that ophiolites represent fragments of ocean crust formed at a constructive plate margin of a major ocean basin (Penrose Conf., 1972). More detailed studies have shown that neither the structure nor the geochemistry of all ophiolites are identical (Saunders et al., 1979; Gass, 1976). In some of them, even in the absence of a complicated post-emplacement metamorphic and tectonic history,

the stratigraphy is far from normal, with entire sections of the more 'typical' ophiolites missing.

The Zambales Complex, for example, lacks a sheeted dyke complex, and consists of an upper layer of gabbroic to trondhjemitic plutonic rocks that show complex intrusive relationships (i.e. they comprise a sill complex?). The rocks below the gabbroic layer consist of an unusually thick ultramafic cumulate series, that is resting on a base composed of depleted (i.e. alpine-type) peridotites. The peridotites are cut by an extensive diabase dyke swarm, indicative of a magma chamber at a much greater depth.

Geochemistry, structural and stratigraphic relationships among the belts and the different rock types, weathering and the orientation of some of the lava flows (and sills) suggests that the Zambales peridotites formed the base of a group of block-faulted subaerial volcanoes, that resemble the stratovolcanoes forming in the Marianas Arc today (Hussong and Uyeda, 1981). Extensional tectonics are dominant during the stage when tholeiitic volcanism is occurring. Scattered between the present volcanic arc and the trench axis (in the fore-arc) are many large seamounts, which may be serpentine diapirs (ref. above, p. 920; the Sierra Madre ultramafics?; see Fig. 3.1).

One possibility seldom considered, until recently, is that some of the less typical ophiolites may correspond to such relief-forming features as oceanic islands (Cendero,

1969; Bosshard and Macfarlane, 1979), seamounts, ridges, plateaus and island arcs (Miyashiro, 1973; Phelps et al., 1980; Gerlach et al., 1981; Himmelburg et al., 1980), as they will be more prone to obduction (Ben-Avraham et al., 1982).

The mechanism of obduction, although poorly understood, may be very important in determining what sort of, or if any, 'crust' is emplaced. Uyeda and Kanamori (1979) have suggested that we classify subduction zones as those activated by either back-arc or ocean ridge spreading. The style of subduction will depend largely on the density differences and the relative motion (rate/speed) of the colliding plates (Uyeda, 1979) progressing, as part of a single evolutionary cycle, from Chilean-type subduction, characterized by strong mechanical coupling (underthrusting, vertical tectonics), to the Marianas-type where the oceanic plate falls freely into the mantle (Kanamori, 1977). For example, the Japan Trench was apparently (Hussong and Uyeda, 1981) M-type during most of the Miocene and has only recently become C-type. It is not hard to imagine the obduction of both relief forming features and some oceanic sediments as thrust slivers (c.f. Oxburgh, 1972; Dewey, 1976) during C-type subduction (e.g. Sierra Madre, Isabela, Philippines (west side of Luzon); Gervasio, 1971). The Zambales Range may represent an additional mechanism for emplacement; i.e. the trapping and upward

squeezing of an arc between two converging plates (c.f. Gass, 1976).

Many of the more typical ophiolite complexes may include the effects of a superimposed cycle of seamount-island arc magmatism prior to and during obduction (c.f. Alabaster et al., 1972, the Oman ophiolite complex), thus further complicating their tectonic and geochemical history. So, while there is little doubt that many 'ophiolites' represent fragments of ocean crust and upper mantle (see also Nur, 1983), it is clear that the term ophiolite (Penrose Conf., 1972) must be expanded to include island-like oceanic features that have not formed at spreading centers, or that have been at least modified so such distinctions are not recognizable.

3.5 Serpentinization

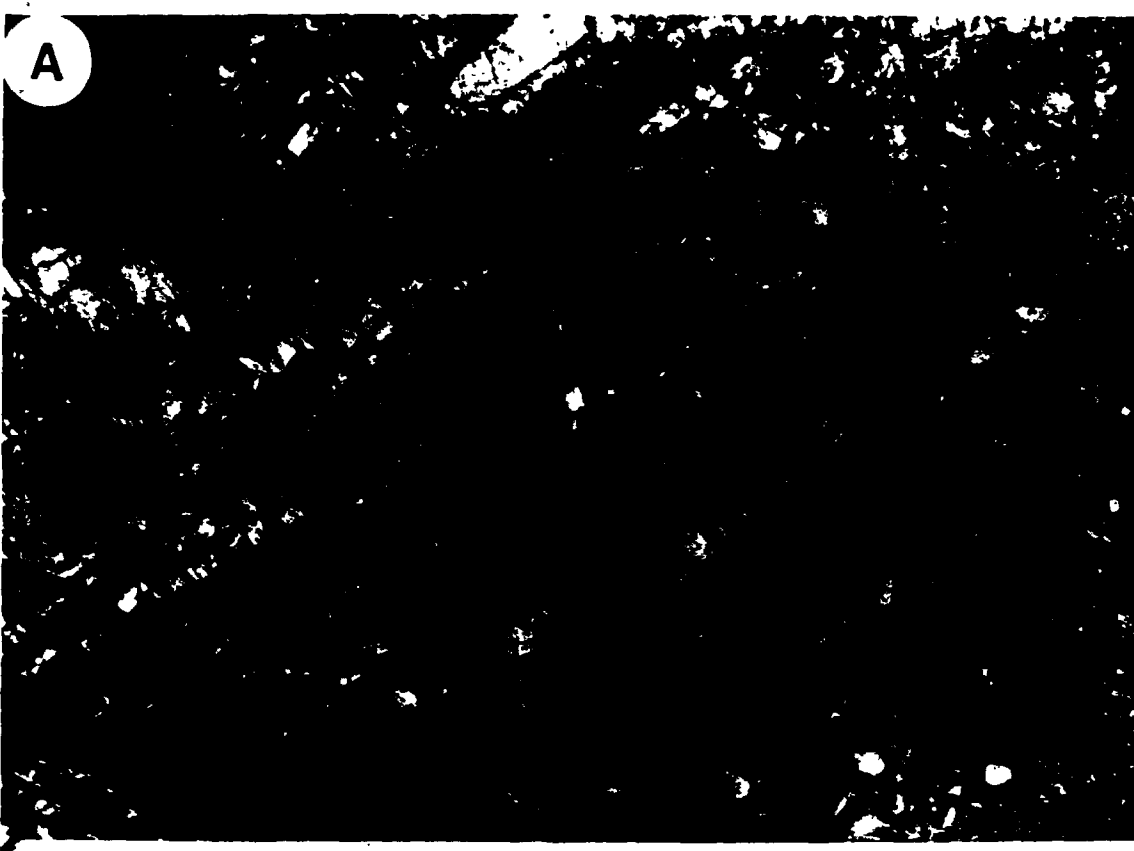
3.5.1 Location and Extent of Serpentinization

The sampling and local mapping for this thesis were done in the summers of 1978, 1980, and 1981. Although the size and ruggedness of the Zambales Mountain Range made any large scale mapping project impossible, the podiform chromite mines at Acohe and Coto (see map Fig. 3.2) provide, fortunately, two well exposed and representative sections of massive serpentinized mafic to ultramafic rocks.

The ultramafic (harzburgites and dunites) rocks and

Plate 3

- A. Diabase textured dykes, 3-4 meters wide, cutting the depleted mantle ultramafic rocks at the Coto mine. Geochemically the dykes are related to an island arc series. Thermal contraction in the dykes produced a large permeability contrast at the dyke-peridotite interface, thus making possible vigorous hydrothermal convection and metamorphism. Note, that in these rocks serpentinization is complete!
- B. Close-up of a densely cracked dyke at Coto mine. Typically the fractures are filled with orehnrite (white material as shown by arrow).
- C. Sheared serpentine zone in blocks of massively seroentinized peridotites (Coto). If water diffusion rates into the peridotite are moderately rapid (see A above), volume strains generated, perhaps syntectonically, by the serpentinization reaction may cause large blocks of massive serpentinite to rise "diapirically" and at the same time to deform ductilly along their margins.



chromite deposits at Coto are cut by an extensive basaltic andesite dyke swarm (Plate 3A). In the vicinity of the dykes peridotites are from 90 to 100% serpentinized (Table IV-2, Appendix). At Acohe the degree of serpentinization is more variable, ranging anywhere from 30 to 90% (Table IV-1; Appendix); the more completely serpentinized rocks are always found immediately beneath the gabbroic layer, and then it decreases with depth.

The degree of serpentinization is always higher in the immediate vicinity of dykes, along the margins of, or within massive chromite pods, and at contacts between different lithologic units. In the peridotite bodies at Coto - and at Acohe - pervasive local tectonic adjustment (joints? shears?) between meter scale blocks has occurred, though little movement is evident (Plate 3A). However, along zones where shearing (and faulting) has been more extensive, as is shown by the presence of sheared serpentine, the displacement (up to 50 meters) of dykes and chromite pods is observed (Plate 3C) (Rossman, 1964).

3.5.2 Serpentine Textures and Mineralogy

In field exposures, massive blocks of unweathered peridotite show a progressive color change from olive-grey to dark greenish-black as the amount of serpentine minerals exceeds 50% (cf. Loney et al., 1981). Serpentinites generally appear a deeper green if the magnetite has migrated

into the veins.

Serpentine minerals (plus brucite and magnetite) found in the massive blocks of serpentinized ultramafic rocks are listed in Table 3.1, along with the mineral assemblages observed petrographically in the diabase dykes and gabbros (at the Coto Mine). Correct identification of the different serpentine minerals (± brucite) is difficult and requires a variety of analytical techniques (Appendix I).

The textural description of the serpentine minerals in thin section follows the comprehensive work of Wicks and Whittaker (1977), Wicks, Whittaker and Zussman (1977), and Wicks and Plant (1979); for serpentine veins see also Cooke (1937) and Riordan (1955). In the partially serpentinized peridotites, mesh textured lizardite \pm brucite \pm magnetite has partially replaced the edges of fragments of pyroxene and olivine grains (Plates 6A to C). The fracture trace is often clearly outlined by a central parting containing anisotropic serpentine. Contacts between the apparent lizardite "fibers" and the unaltered portion of the original mineral may either be sharp or diffuse. The apparent fibers are in reality plates, which often show (001) serpentine oriented roughly perpendicular to the fracture walls and parallel to the [100] parting in forsterite. Brindley and Zussman (1957), Brindley (1963) and Wicks (1969) have shown that the parent mineral exhibits some structural control on the crystallographic

orientation of the serpentine mineral pseudomorphing it.

This translates very roughly into a preservation of the oxygen-anion framework, and the migration of cations (see below, Vein and Crack Formation).

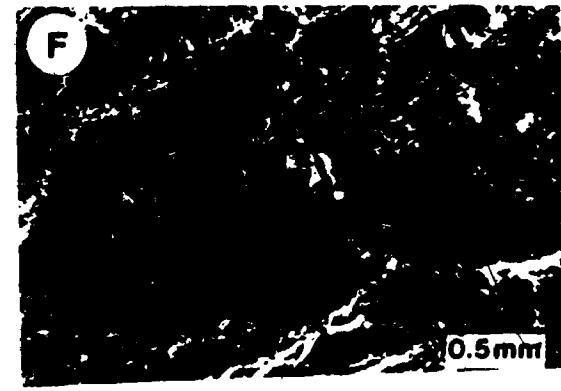
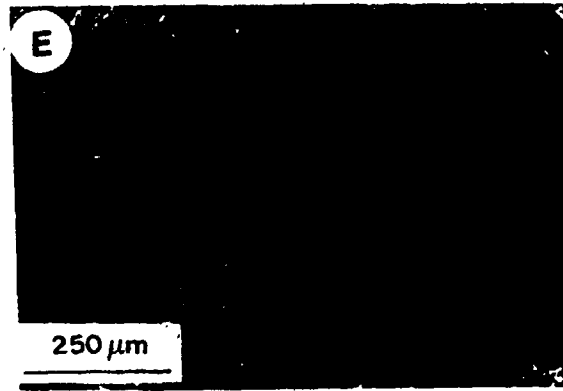
In the more completely serpentized samples, the central portions of grain fragments have been completely pseudomorphed by mesh textured lizardite + brucite + magnetite ± chrysotile (Plates 4A and 4B). If the fluid supply is sufficient, and the temperature is more-or-less constant (Wicks, 1979), the serpentine in the mesh centers tends to become more crystalline and hourglass textures develop (Plate 4C). This was more frequently observed in serpentinites in the immediate vicinity of the diabase dykes at Coto. Serpentine pseudomorphs after pyroxenes are known as bastites (Plate 4E). The amount of chrysotile serpentine appears to increase slightly with the degree of serpentization, but it never appears to constitute more than about 5% of the serpentine minerals in the rock (o.f. Pritchard, 1979); except locally, as veins filling conjugate or en echelon shear cracks (Plate 7; recrystallization textures often evident), or as non-pseudomorphic crack fillings.

A variety of veins showing non-pseudomorphic textures are associated with and grade into the mesh-textured lizardite II + brucite + magnetite ± chrysotile. The veins are composed of both asbestosiform (slip and cross-fibre) and

Plate 4

Serpentine textures (under crossed nicols)

- A. Mesh textured serpentine replacing olivine, as seen in thin section. Well crystallized mesh rims (lighter color), composed of lizardite 1T + brucite + chrysotile, surround finer grained (generally darker colored) mesh centers. Dark lines in mesh rims, which consist of magnetite and fine grained anisotropic serpentine, outline the traces of the original fractures.
- B. Close-up of serpentine mesh cells, showing well crystallized mesh rims enclosing finer grained and randomly oriented serpentine in mesh centers (Mc).
- C. Hourglass textured serpentine (arrow) after olivine, composed of lizardite + brucite + chrysotile. The original fractures, in each textural unit, are visible as fine dark lines.
- D. Ribbon textured serpentine, produced by serpentinization along a network of (usually transgranular) parallel spaced fractures. The dark fractures are filled with magnetite and serpentine.
- E. Close-up of lizardite 1T bastite after orthopyroxene (i.e. a bastite). Serpentine filled fractures, produced by the volume expansion associated with the reaction, are obvious.
- F. Non-pseudomorphic textured serpentine. Yellowish-white areas are "veins" composed of discrete, anhedral grains of brucite, and asbestosiform chrysotile. Black lines are magnetite. When serpentinization rates are moderately rapid, the heat flux generated by hydration may cause the local recrystallization of earlier formed mesh-textured serpentine.



non-asbestiform chrysotile, as well as of lizardite and brucite (Plate 6C).

In the vicinity of the dykes at Coto, however, some of the sections show non-pseudomorphic textures, that have formed by the recrystallization of earlier formed mesh textured serpentine. Serrate-veins of chrysotile + brucite (usually of the Povlen-type, 2mcl or 20rc1; Wicks and Plant, 1979) occur after what appear to be either mesh or hourglass textured serpentine (see above; Plate 4F).

Interlocking and randomly oriented, anhedral grains of lizardite (and antigorite?), and sometimes chlorite-like mineral, are seen scattered throughout the sections. X-ray diffraction patterns of few of the samples, though not a reliable method for identifying the different serpentine minerals, suggest that small amounts of antigorite may be present. The fractures between the grain~~s~~ fragments are filled with a creamy-white mixture of columnar serpentine (probably Povlen-type chrysotile and multi-layer lizardite), brucite, and sometimes asbestiform chrysotile (see Plate 4F).

3.5.3 P-T Conditions of Serpentinization

The successive retrograde mineral assemblages, and hence grades of metamorphism, observed in the diabase dykes and gabbros in the vicinity of the Coto Mine (Table 3.1), are consistent with those determined by Geary and Kay

Table 3.1. The mineralogy and textures of metamorphic minerals in peridotites and associated mafic rocks from the Coto and Acohe Mine Areas, Zamboales Ophiolite Complex, Philippines.

Location	Acohe Mine Area	Coto Mine Area
	Peridotites (dunites, harzburgites)	Peridotites (dunites, harzburgites)
(1) <u>Lizardite</u> + brucite + magnetite + chrysotile	(1) <u>Lizardite</u> + brucite + magnetite + minor chrysotile	(1) <u>Lizardite</u> + brucite + magnetite + minor chrysotile
(a) Mesh (pseudomorphic) and minor veins (fracture fillings)	(a) Mesh, ribbon and hourglass textures (b) Slip and cross-fibre chrysotile veins (c) Minor fracture-filled veins (d) Non-pseudomorphic (recrystallized) "veins" of chrysotile + brucite + chlorite-like mineral	(a) Mesh, ribbon and hourglass textures (b) Slip and cross-fibre chrysotile veins (c) Minor fracture-filled veins (d) - Interlocking, crystals of lizardite after Ca-amphibole (actinolite?) after enstatite and scapolite after plagioclase in chromitite
(1) Gabbro (Both areas)	(2) + remnant Ca-amphibole (actinolite?) after enstatite and scapolite after plagioclase	Dolabase Dykes
(2) Amphibole (actinolite) + epidote chlorite + talc replacing olivine and pyroxene (+ plagioclase)	(2) albite + act iniolite/tremolite + epidote + sphene	
- Veins of actinolite/prehnite	+ muscovite	
(3) Serpentine after actinolite, talc, and chlorite	chlorite	
	- Veins of prehnite, quartz and zeolites	

(1983) for basic rocks in other parts of the Zambales ophiolite complex. The most pervasive metamorphic grade attained was greenschist facies, as defined by the assemblage actinolite + chlorite + albite + epidote, $350 < T < 475^{\circ}\text{C}$ ($\text{P}_{\text{H}_2\text{O}} = \text{P}_{\text{total}} = 2 \text{ Kb}$) (Liou and Ernst, 1979). Although the rare occurrence of blocky, brown or dark green hornblende after pyroxene, and dynamically induced recrystallization textures, indicates that some of the rocks may have been affected by amphibole facies metamorphism. Shrinkage cracks in the diabase dykes are commonly filled with whitish veins of prehnite (\pm quartz, Plate 3B). There is, however, some suggestion that the assemblage prehnite + actinolite + chlorite may represent an equilibrium assemblage; at temperatures $< 380^{\circ}\text{C}$ ($\text{P}_{\text{H}_2\text{O}} = \text{P}_{\text{total}} = 2 \text{ Kb}$). Kuniyoshi and Liou (1976) believe that this may be characteristic of low-pressure metamorphism. The greenschist facies mineral assemblage(s) under conditions where $\text{P}_{\text{fluid}} < \text{P}_{\text{total}}$ and the $a_{\text{H}_2\text{O}} < 1$ - as was certainly the case - is stable at temperatures between approximately 300°C and 425°C (Nitsch, 1971; Liou and Ernst, 1979).

In the diabase dykes, gabbros, and peridotites, serpentine is sometimes seen replacing both actinolite and chlorite (\pm talc) - which had previously replaced olivine and pyroxene. It is not completely clear whether the serpentine phase is antigorite or lizardite, but optically

it appears to be lizardite. In the diabase dykes fractures containing prehnite are cut by "veins" of fibrous, radiating textured zeolites, filling cracks that seem to have formed as a result of brecciation. This evidence, taken as a whole, suggests that the mineral assemblages observed in the surrounding intrusive and basic plutonic rocks can be used to estimate a possible temperature range for serpentinization.

The serpentine assemblage lizardite + brucite + chrysotile (+ magnetite) is stable at temperatures below about 375°C, when water vapor pressures are low (e.g. 1 kb), and where $P_{H_2O} = P_{total}$ (Figure 2.1 curve 1). For conditions where $P_{H_2O} < P_{total} \leq 1$ kb, which is more realistic, if the system is open, 300°C-350°C is probably the upper limit of stability of pseudomorphic serpentine assemblages containing brucite. The development of the transitional assemblage serrate chrysotile + brucite + chlorite-like mineral (\pm very minor antigorite?) plus hour-glass textured serpentine, in the vicinity of the diabase dykes at Coto, indicates that temperatures may have been close to 400°C, but not much higher than this because of the lack of any significant growth of antigorite in association with actinolite + chlorite \pm talc. This is also in accord with the mineral assemblage observed in the more basic rocks.

Concluding then, it appears that serpentinization

began at temperatures near 400°C (depending on P_{fluid} / P_{total} and the $a_{\text{H}_2\text{O}}$). The sharp temperature gradient at the peridotite-dyke interface, as well as a sufficient fluid supply, produced hourglass textured serpentine locally. And then, because of extremely fast reaction rates, heat generated by the serpentization reaction may have caused the local recrystallization of the hourglass textured serpentine (see eq. 1.1 and 1.2). The abundance of mesh textured serpentine clearly indicates, however, that the bulk of the serpentization occurred under retrograde metamorphic conditions (c.f. Wicks and Whittaker, 1977). The close spacing of the dykes (10-20 m) at Coto means that crack permeability was very large (10^{-10} cm^2) and must have led to the rapid and complete serpentization of the surrounding peridotites. The dramatic reduction in permeability which accompanied the precipitation of actinolite, quartz and prehnite in veins implies that most of the serpentization was completed by the time zeolite facies temperatures were reached ($\leftarrow 250^\circ\text{C}$). Finally, as a result of the large volume change (50%) accompanying hydration, tectonic readjustment within the entire block caused the local brecciation of the dykes (c.f. Liou and Ernst, 1979), and at least a temporary increase in permeability. As such water continued to circulate along the dykes and zeolites were able to form.

The same relationships were observed, although much less extensively, at the Acohe Mine. It appears that the large permeability contrast caused by thermal contraction of the diabase dyke swarm at Coto is the main reason for the much more complete serpentinization.

3.6 Strain Fabrics in Serpentinized Peridotites; Including Samples from Newfoundland and Italy

3.6.1. Microstructures in Massive Serpentinized Peridotites

Microstructures, ubiquitous to all serpentinized peridotites, consist of a complex network of intra-, inter-, and transgranular serpentine "filled" fractures that give the rock its distinctive microfabric. This microstructure fabric is seen on all scales (Plate 5).

In partially serpentinized peridotites, the pervasiveness of the microfracturing is clearly visible. Serpentinized peridotites from the Philippines and Newfoundland characteristically show a linear crack density in the range of 50 cracks per centimeter. Such sub-millimeter cracking gives the rock its peculiar shattered and crushed appearance.

In olivine, the microstructure fabric is typically produced by a complex semi-rectangular mosaic of irregularly spaced inter (i.e. grain boundary) and intragranular serpentine "filled" (i.e. mesh rims of lizardite II) micro-fractures (Plates 6A and B; Coleman and Keith, 1971), in

which the trace of the original fracture may be outlined by a thin (central) zone of fine-grained anisotropic serpentine.

In the majority of the serpentized ultramafic rocks studied, however, the microstructure pattern typically consists of, in addition to the "box-like" crack pattern described above, a crosscutting network of transgranular microfractures filled either with complexly banded serpentine (lizardite 1T) and/or more normal mesh textured serpentine fibers (Plates 6D and 6F, respectively). Because the microfractures tend to fork and branch repeatedly, at times even curving somewhat sinuously before tapering into a narrower set of microfractures, the final microstructure pattern is quite complex and heterogeneous. Several generations of microfractures (and hence microfracturing) are recognizable. The microbrecciation, and the displacement of grains observed in some of the transgranular fractures show that a local shear component has been involved in the fracturing process. All of the fabric structures described so far show that fracturing has occurred by a brittle failure mechanism.

Preferential serpentinization along (i.e. perpendicular to) the more closely spaced, sub-parallel network of microfractures (see Plate 6E) tends to produce ribbon textured serpentine (Francis, 1956; Maltman, 1978). Microfractures in the most highly serpentinized peridotites, as

Plate 5

Reaction induced strain fabrics in serpentinized peridotites visible on the hand specimen and the rock scale.

- A. Branching transgranular fracture in partially (60%) serpentinized peridotite (Acohe, Zambales, Philippines). Fracture is filled with complexly banded lizardite \pm brucite. Sample no. H9-82.
- B. Typical fracture distribution in partially serpentinized ultramafic from the Bay of Islands complex, Newfoundland. Fractures contain lizardite (\pm brucite) often banded parallel to contacts. Field sample no. NA-71-16 (collection of W.R. Church).
- C. Typical fracture distribution in totally serpentinized harzburgite (Coto, Philippines). Dark transgranular fractures contain lizardite and magnetite. Sample W-2-11.
- D. Less weathered specimen of the sample above (i.e. C). Magnetite (dark) is clearly visible in fractures.

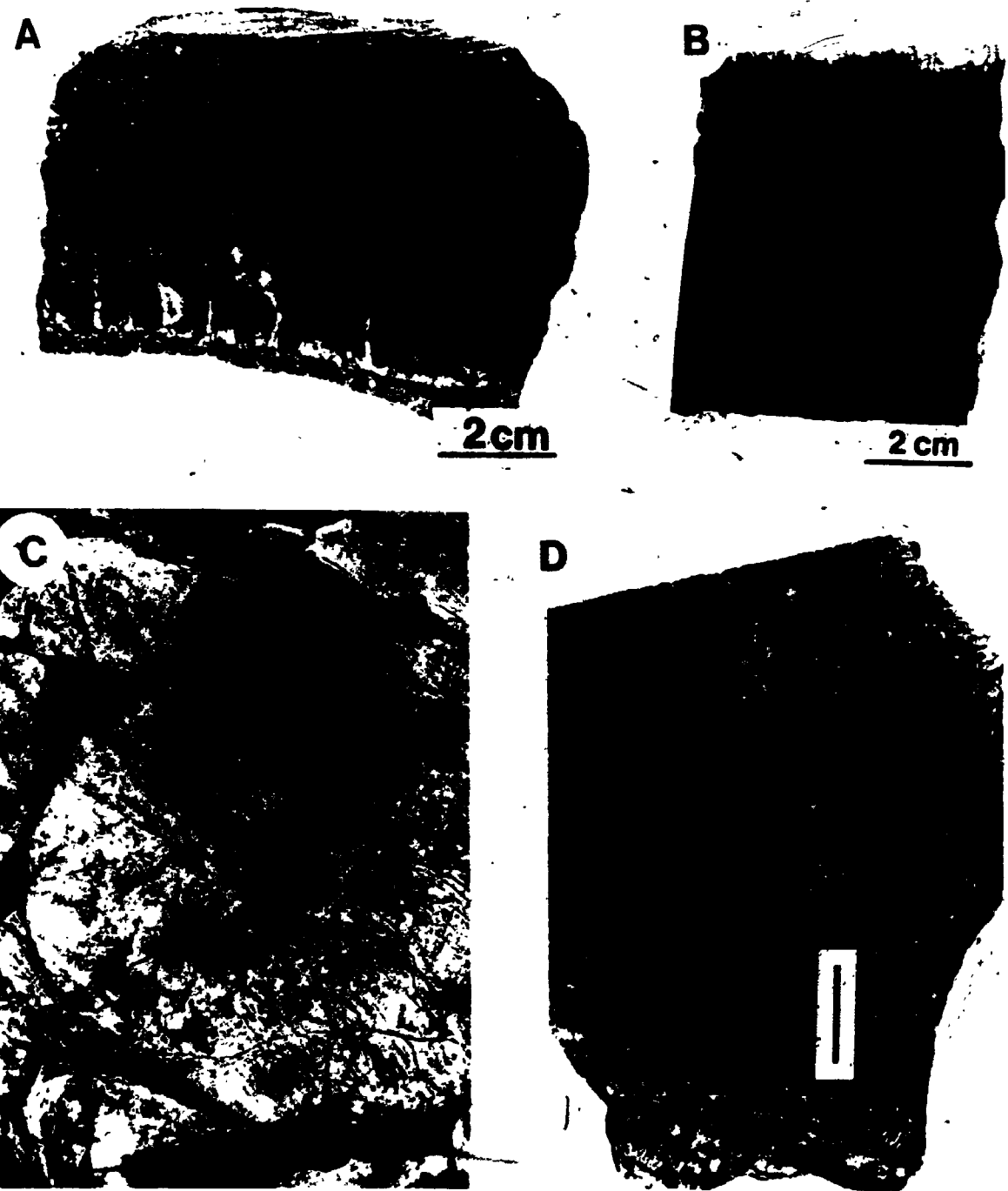


Plate 6

Microscopic strain fabrics in serpentized peridotites.

- A. Typical "cubic" microfractures developed in a single olivine crystal (i.e. the light area) in a dunite (Acohe, Philippines). The fabric structures, composed of mesh veinlets of serpentine (lizardite + brucite) enclosing fragments of remnant olivine (bright white), show no preferred orientation. The dark fracture trace is faintly visible in some mesh rims. Such a fabric is in accord with rather slow reaction rates. Crossed nicols.
- B. Close-up of typical microfracture distribution in a partially altered olivine. Serpentization, as shown by the dark fractures containing lizardite + brucite, is confined to grain boundary and intra-granular cracks. Note how brittely olivine behaves. Crossed nicols. Sample from Acohe Mine, Philippines.
- C. Intensely microfractured olivine, showing cataclastic fabric structures (dark) containing lizardite and brucite. Some of the cracks have been produced by transgranular fracturing. This texture suggests that the reaction induced strain rates may have been locally high. The remnant olivine (ol) fragments are the light colored areas. Crossed nicols. Sample Cevinta (Acohe, Philippines).
- D. Transgranular fracture in partially serpentized harzburgite peridotite, composed of complexly banded serpentine (lizardite) and magnetite (black). The dark serpentine veinlets in the surrounding rock show that microfracturing has occurred on all scales. Lighter areas are unaltered olivine grains. Sample DA-3, Acohe, Philippines. (Similar microstructures have been observed in samples from the Bay of Islands, Newfoundland; c.f. Plate 5A and 5B). Crossed nicols.

Plate 6 (continued)

- E. • Ribbon textured microstructures from E. Liguria, Italy, produced by serpentinization induced swelling in response to a "static" anisotropic stress field. The lizardite fibers, which grow towards the least compressive stress and hence at an oblique angle to the walls of the fracture, are faintly visible. Crossed nicols.
- F. Dark transgranular microfracture (arrow) composed of magnetite (black) and serpentine (greyish-white) in completely serpentinized harzburgite (Cote Mine, Philippines). The fracture is bordered by well-crystallized mesh textured serpentine (lizardite). This type of microstructure is in accord with water diffusion rates that were locally, moderately rapid. Sample DC-5. Crossed nicols.

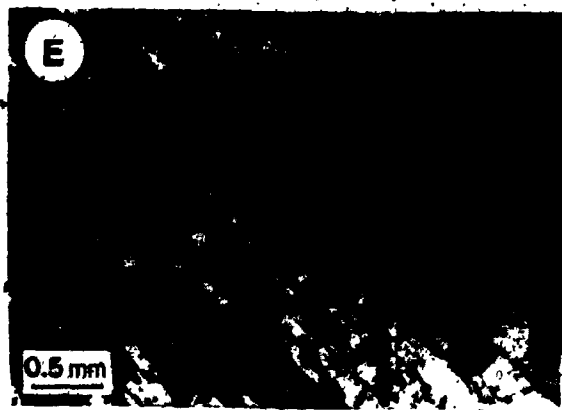
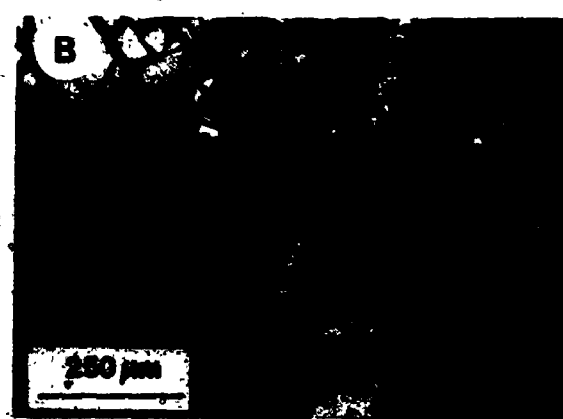
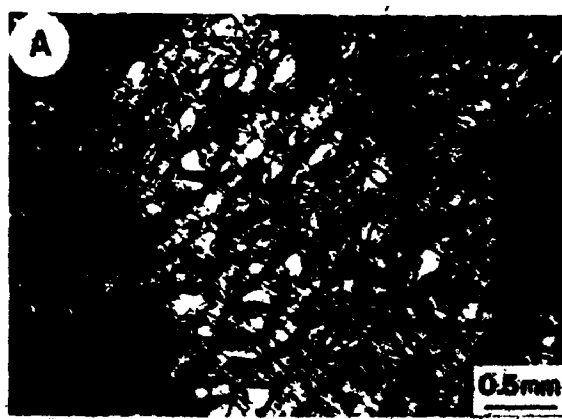
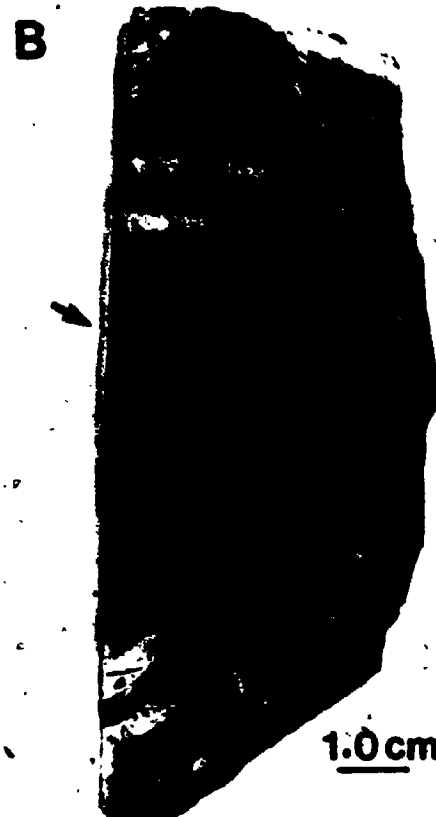


Plate 7

Syntectonic serpentinization fractures.

- A. Conjugate shear fractures cutting massively serpentinized dunite. The fractures are filled with non asbestosform chrysotile serpentine.
- B. Close-up of conjugate shear cracks cutting massive serpentinite (i.e. harzburgite). Fractures consist of cross-fiber chrysotile and magnetite (dark zone indicated by FZ). Yellowish-white (porcellaneous) fracture margins, composed of recrystallized mesh textured serpentine, define the reaction zone. Arrow points to shear surface coated with massive serpentine containing slickensides.
- C. Microscopic shear fractures not easily visible in the specimen above, because of the extensive chrysotile growth, are clearly recognizable in this section. If the tectonically induced strain is large enough, these small scale shear cracks will coalesce to form a major shear fracture (see A and B). The fractures, composed of cross-fiber chrysotile, are outlined in grey while the reaction zone appears blackish. Crossed nicols.
- D. Microscopic view of fracture above, showing the cross-fiber chrysotile asbestos in the fractured zone. The serpentine zone bordering the fracture zone to the left is composed of recrystallized mesh textured serpentine. Crossed nicols.



seen in both thin section (Plate 6) and in handspecimen (Plate 5), are still easily recognizable because of the thick stringers of magnetite that are concentrated in veins composed of well-crystallized mesh (or ribbon) textured lizardite serpentine (Plate 6F). This texture suggests, further, that the penetration of water into the rock was controlled locally by certain major (i.e. transgranular) microstructures that cut across the mesh cell fabric.

Massive blocks of serpentined peridotite are often cut by a conjugate set of "macrofractures" filled with what appears to be massive cross-fiber chrysotile asbestos (+ magnetite + brucite) (Plate 7A and B). When viewed in thin section, the serpentined peridotite is seen to consist of an en echelon array of connected shear fractures, composed of cross-fiber chrysotile (Plates 7C and D). These microfractures crosscut the earlier formed serpentine mesh (pseudomorphic) cells, and are quite commonly bordered by a thin zone composed of recrystallized mesh textured serpentine. In comparison to the micro-fractures described above, these microstructures display a very distinctive morphology (including a strong preferred orientation) and serpentine mineralogy. Often these fractures grade (or are cut by) what appear to be extension or shear joints, whose walls show little evidence of serpentization. (though slickensided serpentine is sometimes observed, coating the fracture walls).

3.6.2 Scanning Electron Micrographs of Serpentine Structures

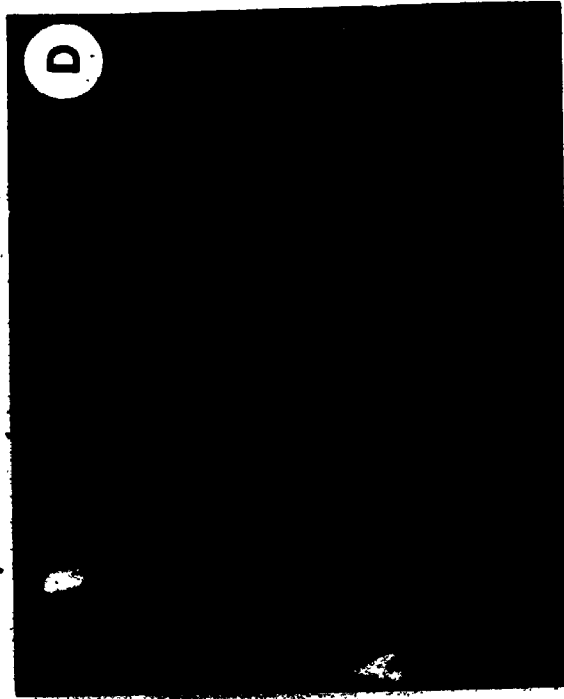
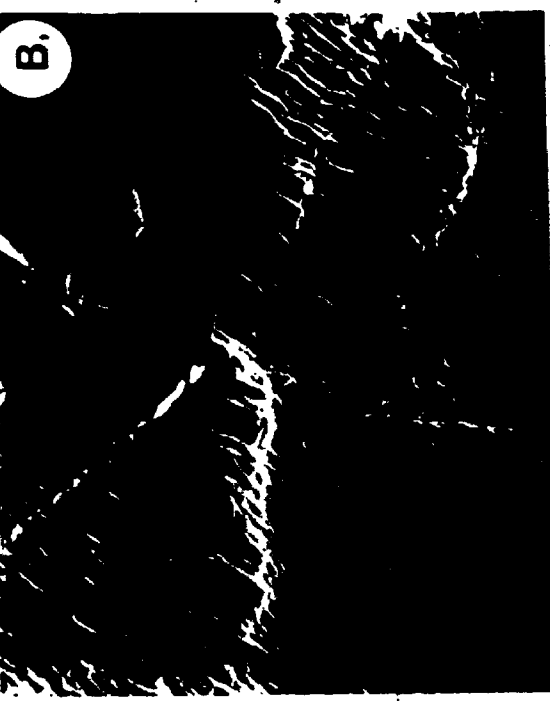
Samples of serpentinized peridotite were ion-etched (Barber, 1970) and then viewed with a scanning electron microscope (made by International Scientific Instruments, model DS-130) in order to study the growth structures of serpentine minerals in fractures. Photomicrographs show crenulated stacks of platy lizardite lying parallel to one another and perpendicular to the fracture walls (Plate 8; c.f. Cressy and Zussman, 1976; Cressy, 1979). In this study, well-crystallized, well-oriented serpentine was observed only in veins and in mesh rims, while the serpentine in mesh centers was found to be generally fine grained and randomly oriented (Plate 9D, c.f. Cressy, 1979). The gaps between the plates in the well-crystallized serpentine are quite variable, ranging from 100-1000 Å (up to 4000 Å). Electron micrographs by Cressy (1979, p. 745) suggest that even poorly-crystalline mesh centers are porous (i.e. gaps on the order of 100 Å). Fine grained material (smectite clay?) is sometimes observed coating plates and filling-in the gaps (see Cressy, 1979; Pritchard, 1979), thus making it impossible to estimate accurately the average size of the pores.

Defects in the serpentine structure must be responsible for the significant volume porosity measured in serpentinites (i.e. 1-3%; this study; Diment, 1964; up to

Plate 8

SEM photomicrographs of microstructures in serpentinized peridotites.

- A. Typical microfracture, containing the platy serpentine mineral lizardite, developed in olivine (ol) (Philippines). Scale bar is 4.33 microns.
- B. Close-up of typical serpentine (lizardite) structures in microfracture above. Defects produced by the buckling of the serpentine plates are obvious. Scale bar is 3.23 microns.
- C. Similar to the photo above, except that some of the lizardite crystals are terminated with needle-like triangular (trigonal) pyramids.
- D. Close-up of crenulated lizardite plates in serpentinite from Liguria, Italy. Voids produced by buckling are again apparent.



6%). In lizardite, because of a stacking disorder and/or compression of the octahedral sheet, the plates tend to be bent around the x and y axes (Rucklidge and Zussman, 1965; Wicks and Whittaker, 1975); while Yada (1967) has found that curling in the chrysotile polymorph produces tubular defects (Plate 1C).

3.6.3 Crack Growth in Rocks in the Presence of Moisture

Stress corrosion cracking is a slow, stable crack growth in the presence of a corrosive environment (e.g. moisture), which catalyses chemical reactions at crack tips, thus reducing the energy required for bond separation (Anderson and Grew, 1977).

Experimental data on corrosive crack growth (e.g. traditionally in studies of alloys, ceramics, glasses) is usually plotted as the logarithm of the stress corrosion crack velocity against the stress intensity. The resulting curve is characterized by three main regions, labelled I, II, and III, after Widerhorn (1967). In regions I through III crack growth is slow ($<10^{-5}$ to 10^{-13} cm/sec) and stable. The rate controlling mechanism in region I is believed to be determined by the reaction rate, whereas in region II crack growth is controlled by the mass transport of reactants (e.g. H_2O) to the crack tip (independent of the stress intensity). In region III, the controlling kinetic factor appears to be a combination of corrosive and

mechanical failure (Evans, 1972). As the critical stress intensity (KIC) is approached, cracks begin to grow unstably (i.e. begin to grow at critical velocities, $>10^{-1}$ cm/sec - 10^5 cm/sec), and the material eventually fails catastrophically (i.e. by Griffith failure).

Slow crack growth in both wet and dry geological materials is characterized by intragranular separation, which gives way to transgranular fractures as the compressive stress is increased (Brace and Bombolakis, 1963; Martin, 1972; Bieniawski, 1967). When the failure strength of the material is reached an increased forking of fractures and shattering of grains is observed, that culminates in the rupture of the specimen. However, silicate materials that are placed under a constant load in the presence of water, will also, given sufficient time, fail (usually violently and internal transgranular cracks may dominate; Scholtz, 1972; Martin, 1972). Such time-dependent deformation (i.e. "creep" failure or strain) is called static fatigue, and is attributed to stress corrosion cracking. According to Martin and Durham (1975), the rate of crack growth (i.e. crack velocity) is proportional to the rate of water transport to the crack tip, which in many silicate reactions may control the rate of the hydration reaction and the strain rate (see also Hillig and Charles, 1965; Wiederhorn, 1972).

3.6.4 Swelling Pressure (Stress) of the Reaction

The swelling pressure of the reaction is the total pressure needed to stop hydration given a definite P_{H_2O} in the environment (i.e. in cracks, see also section 5.1).

This assumes that water is able to flow continuously through defects in the serpentine structure to the reaction interface (see above).

Imagine a block of peridotite under sea floor conditions, covered by 5 km of seawater, and at a crustal depth of 7 km ($P_{solid} = 26000$ bars, hydrostatic ≈ 1200 bars). For the reaction 2 forsterite + 3 $H_2O \rightarrow$ serpentine + 1 brucite, under conditions where $P_{fluid} = P_{total} = 1200$ bars, the pressure that must be applied to stop the reaction (P_s) will be,

$$\Delta G_{reaction} (P = P_{H_2O} = 1200 \text{ bars}) = \int_{1200}^{P_s} \Delta V_{solids} dP, \quad (3.1)$$

where P_s is the swelling pressure. Given the equilibrium vapor pressure data for an open system, it is a simple matter to calculate swelling pressures for any given depth, fluid pressure conditions (Appendix II).

For example, at 1800°C, the equilibrium vapor pressure corrected for the effect of the nonhydrostatic pressure on the solids will be on the order of 2 bars (see Fig. 5.2).

Table 3.2. Typical swelling pressures produced by the reaction 2 forsterite + 3H₂O → 1 serpentine + brucite when Hydrostatic = 1200 bars, and P_{Solid} = P_{H₂O(eq)} + 2600 (bars)¹.

T _{OC}	Swelling pressure (bars)	Effective Swelling ² Pressure (bars)
180.	4323.0	1723.0
200	4980.0	2380.0
240	3894.0	1294.0
260	3206.0	606.0
280	2810.0	210.0
300	2348.0	³

- 1) For a block of peridotite at a depth of 7.0 km, and which is covered by 5 km of seawater. Plithostatic = 2600 bars.
- 2) The effective swelling pressure (P_E) = swelling pressure (P_S) - Load pressure (P_L).
- 3) Above 280°C the load pressure on the solids stops the reaction.

To stop the reaction a load pressure of 4 kb would have to be applied to the system. The effective swelling pressure will simply be the swelling pressure (P_s) - lithostatic pressure (P_{load} (eg. 2600 bars). It is clear that, for these conditions the serpentinization reaction will generate fractures continuously (see Table 3.2). At temperatures above 280°C the vapor pressure for this serpentinization reaction rises steeply, then the lithostatic pressure is sufficiently large to stop the reaction once any open micro-cracks are filled. For serpentine reactions without brucite this upper boundary would be about 100°C higher (i.e. 380°C, $P_{H_2O} < P_{total}$).

3.7 Mineral and Whole Rock Chemistry

Whole rock and selected mineral analyses are presented in Tables IV-1 and IV-2 (Appendix IV), and Tables III-1a to 1e and III-2a to d (Appendix III), respectively.

In the earliest stages of serpentinization, the concentrations of Fe, Mg, and Si in serpentine minerals (and veins) after olivine and pyroxene vary considerably (see Wicks and Plant, 1979). The composition of the serpentine phase (usually lizardite; c.f. Wicks and Plant, 1979; p. 797) is usually intermediate between that of olivine and serpentine. Intermediate compositions were generally found in high relief alteration material - commonly forming mesh rims - which showed anomalous colors

ranging from pale yellow to a reddish-yellow. The pale yellow zones contained higher contents of Si, but less Fe than the reddish-yellow material (see Table III-1d). Pale brown to reddish brown mesh rims and centers, of more normal relief, but showing high Mg and Fe contents, are composed of intermixed lizardite + brucite (which may contain up to 30% FeO) (Page, 1967).

In the more completely serpentinized samples (eg. see Table III-2), serpentine compositions are generally more homogenous, and tend to approach the proportions suggested by the structural formula. At this stage small amounts of Al are found in almost all the serpentines analysed (except in rocks containing little or no pyroxene). Trace amounts of Cr, Ni and Cl were commonly detected in both the partially and more completely serpentinized samples.

Whole rock analyses (see Appendix D) of the serpentinized peridotites, when recalculated to 100%, water free, appear nearly identical to analyses of other dry, alpine-type peridotites. The Mg/Si ratio of pristine alpine peridotites ranges from approximately 1.05, for harzburgites with a 1:1 orthopyroxene to olivine content, to 1.23 as the ideal dunite composition is reached (Coleman, 1971). However, in less depleted oceanic peridotites (and depending on the modal percentage of pyroxene in the rock) Mg/Si ratios may be as low as 0.85 (see Bonatti and Hamlyn, 1981). The majority of the hydrated perido-

tites analysed in this study differ by no more than a few percent from the theoretical value. If their Mg/Si ratio (determined both by point count, Table III-2a and by comparison with whole rock analyses; Table IV-2, samples C-35 and C-31) does deviate from the 'ideal' ratio, it is usually on the low side (i.e. 0.90 to 0.99) and is in samples that contain large chrysotile veins. This seems consistent with most reported analyses from alpine-type ultramafic bodies (Coleman and Kieh, 1971; Aumento and Loubat, 1971; Laurent, 1975).

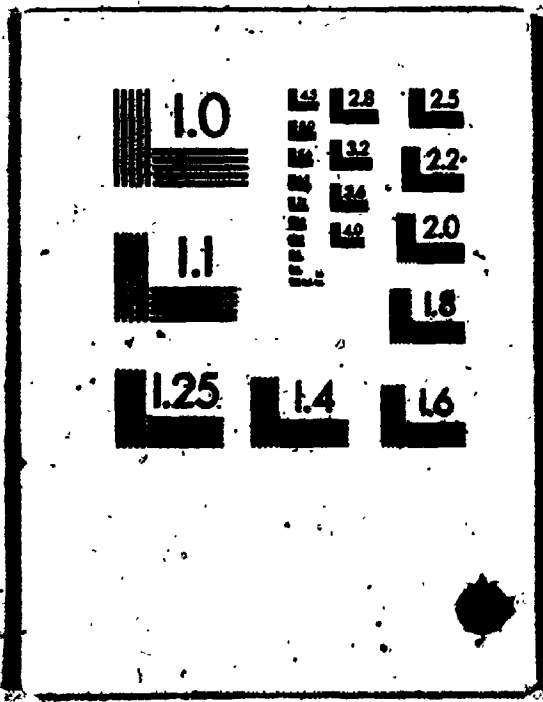
3.7.1. The Mobility of Mg, Si, Ca, Na, Fe and H₂O

The serpentinization of a body of peridotite results, as in any other reaction-transfer system, in the conservation of mass being transported; i.e. the flux of chemical species entering the peridotite = flux leaving the system + rate of accumulation of the quantity in the system due to reaction (e.g. hydration).

High temperature hydrothermal fluids that might react (i.e. enter vs. be produced by serpentinization) with a peridotite in the ocean crust are likely to be highly saline (e.g.) seawater; the major ions in seawater are Cl. $\text{Na}^+ > \text{Mg}^+ > \text{Ca}^+ \approx \text{K}^+$ (Fyfe and Lonsdale, 1980).

Flow and reaction processes in cracked basaltic rocks at elevated temperatures (350°C) tend to enrich the rocks in Na, Mg and possibly Cl (see Edmond et al., 1977), while

9



leaching Si, K, Ca and Fe (see Hajash, 1975; Bischoff and Dickson, 1975; Seyfried et al., 1978; Fyfe and Lonsdale, 1980). The precise behavior of the cations will, of course, vary along the flow path.

Experimental studies have shown further that fluid pH, and the concentrations of Mg, Ca, and Na in solution at temperatures between 150-350°C are determined (primarily) by the relative rates of reactions which remove aluminosilicates from solution and produce H⁺, versus rates of fluid flow (Ellis, 1971; Seyfried and Mottl, 1982). At low water/rock ratios Mg(\pm Ca,Na)-hydroxy-silicate reactions rapidly remove these ions from solution (eg. the greenschist facies assemblage chlorite + albite + epidote + tremolite + sphene \pm quartz), while maintaining a near neutral solution pH. Under fluid dominated conditions (water/rock mass ratio > .50), the solute supply exceeds the reaction rate, so the pH will be on the acidic side, and the concentration of Mg, Ca, and Na in the solution will be relatively high (eg. talc, smectites and chlorites will be favoured). However, at elevated temperatures (>300°C) there is an increased tendency for ions to form complexes of weak acids, hence reducing the pH (Fyfe et al., 1978; Ellis, 1979).

Although the permeability of ocean crust at depths of 5-8 km is unknown at present, it is probably relatively low. Moderately saline fluids ($T < 400^{\circ}\text{C}$) circulating in

cracks near a peridotite body in the ocean crust are likely to be somewhat acidic, contain very low (but saturated) concentrations of Si ($0.16 - 0.77 \text{ m mol/l}$), low-moderate amounts of ($1-50 \text{ m mol/l}$), Ca, K, Fe, and Mg and high ($400-500 \text{ m mol/l}$) concentrations of Na, and Cl (Edmonds et al., 1979; c.f. Ellis, 1979 for analysis of land based geo-thermal systems).

Fluid reacting with a peridotite body at temperatures $<400^\circ\text{C}$ ($P_{\text{H}_2\text{O}} < P_{\text{solid}}$) will rapidly seal all the available cracks; water, however, will have continual access to fresh (i.e. dry) peridotite by moving, probably by diffusion, through defects (pores) produced by the growth structures in the serpentine minerals - especially the lizardite polymorph. The fluid velocity in this channel system must be low, hence the serpentinization reaction will control the chemistry of the water moving into and through a peridotite ($1000^\circ\text{C} < T < 400^\circ\text{C}$).

For a chemical species (including H_2O) to be transported, into and through a peridotite during serpentinization, either a chemical potential gradient must exist, or micro-cracks must open at least temporarily to allow the influx of material by convection and dispersion. In the case of Si, Mg, and Fe - given the composition of a peridotite - any concentration gradient, if present at all, will be small. This suggests that any addition of these ions will be limited to local infiltration metasomatism.

(see Bloch and Hoffman, 1978), which may occur when the swelling pressures of the reaction crack the rock (see Vein Formation below). Because of the defects in the serpentine structure, the interface between a peridotite and a circulating fluid may act not only as a semipermeable membrane, if charged, but by slowing the rate of fluid flow, and raising the pH (see Brennan, 1983) it will filter the solutions entering the rock and increase the rate of those reaction(s) forming chlorite, tremolite, epidote, talc and brucite (etc.). It is clear that Mg, Si, Fe, Na, and Ca will not penetrate far into a peridotite.

What geochemical evidence is there for the loss and gain of components from the system? Hess and Otalora (1964), Page (1967), Miyashiro et al. (1969); Condie and Madison (1969) suggest that with increasing serpentinization small amounts of Ca, (K), Al₂O₃ and alkalis may be leached from the rock. However, as pointed out by Miyashiro et al. (1969), most of this apparent change may reflect the chemical heterogeneity of the peridotites themselves. The loss and/or gain of Mg and Si during active serpentinization, as shown by an extensive comparison of Mg/Si ratio of altered and unaltered peridotites has been, if it occurs at all, extremely small (see Table IV-1 and IV-2); except perhaps during rodingitization (Honnerez and Kirst, 1975; Wares and Martin, 1980), or in serpentinite bodies regionally metamorphosed, where some chemical

(metasomatic) readjustment at contacts is to be expected (cf. Le Chatelier's rule; Fyfe et al., 1978, pp. 166-170), and is observed (Chidester, 1962; Philipps and Hess, 1963; Jahns, 1967; Sanford, 1982). The one other exception appears to be in the case of massively serpentinized peridotites which are cut by veins, usually of cross-fibre chrysotile (eg. C-31, Table IV-2). The low Mg/Si reported in these samples may be the result of the addition of some silica (3-5 wt. %, or 23 g/kg Si); and/or it may simply be due to processes associated with reaction-vein formation (see below; Coquulu and Laurent, 1984) and the growth of stoichiometrically pure chrysotile serpentine.

In conclusion, geochemical and mineralogical evidence suggests that the major chemical change associated with the serpentinization of dry peridotites has been the introduction of H₂O (plus Cl 400-800 ppm, Na ± F, B, Sr, He? (see Hess and Otolora, 1964; Nelson and Thompson, 1971; Aumento and Loubat, 1971); i.e., the

$$\begin{aligned} \text{influx of H}_2\text{O} (\pm \text{ ppm Cl, Na, F, B etc.}) = \\ \text{rate of H}_2\text{O consumption by the hydration} \\ \text{reaction} \end{aligned}$$

Peridotites act as sponges and must swell by 40-50% (depending on mineralogy) if the reaction is complete. Some of the ions (eg. Cl) that enter the peridotite may simply be absorbed on the surfaces of minerals (c.f. Kohls and Rodda, 1967; Poty et al., 1972; Patterson and

Rucklidge, 1977).

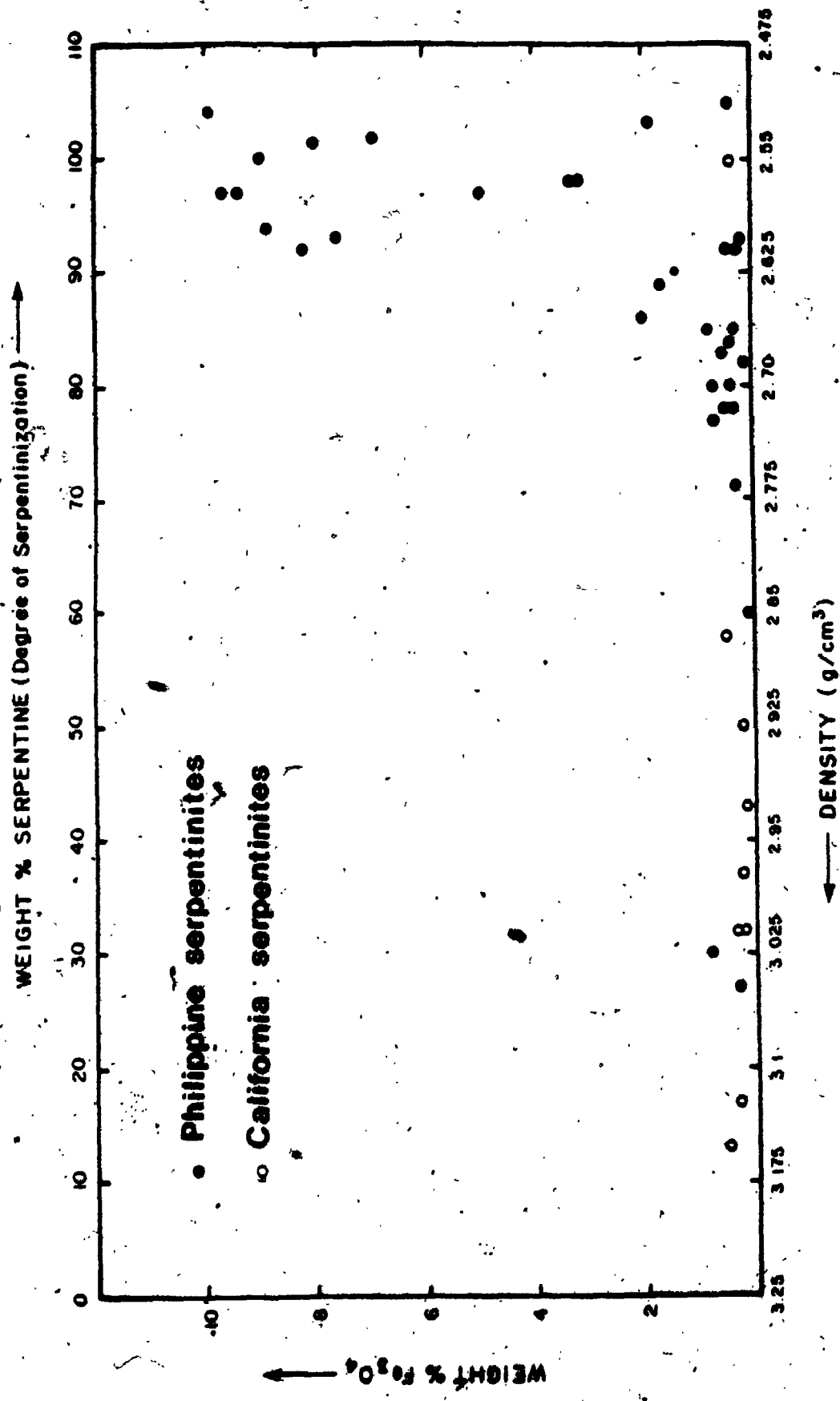
3.7.1 The Oxidation of Fe

Serpentinization is accompanied by an increase in the oxidation ratio $\text{Fe}_2\text{O}_3 \times 100 / (\text{Fe}_2\text{O}_3 + \text{FeO})$ (Coleman and Kieth, 1971; Nelson and Thompson, 1971; Bonatti and Hamlyn, 1981; this study). Coleman and Keith (1976) found that this ratio increases with the degree of serpentinization (total Fe remained constant), although the amount of magnetite (Fe_3O_4) formed was always less than 0.6 wt. % and was not a simple function of the degree of serpentinization. In this study, the amount of magnetite was determined by measuring the magnetic susceptibility against a known standard (Appendix I), and then plotting it against the % of serpentine 'minerals' (serpentine + brucite) found in the sample (Table 3.3). Again no linear correlation with degree of serpentinization was observed.

The results suggest that ferrous iron is gradually expelled from the primary silicate phases (olivine and pyroxene). At very low water/rock ratios, little of the iron is oxidized; instead a great proportion of it may enter the brucite structure as ferrous Fe (Coleman and Kieth, 1971; this study, samples from Acohe). In peridotites that have been serpentinized more rapidly, as shown by the pervasive microstructures (eg. Coto samples or sea-floor serpentinites), water/rock ratios were slightly high-

Figure 3.3

Diagram showing the concentration (in wt. %) of magnetite in serpentized peridotites from the Zambales complex, Philippines, and Burro Mountains, California, plotted as a function of the degree of serpentinization (i.e. density).



er and most of the iron, ferrous and ferric, in the rocks has ended up in the ubiquitous magnetite veins. These observations show that, ultimately, the partial pressure of oxygen (P_{O_2}) in a peridotite being serpentinized is buffered by the large reservoir of ferrous Fe in the rock itself:



(Fyfe et al., 1978). Fig. 3.3 shows, most importantly, that regardless of the degree of serpentinization some or even a large proportion of the Fe may remain as ferrous iron in the hydrated magnesium silicate phases and in brucite; i.e. it takes a great deal of water to oxidize the iron in a rock.

3.8 Vein and Crack Formation During Serpentinization

3.8.1 Reaction induced volume strains

Most of the deformation recorded by the microstructures (i.e. veins) in massively serpentinized peridotites, from this study and others, has occurred by brittle failure (Plates 5 and 6), or by a failure mechanism that is transitional between brittle and ductile failure (c.f. Aumento and Loubat, 1971; Coleman, 1971; Wicks, 1984b).

The alteration observed in ophiolitic gabbros, while pervasive on a large scale, is quite heterogeneous on the

scale of a centimeter or millimeter (see Fox and Stroup, 1981). The alteration fabric follows an 'open' fracture network that is the product of thermal contraction cracking (c.f. Lister, 1974). This contrasts quite strongly with the quasi-regular microstructure fabric seen in all serpentized peridotites, in which the cracking and alteration has occurred pervasively on all scales - centimeter to sub-millimeter. This alteration texture is in accord with a reaction induced cracking process, and not with a simple fluid infiltration and metasomatic model appropriate only for reaction processes in an open micro-crack system!

The expansion stresses associated with the reaction must impose their own deformational fabric on the rock by gradually extending 'old' cracks (Wicks, 1984c) - which are not all interconnected - and by producing new cracks. As serpentization is occurring in rocks which are themselves affected by a regional stress field, the final microstructure fabric will also reflect the tectonic history of the system, and hence is likely to be complex. The quasi-regular, i.e. little preferred orientation - "box-like" microfabric structures observed in almost all massively serpentized peridotites suggests that the regional and the reaction induced stress field during serpentization was fairly isotropic. This microfabric is in agreement with a water diffusion controlled process:

However, on a local - centimeter to millimeter scale, the stress and strain distribution may not be homogeneous. Because of very high local strain rates, the reaction process generates a complex array of cross-cutting fractures, which include complexly banded transgranular microstructures. These fabric structures are consistent with the moderately rapid, local diffusion of water into the peridotite. If the local strain rates are lower, the primary igneous minerals may deform brittly by slow intra- and intergranular crack growth. This generalization is complicated, however, by the apparent tendency of olivine to behave in a more brittle manner than pyroxene.

When the stresses in an ultramafic rock are somewhat inhomogeneous, the reaction strains produce a set of parallel - i.e. well oriented -- and closely spaced micro-fractures. The serpentine "fibers" grow in the direction of the least compressive stress, and hence at oblique angles to the fracture itself. This process forms ribbon textured serpentine (c.f. Wicks, 1984c). The patchy distribution of these microstructures in many serpentinites, for example those found in the Philippines and the Bay of Islands complex, Newfoundland, suggest that it may only be the local stress field which is anisotropic. In the Ligurian serpentinites this texture is more commonly developed, indicating that it is the product of serpentinization in response to a more inhomogeneous regional stress

distribution; for example, as must occur near a transform fault.

The successive generations of cross-cutting microstructures seen in a serpentinized ultramafic rock must, quite clearly, be recognized as having been generated dynamically by the swelling pressures of an on-going chemical reaction: the serpentinization reaction!

The final crack (vein) pattern seen in a serpentinized peridotite massif is a function of both continued "low temperature" (see Chapter 5) serpentinization strains, which weaken the rock by producing microscopic cracks, and tectonically induced - large scale (regional) - elastic strains which, when they reach a critical level, cause the microscopic cracks to extend and then coalesce to form a macroscopic shear fracture (Plate 7; cf. Ramsey, 1980). In such a system, crack and vein formation will be occurring synchronously. However, in contrast to the observed microstructure pattern discussed above, which appears the result of reaction induced volume strains accumulating under conditions where the confining pressure is moderately high, the development of late stage conjugate shear fractures suggest that the confining stress σ_3 was relatively low (i.e. $\sigma_1 - \sigma_3$ is large). The necessary large scale strain and stress conditions can be reasonably generated during the tectonic obduction - and concurrent unloading - of an ophiolite complex. Finally, following

the partial erosion of the overlying carapace of volcanic and gabbroic rocks, residual expansion stresses rupture the rock and form the ubiquitous, largely unserpentinized conjugate joint set.

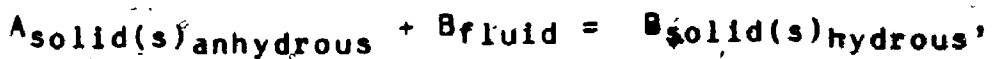
3.8.2 Serpentine veins

Most 'veins' (i.e. mesh rims) seen in serpentинized peridotites are not the result of true fracture filling, but are produced by the inward diffusion of water into a pyroxene or olivine crystal, and the subsequent growth of the serpentine vein - or reaction zone - into the crack. This crack accommodates the volume change of the reaction by expanding (see Harker, 1935; Fig. 1.1). Single crystals are repeatedly cracked into a mosaic of smaller grain fragments, perhaps initially by the stresses generated by the brucite reaction; i.e.



At some critical size the hydration of the remaining sub-millimeter fragment is able to proceed at constant volume, by the relatively strain free reorganization of the primary crystal structure (c.f. Wicks and Whittaker, 1977). On a local scale Si, Al, Cr, Ni, Fe, Mn (etc.) are mobile (see Wicks and Plant, 1979; Brennan, 1983); yet, in terms of the entire system it appears negligible (see above) and therefore in regards to mass transfer only the chemical potential of H_2O , $\mu_{\text{H}_2\text{O}}$, need be considered (see Thompson,

1959). Heterogenous reactions of the type (Pannetier and Souchay, 1967),



(3.4)

where V_2 products > V_1 reactants may adequately describe reaction processes in peridotites that are being serpentinized. Such reactions, as the alteration texture suggests, are generally diffusion controlled after a certain period of time (c.f. Martin and Fye, 1970).

The small degree of displacement seen in the dykes (etc.) in the Zambales ophiolite suggests that most of the volume increase in large, totally serpentinized bodies (e.g. Coto, this study) is accommodated by the upward movement of large blocks along widely spaced (conjugate) shear zones (c.f. Coleman and Keith, 1971). This adjustment may give the appearance of having been produced by diapiric intrusion.

3.9 Conclusions

(1) The major chemical change accompanying serpentinization is the introduction of water.

(2) Retrograde hydration of the Philippine peridotites produced the serpentine assemblage lizardite-1T (+ minor chrysotile) + brucite + magnetite. Volume changes, given

the minimal gain of material and mineralogy, were on the order of 40-50% in the most highly serpentinized samples.

(3) Calculated swelling pressures for the serpentine reaction are on the order of a few thousand bars at typical serpentinization temperatures. The morphological characteristics and the pervasiveness of the fracture network (now serpentine veins) is in accord with both the stable and critical growth of cracks; as a result of reaction induced strains. Thus if defects produced by the buckling of plates of lizardite result in a "structure" that is permeable to water, hydration rates and local volume strains will depend only on the rate of water transport through a serpentine reaction layer. The availability of water and thus the overall macro-permeability of the system will determine both the extent and violence of serpentinization (e.g. Coto area), but clearly given a sufficient fluid supply fracturing will be a continuous process.

(4) Chemical, mineralogical, and textural evidence suggests that the local hydration of olivine, and to a lesser extent pyroxene, proceeds via a complex heterogenous (brittle) reaction which results in the rapid precipitation of brucite (i.e. $MgO + H_2O \rightarrow Mg(OH)_2$). This reaction may be very important in the initial stages of new crack formation.

(5) Locally formed cracks (i.e. veins) act as sinks for the excess Mg, Si, and Fe (Al, Ca, etc.) released

during the hydration of olivine and pyroxene and accommodate most of the volume expansion. As an example consider the effect of 100% serpentinization of a block of peridotite 1 m³. If the resulting volume expansion is 40%, the block must increase in size by 11.9 cm on a side (i.e. 11.9 cm x 11.9 cm x 11.9 cm). If the linear crack density is 50 cracks/cm (observed in Philippine serpentinites) the block contains 5595 cracks/cm; therefore each crack (vein) had to expand by a mere 2/100 mm. This means that 50% of the volume of the rock is occupied by cracks which are now veins. Clearly, this sort of volume expansion will be barely visible in the scale of a thin section!

(6) Until serpentinization is complete, the swelling pressures of the reaction will generate fractures in peridotites by cataclastic flow. However, once the reaction is finished blocks of serpentinites may begin, at high confining pressure (i.e. >2 kb), to deform ductilly (Raleigh and Patterson, 1965). As the volume strains produced by the serpentinization reaction must cause the large scale expansion of the rock this process must cause some sort of mechanical displacement in the surrounding rocks. Shear zones (e.g. block faults in Cyprus; W.S. Fyfe, personal communication), common in all serpentinized ultramafic complexes, provide visible evidence for the development of such stresses and strains, and the consequent upward (diapiric) movement of overlying blocks of rocks.

CHAPTER 4

SOME MEASUREMENTS OF WATER AND SALT TRANSFER THROUGH SERPENTINIZED PERIDOTITES

4.1 Purpose of Study

Solid state diffusion processes will generally only affect fairly small thicknesses of bulk rock at elevated pressures and temperatures (ie. a few tens of meters at 300°C; Fyfe et al., 1978; Nigrini, 1969). This must also be true for perfect solids. But when a medium is cracked, or porous, or if defects occur in the crystalline structure of solids, fluid diffusion may be more rapid. In terms of water penetration into serpentinized peridotites, defects resulting from plate buckling in the serpentine mineral lizardite (Plates 8A to D) imply that the rate of water transport may be similar to that observed in other porous materials (eg. zeolites and compacted clays), in which the diffusion coefficient of water is close (i.e. 1 or 2 orders of magnitude less) to its free solution value of $\approx 10^{-5} \text{ cm}^2$.

sec⁻¹ (at 25°C). As all observations of serpentinites show ubiquitous microscale cracking direct measurement of the diffusion permeability must be made.

4.2 Transfer Processes in Open Systems

Consider a system containing two reservoirs A and B, separated by a membrane (i.e. membrane, porous clay layer, etc.) (see Denbigh, 1981, p. 64). Given that the chemical potential (μ_i) of B is less than A, energy and matter will flow from A to B in an attempt to eliminate the gradient. If the reservoirs A and B are infinitely large (i.e. are open ended) there will be an irreversible and continuous transfer of material within the system, as well as between the system and the surroundings. In such a system the stationary state will not be characterized by thermodynamic equilibrium (eq. closed system), but instead a time invariant condition called the steady-state, in which the concentration(s), c, (or activity, a) of the material that is being transferred is constant with time, t; ie.

$$\frac{dc}{dt} = 0 \quad (4.1)$$

At the steady state, material (mass or volume) flows are constant (see Lerman, 1979, p. 73-5). The flux is a measure of the rate of transfer of material (or energy) between any two reservoirs, and from one chemical or

physical state to another (Lerman, 1979). A more general definition of the flux is,

$$\text{flux}_{\text{system}} = \text{proportionality constant} \times \text{driving force}$$
$$[\text{ML}^{-2} \text{t}^{-1}] \text{ or } [\text{Mt}^{-1}] \quad (4.2)$$

where M is a measure of the quantity of material transferred, L is a linear dimension, and t is the time.

However, in flow systems involving a reaction in which the steady state concentration gradient is changing with time, kinetic information (ie, rate constants) will be needed to describe the rate of approach to the steady state (see Stumm and Morgan, 1981 for a discussion). If the concentration gradient changes slowly (or linearly, as is the case with many reactions) with time, the system may be said to be quasi-stationary (Jost, 1960, p. 8-11). In other systems in which the change in the flux is strongly dependent on time, as well as distance, transient state models (ie. partial differential equations) are needed to completely describe the system (see Lerman, 1979, Chapter 8).

4.2.1 Transport Equations for Diffusive Flow

Diffusion is a process which results in the elimination of concentration gradients (ie. chemical potential gradients) within a single system as a result of the

dispersal and migration of a material(s) by random molecule-molecule interaction (Jost, 1960; Lerman, 1979). Ficks first law, empirically derived by Adolf Fick in 1855, states that the diffusive flux of a species, i , in a plane perpendicular to the direction of mass transfer, is proportional to the concentration gradient of i , ie.

$$J_i = -D_i \frac{dc}{dx} \quad (4.3)$$

where J_i is the quantity of material passing through a reference plane, x , per unit time ($\text{g cm}^{-2} \text{ sec}^{-1}$), D_i is the diffusion coefficient with dimensions of $\text{cm}^2 \text{ sec}^{-1}$, and dc/dx is the concentration gradient (g cm^{-4}) in a direction perpendicular to the reference plane. The negative sign is necessary because the mass transport is in the direction of decreasing concentration. A more general (ie. fundamental) form of the diffusion equation for non-ideal solutions, given by Jost (1960, p. 240-1), relates the flux J (moles $\text{cm}^{-2} \text{ sec}^{-1}$) of a material to its chemical potential gradient ($d \mu / dx$); ie.

$$J_i = -c \frac{D}{RT} \frac{d\mu}{dx} \quad (4.4)$$

where c is the average concentration (moles cm^{-3}) of the species, i , in the diffusion current, D is the diffusion coefficient ($\text{cm}^2 \text{ sec}^{-1}$), R is the gas constant (1.987 x

10^{-3} kcal deg $^{-1}$ mol $^{-1}$), and T is the temperature in degrees Kelvin. Note that D/RT is equal to u, the mobility of the diffusing particle per unit force (see Jost, 1960, p. 139). D in Fick's law above (eq. 4.3) is thus equivalent to RTu.

In general, the diffusion coefficient (or diffusivity), indicates the ability of a material (eg. water, salt ion) to move through a particular medium. This definition is applicable to all transport coefficients (see Bear, 1972, eq. the conductivity coefficient in Darcy's or Fourier's law). The diffusion coefficient, D_f , depends on the nature (i.e. physical, electrical properties) of the diffusing material as well as the medium itself (Lerman, 1979). For diffusion through a porous medium, the porous system diffusivity, D_p , is a strong function of porosity (i.e. viscosity, pore size) and the tortuosity of the channel system (Li and Gregory, 1974; Lerman, 1979, p. 86-93). Because of the effect of such parameters, porous system diffusivities will be lower in comparison to their respective self-diffusion values in bulk solution (which are on the order of 10^{-5} cm 2 sec $^{-1}$; Robinson and Stokes, 1970; Li and Gregory, 1974). The diffusion coefficient of water in a (or through) porous material measures in effect the permeability of the medium - that is the capacity of a porous material for transmitting a fluid.

For all practical purposes the diffusivity can be

considered to be invariant with changes in concentration (i.e. activity, see Jost, 1960, p. 241; Kemper and Shaik, 1966) along the path of diffusion. Hence diffusion coefficients of ions or water molecules determined using Ficks first law, when the bulk flux and concentration gradient of the material are known, should not vary appreciably from self-diffusion coefficients obtained using a tracer isotope of the species that is diffusing.

The diffusion coefficient is, however, strongly dependent on temperature as is shown by an equation analogous to the Arrhenius relationship; i.e.

$$D = D_0 \exp(-E/RT) \text{ (cm}^2 \text{ sec}^{-1}) \quad (4.5)$$

where E is the activation energy for diffusion (kcal mol⁻¹), T is the temperature in degrees Kelvin, R is the gas constant, and D₀ is a constant coefficient, with units of cm² sec⁻¹. Plots of experimentally determined values of ln D versus the reciprocal of temperature, 1/T, generally give a straight line with a slope of -E/R, and a y intercept D₀ at 1/T = 0. When the slope (E/R) is known, the value of the diffusion coefficient D_{T₂} at some temperature T₂ can be estimated from the equation,

$$\ln \frac{D_{T_2}}{D_{T_1}} = \frac{E}{R} \left(\frac{1}{T_1} - \frac{1}{T_2} \right) \quad (4.6)$$

(Lerman, 1979, p. 116) where D_{T_1} is an experimentally known diffusion coefficient at some temperature T_1 . This of course may not be completely valid in porous media in which the transfer of water is quasiviscous (i.e. it will be more strongly a function of the change in viscosity with temperature and pressure; see Lerman, 1979, pp. 86-87).

The quotients $\frac{D}{dx}$ (equation 4.3) or $\frac{D}{RT} \frac{d\mu}{dx}$ (equation 4.4) have the dimensions of a velocity (cm sec^{-1}), and thus represents the velocity of diffusional transport of a material across a layer of thickness x (Lerman, 1979, p. 59). One can thus predict on dimensional grounds - and this is born out by all formal solutions (see Jost, 1960; Crank, 1956) - that a typical diffusion distance, (or "penetration distance"), x , will be given by the equation,

$$x = (Dt)^{1/2} \text{ (cm)} \quad (4.7)$$

If this equation is rewritten as $t = x^2/D$, one can predict the transfer times, t (i.e. the time needed to reach a quasi-steady state; see equation in Wadden and Katsube, 1982) of a material given a diffusivity and a distance (x). A similar equation can be written for heat conduction, thus allowing one to estimate the quasi-steady state cooling (or heating) times of a body of rock at a specific depth (see Verhoogen et al., 1970).

4.2.2 Osmotic Flow

Consider a concentration cell composed of two compartments I and II, one of which (I) contains a pure solvent (eg. water), A, and the other (II) a solution of a solute (eg. salt), B, in the same solvent, A. The two compartments are separated by a membrane that is permeable only to the solvent (A) water (i.e. the membrane is semi-permeable). Because the activity of the water is lower in the solution, water will tend to flow through the slice and into the solution compartment. This is the phenomenon of osmotic flow or osmosis (Lorrimer, 1979).

The osmotic flow of water causes the fluid level in compartment II to rise slowly with time, with the result that a pressure difference develops across the membrane. When this hydrostatic pressure reaches its maximum value, called the osmotic pressure, π , the flow stops. The osmotic pressure is thus the pressure that must be applied (eg. by a piston) to a solution, separated by a semi-permeable membrane, to stop the solvent flow and make the chemical potential of the solvent in the solution equal to that of the pure solvent, when both are at the same temperature (Thain, 1967). Osmotic equilibrium is defined as (see Lewis et al., 1961),

$$\Delta P = \pi = -\frac{RT}{V} \ln \frac{a_{H_2O}}{a_{H_2O^*}} \quad (4.8)$$

where π is the osmotic pressure (bars), P_{II} is pressure applied to the solvent (H_2O) in the solution, P_I is the pressure (usually atmospheric) on the solvent in the pure solvent phase, R is the gas constant ($83.1421 \text{ cm}^3 \text{ bar mole}^{-1}(\text{K})^{-1}$), T is the temperature (degrees Kelvin), v is the partial molal volume of the pure solvent (liter mole $^{-1}$), a_{H_2O} and $a_{H_2O}^*$ are the activities (moles liter $^{-1}$) of water in the solution and pure solvent phase, respectively (see Appendix II).

The flux of water by osmosis is similar to other mass transfer processes in that the driving force is a free energy gradient. If the concentrations of the solutions in the two compartments remain constant with time the system can be considered to be open, and the flux of water (and solutes if the membrane is not perfectly semi-permeable, but "leaky") can be described by an appropriate transfer equation.

Although differences in chemical potential may be regarded as the origin for all diffusion processes, it is not equally true, as suggested by Denbigh (1981, pp. 262-4), that diffusion is always responsible for an osmotic flow. This has been shown by a number of workers (cf. Kemper and Evans, 1963; Mokady and Low, 1968). The results suggest that in some porous materials (eg. clay systems), water may be transported by viscous or quasi-viscous bulk (i.e. "convective") flow. In such cases the transport

(i.e. not the self-diffusion) coefficient D of water obtained experimentally using Fick's first law (see study by Mokady and Low, 1968, in which D_{H_2O} is on the order of $10^{-3} \text{ cm}^2 \text{ sec}^{-1}$) may represent combined effect of both convection and diffusion; and so appear much larger than its self-diffusion coefficient for that temperature. It is thus not surprising that fluid transport through some membranes may obey Darcy's law (see Bear, 1972; Freeze and Cherry, 1979). This equation describes the viscous (i.e. the fluid behaves as a Newtonian liquid) transport of a fluid in response to a hydraulic gradient:

$$Q/A = -\frac{k}{\eta} \frac{\Delta P}{L} \quad (\text{cm}^3 \text{ cm}^{-2} \text{ sec}^{-1}) \quad (4.9)$$

where Q/A is the volume of water flowing per unit area per unit time ($\text{cm}^3 \text{ cm}^{-2} \text{ sec}^{-1}$), k is the permeability (darcy or cm^2), P is the pressure (in bars if k is in darcy units, in dynes cm^{-2} if k has dimensions of cm^2), η is the viscosity (centipoise or dynes sec cm^{-2} respectively), and L is the length of the porous column (cm). The permeability k depends on the grain size, packing and porosity of the medium (Lerman, 1979); it measures, as does the porous system diffusion coefficient D, the (relative) resistance felt by the material as it is transported through a porous medium (see Bear, 1972).

Whether water moves viscously or not in response to a

chemical potential or hydraulic gradient will depend strongly on the average pore size in the medium being studied (eg. clay, cracked rock, etc.), and thus must be experimentally verified in each case (see Scheidegger, 1960; Swartzendruber, 1961).

4.3 Experimental Methods

4.3.1 Samples

The samples of partially and totally serpentinized peridotites used in the experiments were carefully chosen to be free of macrofractures by collecting boulder-size samples along vigorously flowing streams in the Zambales Ultramafic Complex, Philippines. A few additional samples were provided by W.S. Fife from the Ligurian Ophiolite in Italy (Appendix VIID) and, by W.R. Church from the Bay of Islands Ophiolite in Newfoundland (see Appendix VII).

Three "types" of samples were used in the diffusion experiments: 1. partially serpentinized peridotites (a) containing fracture-filled veins visible in hand specimen (Plate 5B and 6D), and those showing (b) dominately pseudomorphic textures (Plate 6A); 2. totally serpentinized peridotites that are extensively veined; as is clearly shown by the stringers of magnetite (see Plates 4A to D and 6F).

4.3.2 The Diffusion Cell

Steady state diffusion coefficients can be determined by studying the mass transport from one solution to another, separated by a thin slice of the solid.

The experimental apparatus consisted of two cylindrical glass cells, both open at one end (Figure 4.1). Glass capillary tubes with an internal diameter of 2 mm were attached close to the closed ends, and shorter, larger diameter (1.0×6 mm) filling tubes were attached near the open ends. Semi-circular slices, 3 to 5 mm thick, were cut from the stream boulders with a water or kerosene lubricated saw, and then polished by hand until the sample faces were parallel. Next, the samples were placed in an ultrasonic vibrator in a beaker of methyl-alcohol or acetone, in order to remove any fine rock particles or kerosene that might have clogged the pore system. Finally, the slices were oven dried in order to evaporate any remaining oil.

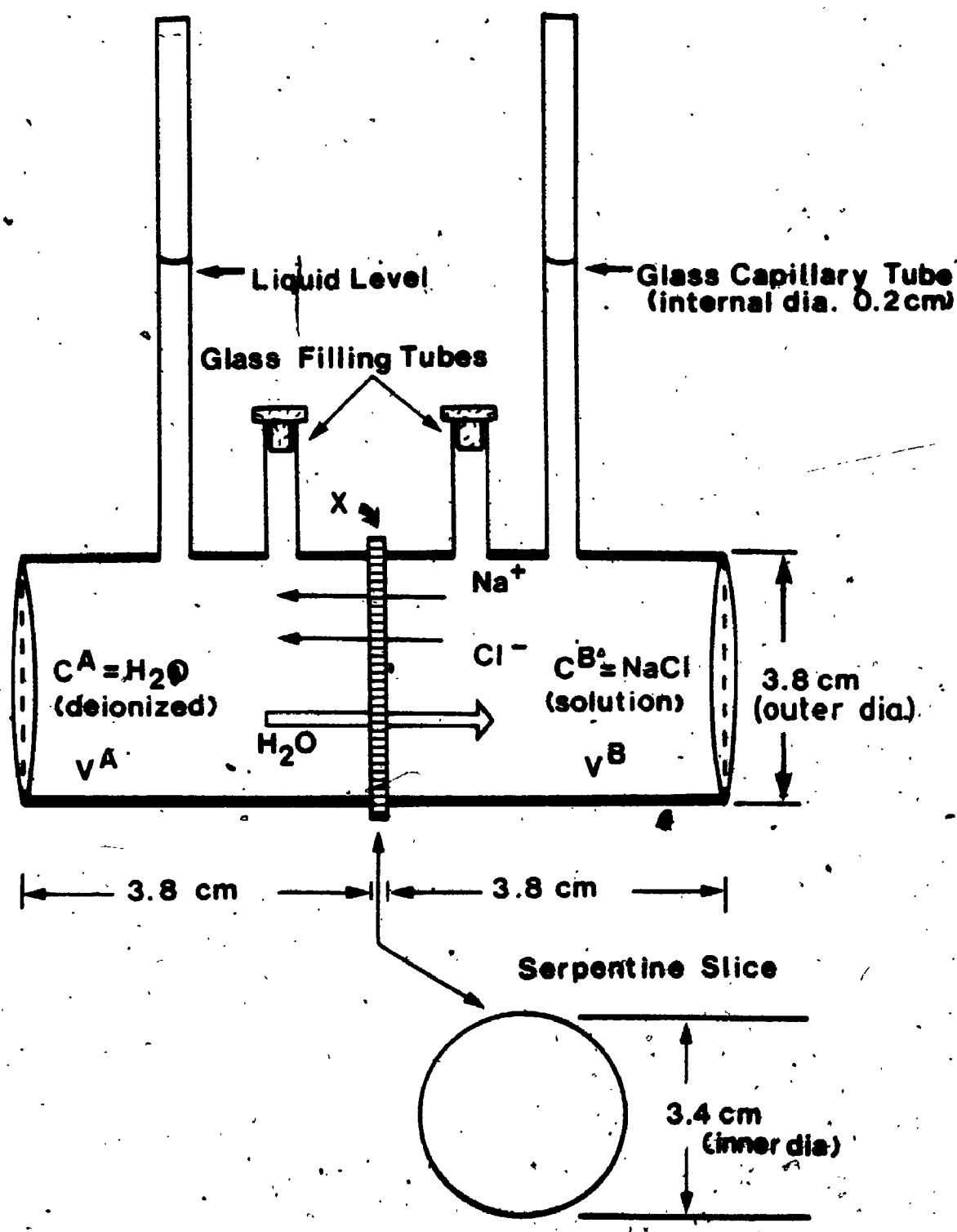
The samples were all carefully studied under a binocular microscope to see if they contained any open microcracks.

Tables V-1 and 2 (Appendix V) summarizes the various physical and mineralogical characteristics of the samples.

Cementing the slices to the glass cells proved to be the most difficult and time consuming aspect of the experiments. In the initial runs fast-curing epoxy (Lepage) was employed as the bonding agent, but with time the epoxy tended to become plastic and to peel away from one of the

Figure 4.1

Schematic diagram of the diffusion (concentration) cell used to study the transport of salt and water across thin slices of serpentinized peridotite.



surfaces. For the later runs a fast-curing anaerobic adhesive (Speed Bonder #324) manufactured by the Loctite Corp. was used. Although the improved heat, water and impact resistance (as well as the gap filling ability) of adhesives are remarkable, the bond strength of the seal between the glass and the rock specimen was not substantially improved (ie. and at a much higher cost). To fully prevent any lateral migration of fluids through the samples or between cracks at the glass-rock interface, and to provide some additional (albeit elastic) strength to hold the cell apparatus together, copious amounts of silicone rubber sealant (Dow Corning) were applied to the outer surfaces. This held the cylinders tightly together for experimental runs lasting a few months.

After the serpentine slices were cemented between the glass cells, one of the compartments was filled with de-ionized water, and the other with a NaCl solution ranging from 2 to 6 molal. Fluid levels were equalized and then the filling tube was sealed. The cells were then placed in a circulating water bath (Heto, model W3241-3) at a constant ($\pm 0.1^{\circ}\text{C}$) temperature.

4.3.3 Measurement of Sodium Chloride and Water Fluxes

Quasi-steady state fluxes of sodium chloride and water were determined for 18 serpentized peridotite slices by measuring the rate of change in the concentrations of the

diffusing species in the external solutions in cells A and B, respectively.

The diffusion of sodium chloride through the serpentine slices resulted in an increase in the salt concentration in compartment A (Figure 4.1). In order to maintain electrical neutrality in the system, the quantity (grams, moles) of cations (eg. Cl⁻ ions) and anions (eg. Na⁺ ions) leaving the membrane must be equal. Therefore, the flux of only one ion (in this case chloride) need be measured to determine the total sodium chloride flux, i.e. $J_{Na^+} = J_{Cl^-} = J_{NaCl}$. These measurements were made on the average of every 15 days with an ion-sensitive electrode (Orion). The cell was then refilled with de-ionized water if the sample was to be in another experimental run. The equation for the total mass transfer of chloride through the serpentine slice in a time t, is

$$J_{Cl^-} = \frac{(C_{t2} - C_{t1})}{A \cdot t} \quad (4.10)$$

where J_{Cl^-} is the net flux of chloride ions (moles cm⁻² sec⁻¹)

$C(B)$ is the measured chloride concentration in compartment B (moles liter⁻¹)

V is the volume of solution in each cell (35.38)

A is the area of the serpentine disc (9.0746)

t is the time (seconds)

At the same time that salt is diffusing from B → A, water is flowing from A → B by osmosis. This volume transfer of water causes a rise in the fluid level in the capillary tube on side B; and during the steady state a corresponding decrease in the level of pure water in the capillary tube in cell A. The flow of water through the solid slices was measured by recording daily the rate of displacement of the meniscus in a calibrated capillary tube attached to cell B, and then calculating the flux (J_{H_2O}) using the equation,

$$J_{H_2O} = \frac{\frac{1}{v} \Delta V}{A \times t} = \frac{(πR^2 h) \cdot 1/18 \text{ moles g}^{-1}}{A \times t} \times C_w \quad (4.11)$$

where J_{H_2O} is water flux (moles $\text{cm}^{-2} \text{ sec}^{-1}$)

$πR^2$ is the internal area of the capillary tubes ($3.14 \times 10^{-1} \text{ cm}^2$)

h is change in fluid level in cell B (cm)

$ΔV$ is the change in the volume of water (cm^3)

A_s is the area of the serpentine discs (9.0746 cm^2)

t is the time (seconds)

C_w is the water concentration on the solution side (g/cm^3)

v is the partial molal volume of water ($\text{cm}^3 \text{ mole}^{-1}$)

Because the concentration of the salt solution in cell B changes negligibly (i.e. in cell A), what we are really measuring is the rise of the salt solution; so it is necessary to multiply this rise by the water concentration of the solution C_w (g l^{-1}) in order to obtain the actual water flux (see Appendix II).

It is assumed, given the time span of each experimental run, that the hydrostatic pressure that builds up across the slices as a result of the transport of water isn't significant, and doesn't affect the quasi-steady state gradients that develop. In order to insure that the gradients remained roughly constant with time - and were controlled by the physical properties of the membrane - the solution in compartment A was replaced frequently (i.e. generally when salt measurements were made).

4.3.4 Determination of the Diffusion Coefficients of Sodium Chloride and Water

The quasi-steady state porous system diffusion coefficients for sodium chloride and water can be obtained, if their respective fluxes are known, from Fick's first law (eq. 4.3); i.e.

$$J_1 = -D_F \frac{dC}{dx}$$

Therefore for sodium chloride this becomes,

$$D_{\text{NaCl}} = \frac{J_{\text{NaCl}} \cdot x}{(C^A - C^B)} \quad (4.12)$$

and for water,

$$D_{\text{H}_2\text{O}} = \frac{J_{\text{H}_2\text{O}} \cdot x}{(C^B - C^A)} \quad (4.13)$$

where D_i is the diffusion coefficient of water or salt
 $(\text{cm}^2 \text{ sec}^{-1})$

J_i is the flux (moles $\text{cm}^{-2} \text{ sec}^{-1}$)

x is the thickness of the serpentine disc (cm)

4.4 The Results of the Diffusion Experiments

4.4.1 Fluxes of Water and Sodium Chloride in Response to a 6 Molal Sodium Chloride Concentration Difference at 34°C¹

The experimentally measured rates of water flow in moles per day through each of the serpentine slices studied are shown graphically in Figures VII-1A to J (Appendix VII; salt was not plotted). The total volume of water accumu-

¹Results of the experiments at 25°C and 40°C, and different salt concentrations (2, 3, and 4 molal NaCl) are not included or discussed in the main text (see Appendix VI).

Table 4.1. Observed fluxes of water and sodium chloride through totally serpentinized peridotites at 34°C in response to a 6 molal NaCl concentration difference.

Sample and Run No.	Time ¹ days	Average H ₂ O Flux (J) moles cm ⁻² day ⁻¹ $\times 10^{-6}$	Time ² days	Average NaCl Flux (J) moles cm ⁻² day ⁻¹ $\times 10^{-6}$	$\frac{J_{H_2O}}{J_{NaCl}}$
DC-511 (45)		102.2			
	2 (7)	137.9			62.96
	4 (15)	108.7	(77)	2.19	49.52
DC-521 (49)		37.82	(50)	2.8	13.5
DC-532 (39)		99.19	(180)	3.02	32.84
DC-711 (45)		107.3			
DC-733 (38)		142.9	(180)	4.4	32.46
DC-751 (8)		211.67	(10)	5.15	41.1
	3 (25)	122.44			
DC-761 (8)		183.33	(10)	5.55	33.02
Liguria-11* (38)		13.49	(59)	.049	710.0
			(8)	17.28	
Liguria-21 (8)		44.26	(10)	0.07	632.28
	(58)	26.91	(90)	0.45	59.0

Not Measured.

(1) Time of run during which the quasi-steady state transport of water was measured.

(2) Time of salt measurement.

* Reverse flux of salt and water observed.

Table 4.2. Observed fluxes of water and sodium chloride through partially serpentinized peridotites at 340°C in response to a 6 molal NaCl concentration difference.

Sample and Run No.	Time ¹ days	Average H ₂ O Flux (J) moles cm ⁻² day ⁻¹ $\times 10^{-6}$	Time ² days	Average NaCl Flux (J) moles cm ⁻² day ⁻¹ $\times 10^{-6}$	J_{H_2O} J_{NaCl}
DA-611	(76)	24.62	(96)	1.025	24.0
DA-621	(38)	15.13	(180)	0.0194	786.64
DA-911	(62)	18.22	(80)	1.53	11.9
DA-411	(60)	13.50	(130)	0.505	6.72
DA-311	(36)	51.52	(50)	1.55	33.23
DA-321	(39) (30)	39.55 57.62	(74)	1.29	44.48
Bay-11	(41) (30)	32.0 73.0	(74)	1.47	21.76

- Not Measured.

1,2. See Table 4.1.

* See Table 4.1.

lated is plotted against the time in days: The average fluxes of water and salt through each sample slice at 34°C are reported in the main text in Tables 4.1 and 4.2.

After an experiment had been completed, the serpentine sample was removed from the diffusion cell and studied optically with a binocular, scanning electron and petrographic microscope. In all the samples, except those from Liguria, the unpolished surfaces and thin sections (cut parallel to the diffusion direction) of the serpentine slices showed signs of secondary ferrous iron oxidation. This staining, which was produced during the transport of water through the diffusion slices, was observed almost always within the serpentine mesh rims and in major cross-cutting veins (Plates 9 and 10). On the surface that was immersed in the concentrated salt solution, the color of the alteration material is greenish-white (this was observed in only the longest experimental runs), whereas on the side immersed in distilled water, and in the thin sections, the color is a distinctive reddish-brown. Although the greenish-white alteration material was too fine grained and amorphous to be resolved under even the scanning electron microscope, it appears to be coating the serpentine plates (i.e. lizardite; Plate 9D).

A qualitative analysis of this material - which appears "whitish" under the SEM - using the energy dispersive unit attached to the SEM (see Hayashi *et al.*,

Plate 9

The serpentine diffusion slices

- A. A typical serpentine diffusion slice used in the experiments. The brown ferric iron staining along mesh rim veinlets is faintly visible. The dark circle shows where the slice was attached to the glass diffusion cell walls.
- B. Close-up of altered surface of diffusion slice immersed in de-ionized water. Serpentinite surface shows typical iron oxidation staining (brownish color) along mesh rim veinlets. Blackish band in the upper right hand corner of photo shows where the glass diffusion cell wall was cemented to the slice. Sample DC-7.
- C. Binocular microscope view of altered surface of diffusion slice imbibed in salt solution. The surface of the serpentinite slices shows typical intense dissolution-oxidation (greenish-white material) along mesh rim veinlets. Alteration material is believed to be composed of Cl bearing ferric oxyhydroxides of iron (i.e. green rust). Sample DC-7.
- D. Close-up of amorphous green rust coating well-crystallized lizardite serpentine plates in mesh rim. The serpentine in the mesh centers (MC) appears fine grained and randomly oriented, and shows no sign of alteration. Sample DC-7. SEM photo.
- E. Photomicrograph showing location of ferric iron staining inside the diffusion slice. The iron oxidation is clearly limited to the serpentine in the mesh rims (arrows). Dark lines are magnetite that are concentrated in fractures bordering mesh centers (i.e. in mesh rim veinlets). Section was cut parallel to the direction of diffusion (x). One nicol. Sample DC-5.
- F. Close-up of iron staining (arrow) in above sample (MC = mesh center). This series of photos show clearly that the transfer of water through the slices has occurred in an interconnected network of well-crystallized mesh rim veinlets, and not through finite open microcracks! One nicol.

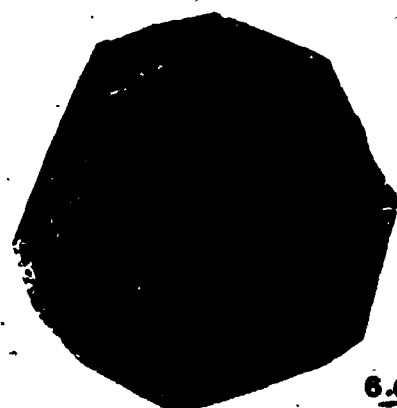
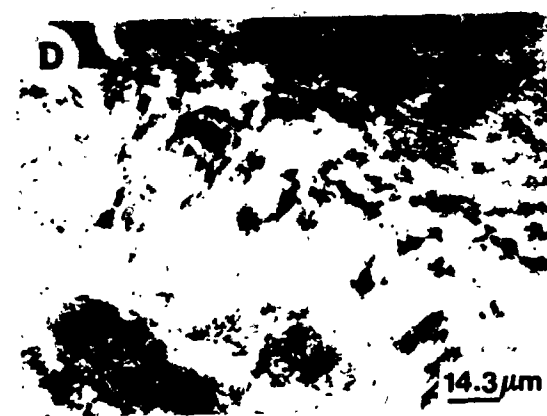
A**C****D****E****F**

Plate 10

The serpentine diffusion slices (con't.)

- A. Surface of slice showing ferric iron staining along cross-cutting veins in sample from Islands, Newfoundland. Degree of serpentinization is 60%.
- B. Same as above, in sample DA-3 from Acohe Mine, Philippines. Note that the diffusion of water has occurred preferentially through this microstructure. Serpentinization is 30%
- C. High magnification photomicrograph showing iron staining in mesh rim veinlets. White patches are unaltered olivine grains. Sample DA-6. 80% serpentinized. One nicol.
- D. Photomicrograph of serpentine in a non-experimental slice, given for comparison. Little iron oxidation is apparent. One nicol.



1978), gave only the iron peaks + Cl. An analysis of the greenish-white material (plus minor serpentine) by x-ray diffraction, while showing no visible change in the sharpness of most of the serpentine peaks, indicates that an amorphous oxyhydroxide, perhaps lepidocrocite mixed with green rust (oxyhydroxide + Cl), may be forming (see Misawa et al., 1974; Murray, 1979). In the Ligurian samples, which contain only very small amounts of brucite, none, or little of, the ferrous iron has been oxidized.

Energy dispersive spectra, obtained from traverses across sections parallel to the direction of diffusion, detected Cl within well-crystallized mesh rims or in veins. Sodium was not found, because it is much less sensitive to detection at very low concentrations. An attempt to determine the relative concentration distribution of Na and Cl across the slices, using an electron microprobe, was not very successful. This was again due, in part, to the very low concentrations being measured. Yet, in several slices a similar concentration distribution was observed (see Figures 4.2a, b).

4.4.2 Diffusion Coefficients of Water and Sodium Chloride

Average porous system diffusion coefficients of water (D_w) and sodium chloride (D_s) at 250, 340, and 400°C were calculated using Ficks first law (equations 4.12 and 4.13), once their respective fluxes had been measured. The

Table 4.3. Calculated average diffusion coefficients for water (\bar{D}_w) and sodium chloride (\bar{D}_s) through partially serpentinized peridotites at 34°C in response to a 6 molal NaCl concentration difference.

Sample and Run No.	\bar{D}_w moles cm^{-2} sec $^{-1}$	\bar{D}_s moles cm^{-2} sec $^{-1}$	\bar{D}_w/\bar{D}_s
DA-611	1.34×10^{-8}	5.9×10^{-10}	22.6
DA-621	8.38×10^{-9}	1.1×10^{-11}	761.82
DA-911	7.6×10^{-9}	6.5×10^{-10}	11.68
DA-411	6.7×10^{-9}	2.55×10^{-10}	26.26
DA-311	2.8×10^{-8}	9×10^{-10} $4.5 \times 10^{-10}*$	31.11
DA-321	2.3×10^{-8} 3.3×10^{-8}	7.5×10^{-10}	44.0
Bay-11	1.5×10^{-8} 4.2×10^{-8}	7.5×10^{-10}	22.0

*see Table 4.1.

Table 4.4. Calculated average diffusion coefficients of sodium chloride (\bar{D}_s) and water (\bar{D}_w) through completely serpentinized peridotites at 340°C in response to a 6 molal NaCl concentration difference.

Sample and Run No.	\bar{D}_w moles $\text{cm}^{-2} \text{ sec}^{-1}$	\bar{D}_s moles $\text{cm}^{-2} \text{ sec}^{-1}$	\bar{D}_w/\bar{D}_s
DC-511	6.5×10^{-8}	N.M.	-
2	8.8×10^{-8}	N.M.	-
4	6.3×10^{-8}	1.4×10^{-9}	45.0
DC-521	3.0×10^{-8}	2.4×10^{-9}	12.5
DC-532	5.7×10^{-8}	1.8×10^{-9}	30.8
DC-711	6.6×10^{-8}	N.M.	-
DC-733	7.8×10^{-8}	2.5×10^{-9}	30.58
DC-751	1.15×10^{-7}	3.0×10^{-9}	38.32
3	7×10^{-8}	N.M.	-
DC-761	9.3×10^{-8}	3.0×10^{-9}	32.0
Liguria-11	7.3×10^{-9}	1.1×10^{-11} $1 \times 10^{-8}*^$	663.64
Liguria-21	2.7×10^{-8} 1.0×10^{-8}	4.6×10^{-11} 4.5×10^{-10}	586.96 57.78

* See Table 4.1

N.M. Not measured

results are listed in Tables 4.3 and 4.4.

The diffusivities of water through the serpentine slices range from 10^{-7} to $10^{-8} \text{ cm}^2 \text{ sec}^{-1}$; whereas those of sodium chloride range from 10^{-8} to $10^{-11} \text{ cm}^2 \text{ sec}^{-1}$. Values of Dw in the completely serpentinized samples differ generally by less than an order of magnitude from those in the partially serpentinized peridotites. Although the same trend is observed with respect to values of Ds, its value for a particular sample is almost always an order of magnitude lower than that of Dw, sample, as shown by the ratio Dw/Ds.

4.4.3 Discussion of Results

a) Fluxes and diffusivities

In terms of water transoort, a quasi-steady state condition within the serpentine slices was assumed to exist when the flux of water leaving the slices was equal to the flux of water entering the slices: the net flux = influx - outflux = 0. The times required for the systems to reach a quasi-steady state were variable, ranging from 10-20 days in the more completely serpentinized samples, to about 40-60 days in the partially serpentinized peridotite samples, including those from Liguria (see equation 4.7). According to this equation, the salt flux in the majority of the slices would have approached a quasi-stationary value only after about 200 days (or 7 months) had elapsed. However,

in membranes in which the solvent flow experiences little resistance, in contrast to ions, osmosis may strongly affect the electrolyte flux by transferring salt ions back towards the concentrated solution against their chemical potential gradients (Helfferich, 1962, p. 390). Therefore, the measured diffusion coefficients may actually be quasi-steady state values. But considering the very low diffusivities observed for salt in some of the partially serpentinized samples, non-steady state transport coefficients may also have been measured.

The observed diffusive fluxes of water through the serpentine slices by osmosis is at least an order of a magnitude greater than the reverse flux of sodium chloride. This is clear evidence that finite, open microcracks didn't contribute to the measured diffusion permeability. Support for this important observation comes from both the SEM and post-experimental photomicrographs (Plates 9 and 10) of the serpentine slices which show, by the ferric iron staining, that most of the fluid flow occurred through serpentine "veins" that make up the mesh rims or fill transgranular fractures.

This difference (above) in the rates of transport of salt and water is a reflection of the relative ability of water and sodium chloride to move through the serpentine slices, as indicated by the ratios of their respective diffusion coefficients, D_w and D_s . The physical parameters

responsible for this variation in mobility within individual samples - and more importantly between the samples - of a porous material can be generally ascribed to the porosity, the constrictivity (pore size), and the tortuosity of the diffusional path. Ion retardation due to sorption mechanisms, such as simple adsorption on solid surfaces, may also be important. These physical parameters are also responsible, as discussed earlier, for the reduced diffusivities of both ions and solvent species in porous media, in comparison to their measured values in free solution.

The larger diffusion coefficient of water and salt through the more extensively serpentinized slices (excluding those from the Ligurian ophiolite) appears to be a function of their higher apparent porosity (2 to 3% vs. 1 to 2%, Table V-1; Appendix V), and what is apparently a less tortuous channel (vein) system. Given the polar structure of the water molecule, an absorbed water film (i.e. interlayer water in swelling clays) of higher than average viscosity will always be present on pore walls (cf. Pundsack, 1956). This means that as the average pore size decreases - as is indicated by the lower porosity of the partially serpentinized peridotites - and the constrictivity increases, the diffusive movement of both water and salt will tend to be reduced because of the increased viscous drag (Kemper et al., 1964; Low, 1976).

Why is the effective diffusion coefficient of NaCl (Na^+ and Cl^-) smaller than that of H_2O ? The diffusional resistance felt by an ion migrating through a porous material is a function of the reduced surface area (as indicated by the porosity and density), the tortuosity of the void system, the size, valence and degree of hydration (ions may move through a membrane partly to fully stripped of their hydration shells; Erickson and Jacobsson, 1981) of the ion, and sorption processes: (1) In true ion-exchange minerals the crystal structure contains surplus electric charge (either positive or negative) which is compensated for by ions of opposite charge - which in turn can be replaced by other ions of the same sign. These are called counterions. Ions sorbed from the pore solution fill interlayer sites in the swelling clays - e.g. smectite and illite clays - while in zeolites they don't occupy fixed positions in the porous solid but are 'free' to move in the channels of the lattice framework (Helfferich, 1962); OR (2) the physical (and essentially irreversible) adsorption of ions on crystal (i.e. pore) surfaces that have developed a net charge as a result of the loss or gain of protons on surfaces containing exposed hydroxyl groups (i.e. at broken bonds, edges, etc.; e.g. kaolinite, Dixon, 1977). Such a charge is dependent on the pH of the solution that is in contact with the clay structure.

Unless pore sizes in the membrane matrix are very small - i.e. the diameter approaches that of the diameter

of a partially or unhydrated ion (see Erickson and Jacobsson, 1981; Monk, 1961) the effective diffusion coefficient of an electrolyte (vs D_{H_2O}) for the mass transport through a porous and permeable material will depend more strongly on the charge (i.e., ion sorption capacity) of the matrix structure. The 1:1 layer-type phyllosilicates serpentine (trioctahedral) and kaolinite (dioctahedral) have no interlayer cations, and as indicated by differential thermal analysis a low adsorption capacity (serpentine < kaolinite, Lambe and Whitman, 1969; Dixon, 1977; Brindley, 1981). Nonetheless, iron oxides such as magnetite or goethite (or orthohydroxides) and broken (i.e., at octahedral) sheet edges will develop a net surface charge in strongly basic or acidic solutions (Drevor, 1982, p. 78-79). In aqueous solutions of high pH produced during serpentization or the dissolution of hydrated magnesium silicates at low temperatures (Nesbitt and Bricker, 1978), the surfaces of these minerals will become negatively charged. If this occurs the adsorption cation capacity of the "rock" as a whole may become significant.

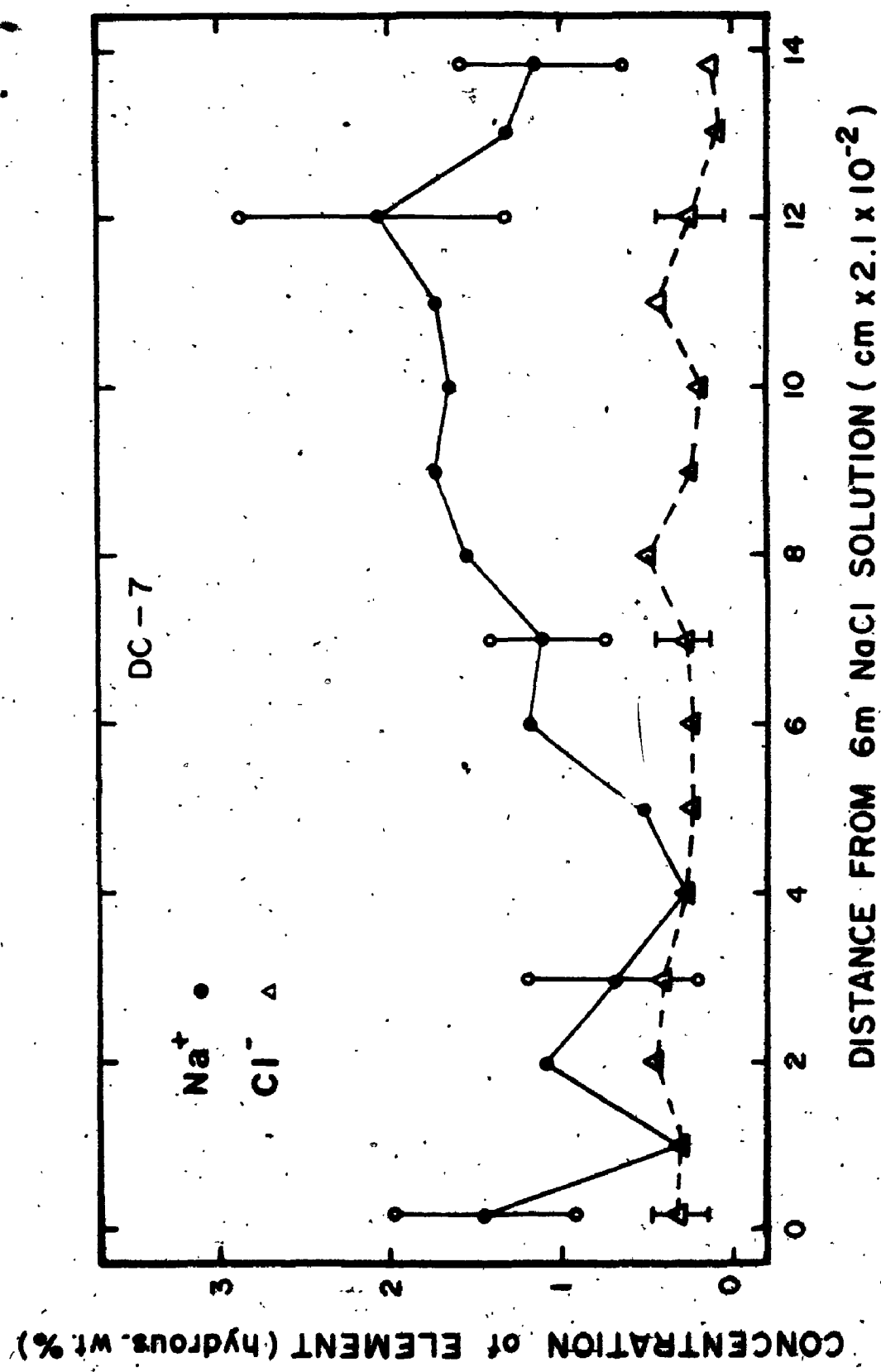
Because of this excess negative charge on the surfaces of the serpentine minerals cations - Na^+ in this experiment - will have no trouble entering the slices, but once inside they will be strongly adsorbed on pore surface to form a layer of so-called counterions. Co-ions - the anion Cl^- in these experiments - on the other hand will have difficulty

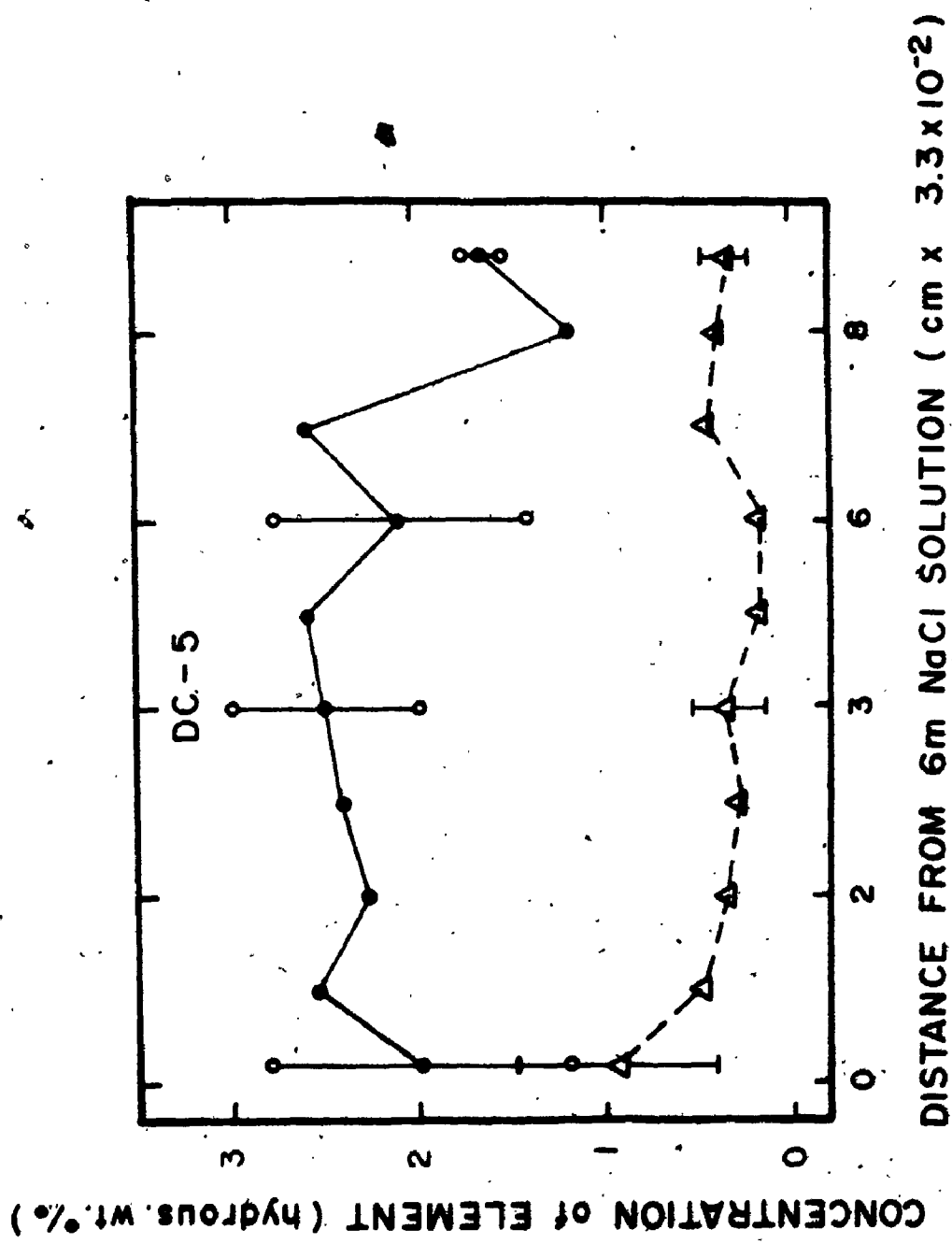
diffusing into the membrane because of this charge. They are, it is believed, repelled at the concentrated solution-membrane interface. Thus inside the serpentine slice the concentration of counterions (e.g. Na^+) will be very high (e.g. 10x background; c.f. Table III-2b; analysis no. 9, 909-1), and the concentration of co-ions (Cl^-) will be relatively low (e.g. 1.5x background; c.f. Table III-2d; average of analyses 1-13 of DC-5), as is clearly shown in Figures 4.2a and b. This Na/Cl ratio, observed in some of the experimental slices, is in agreement with analyses published by Hess and Otalora (1964). Due to the difficulty of measuring the Na concentration, however, more detailed work is necessary before these results can be extrapolated with a full measure of confidence to the natural system.

In order that electroneutrality be conserved everywhere in the system, the fluxes of co-ions (eg. Cl^-) and counterions (eg. Na^+) through a membrane must be stoichiometrically equivalent; i.e. $J_1 = J_2 = J_{12}$ or $J_{\text{Na}^+} = J_{\text{Cl}^-} = J_{\text{NaCl}}$. This condition is enforced by the electric potential (Donnan or diffusion) potential established by the diffusion process itself: the faster ion - usually the counterion (Na^+ in this study) - tends to build up a positive space charge at the exit interface, which speeds up the slower ion (eg. Cl^-). In essence the slower ion (usually the co-ion) determines the diffusion

Figure 4.2a,b

Diagrams illustrating the variation in the concentrations of Na^+ and Cl^- plotted as a function of distance from the side of the slice imbibed in the salt solution. Sections are perpendicular to the direction of diffusion (i.e. 'x'). Vertical lines marked by an open circle or bar represent the standard deviation.





coefficient and the rate of migration of the electrolyte (see Hellferich, 1962).

The "effective" average diffusion coefficient of NaCl through the serpentine slices will tend to be lower than D_{H_2O} as a result of this electrical reduction in mobility - which is probably most important at the solution-membrane interfaces (Dutt and Low, 1961; Kempler and Shark, 1966; Neretnieks, 1983) - and geometric effects which tend to reduce differentially ion diffusivities and thus contribute to the development of an electric field. This may be especially important when void sizes are relatively small (e.g. un-solvated radius of Na^+ (1.08 Å) < Cl^- (1.5 Å) and $D_{\text{Na}^+} > D_{\text{Cl}^-}$; Erickson and Jacobsson, 1991).

The very low salt diffusivities (i.e. high D_{H_2O}/D_{NaCl} value) determined in the initial stages of some of the diffusion experiments is believed to be the result of both steric effects (i.e. geometric exclusion of ions) and the nearly complete adsorption of the diffusing counter-ion. Hence, what one really measures is the apparent (although this is by definition used only in the case of strong sorption during diffusion; Manheim, 1970; van Schaik and Kemper, 1966) diffusion coefficient. This is, however, only a temporary (i.e. transient) phenomenon, and is soon replaced by a quasi-stationary concentration gradient and flux of salt.

A few of the longer (6 month) experimental runs showed

a gradual decrease in the flux of water across the slice (see Appendix VII). Although some of this change may be due to a partial sealing of pores by secondary iron-oxide-hydroxides, most of the decrease is probably due to the progressive increase in the internal salt concentration (Hanshaw and Coplen, 1973). As the solvent flux is coupled to the mass transfer of sodium chloride in the reverse direction, this effect is not surprising.

b) Salt filtration

The salt filtering - or osmotic - efficiency of a membrane separating a concentrated solution from a dilute one is a strong function of its ion sorption capacity, porosity (and pore size), and the ionic strength of the solution migrating through it (Kemper and Maasland, 1964; Fritz and Marine, 1984). The serpentine slices act as leaky semipermeable membranes - i.e. permselective to counterions - because of these properties. For example, in 6 months the concentration of NaCl in the dilute solution side of the cell was found to be on the order of 1×10^{-1} moles liter⁻¹ or 30-40 times lower than that of the (6 molal NaCl) concentrated solution. This ratio is also apparent in the daily average value of $\delta\text{H}_2\text{O}/\delta\text{NaCl}$ (or $\Delta\text{H}_2\text{O}/\Delta\text{NaCl}$). If dilute electrolyte solutions are used, "salt filtration" ratios of 300/1 may have been observed (but see below also). This is similar to that observed in

bentonite clays (cf. Mokady and Low, 1966). Because of the difficulty of quickly saturating the samples with water at the start of an experiment, the filtering capacity of the serpentine slices imbibed with low salt concentrations (<< 2 molal NaCl) was not investigated.

How much of the sorption capacity of the slices was due to the growth of secondary ferric iron-oxide-hydroxides, which are believed to be forming as a result of the dissolution of ferrous iron rich brucite and serpentine(?) (Plates 9 and 10), is not known. But the absence of any observed ferric iron oxidation in the Ligurian samples, which exhibit similar flux ratios, suggests that it was not important during the life span of most of these experiments. As mentioned before, these samples have very low amounts of brucite.

In a few of the slices - noticeably the partially serpentized slices containing visible cross-cutting micro-veins of serpentine-negative osmosis was observed (i.e. the level of the fluid in the capillary-tube on the dilute side (A) of the cell tended to rise, while that on the concentrated side was dropped). In membranes where the mobilities of the counterion and co-ion are quite different, the pressure (osmotic) gradient driving the solvent flow may be partly balanced or outweighed by the resulting electrical (diffusion) potential gradient driving the transfer of ions (Helfferich, 1962, pp. 389-390). If the

co-ion is much faster than the counterion, it "pushes", because of ion-water dipole interaction, the electrically charged pore fluid in the direction of the dilute solution; instead of simply balancing the fluxes of the diffusing ions (eg. Na^+ and Cl^-). This transfer phenomenon is characteristic of rather open-structured exchangers, where the permeability to water is high (i.e. low flow resistance), and the membranes typically "leaky" (Patterson, 1970). It also points out the fact that the pore sizes in a brittle porous medium, such as a serpentinized peridotite, are probably quite heterogeneous.

c) Temperature dependence of D

The temperature dependence of D_w or D_s is given by the Arrhenius relationship (equation 4.5). The scatter in the values of the diffusion coefficients (especially in the partially serpentinized samples) for a particular sample type is probably caused by small differences in the water contents of the slices (cf. Barrer, 1961, pp. 97-101; as a result, the small difference in E between sample types is not noticeable). Barrer (1961, p. 103) gives values of $5.4 \text{ kcal mol}^{-1}$ and $9.4 \text{ kcal mol}^{-1}$ for the diffusion of water parallel (to 001 plane) to the main channel (aperture) system and at an oblique angle (parallel to 201) to it, respectively, in the zeolite heulandite. The activation energy, E , for the diffusion of water through the slices

Figure 4.3

Arrhenius plot for the diffusion of water and sodium chloride through serpentinized peridotites, based on the experimentally measured values of D_{H_2O} and D_{NaCl} at 25°, 340 and 400°C. Solid points = H_2O through Coto serpentinites, crosses = H_2O through Acohe serpentinized peridotites, and open circles = $NaCl$ through Coto serpentinites.

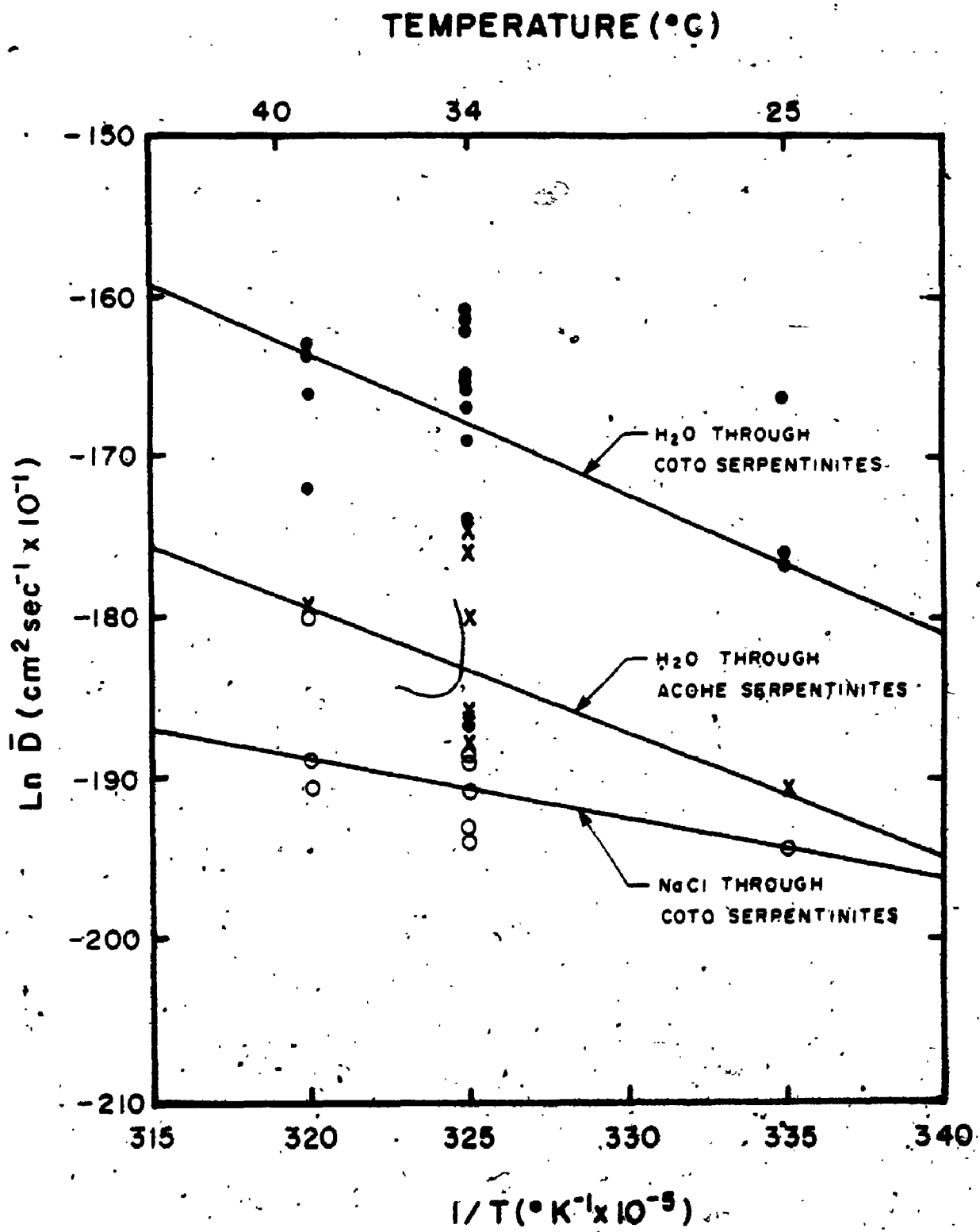
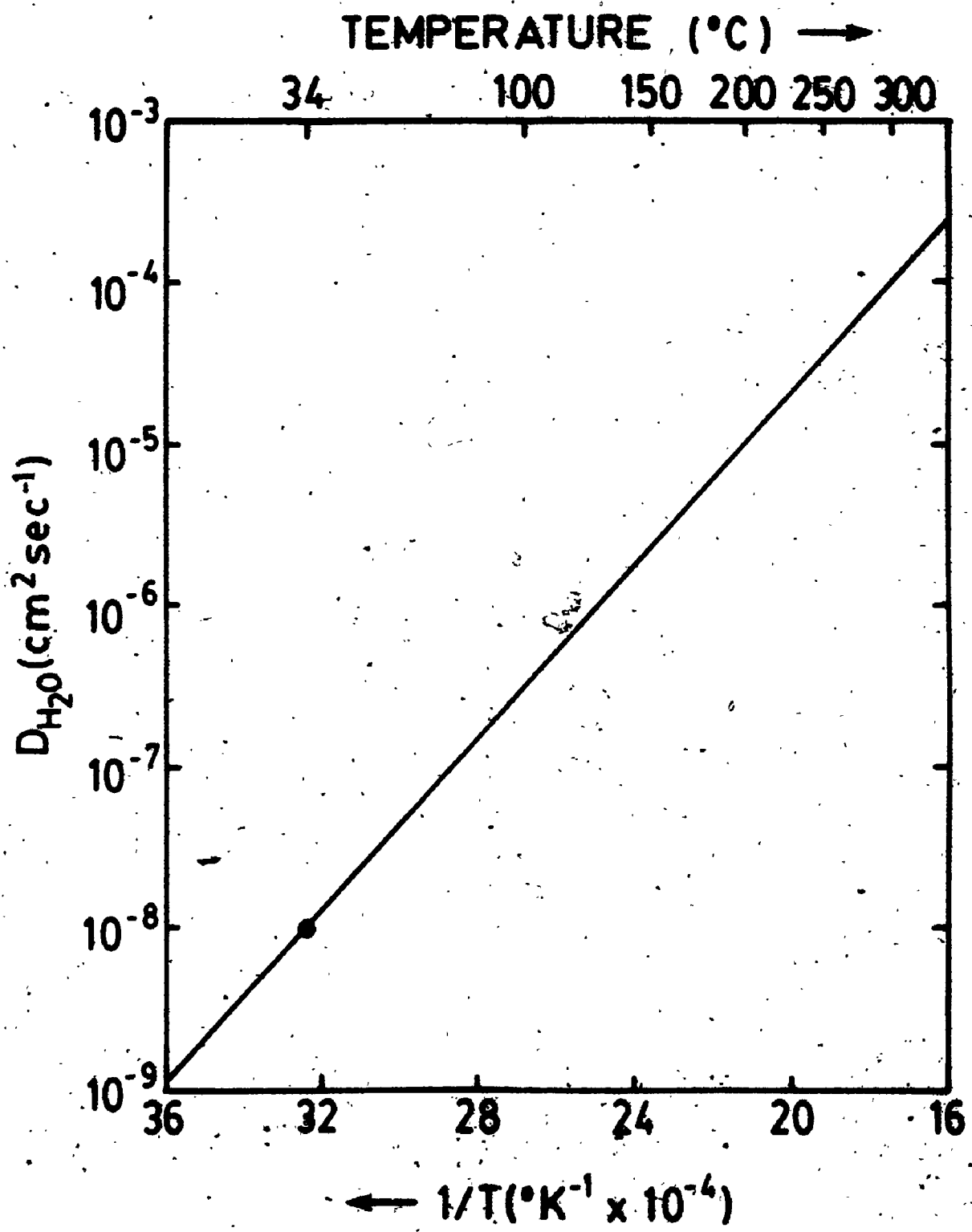


Figure 4.4

Graph showing the estimated average diffusion coefficients of water plotted as a function of the reciprocals of temperature. The measured value of D_{H_2O} at 34°C is taken as T_1 ; i.e. therefore, in $D_{T_2} = E/R (1/T_1 - 1/T_2) + \ln D_{T_1}$ (see text).



was found to be on the order of $10-12 \text{ kcal mol}^{-1}$, whereas more limited data for salt suggests a similar value (see Figure 4.3). This relatively high value of E , in comparison to that reported for diffusion in aqueous solutions, means that D will increase fairly rapidly as the temperature increases. And so in diffusing through the serpentine "structure" a species behaves more as if it were moving in a solid, albeit porous solid (see Lerman, 1979, pp. 116-17). Figure 4.4 is a plot showing the estimated values of D_{H_2O} at higher temperatures. These were determined using equation 4.6, and assuming an activation energy of 10 kcal mol^{-1} .

d) Transport coefficients of H_2O

Several studies (Durbin, 1960; Kemper and Evans, 1963; Hammel and Scholander, 1976) have shown that if a porous membrane separating two solutions behaves semipermeably, the osmotic flux is equivalent to that produced by a hydraulic gradient (bars/cm) equal to the measured osmotic pressure difference (eq. 4.8) of the system (above). It has also been found that in some cases the solvent (eg. H_2O) moves through the solid membrane (eg. clay paste) primarily by viscous or quasi-viscous flow. Kemper (1961) calculated that the diffusive flow becomes dominant only when the pore size (or water film thickness) falls below about 40 Å (how tightly the adsorbed water film is held may-

also be important).

Deviations from Darcy's law - determined by plotting the flow rate against the hydraulic gradient (Dullien, 1979) - are common in compressed clays (eg. bentonite, Push, 1983), especially at low hydraulic gradients. This has been attributed to the non-Newtonian behavior of strongly adsorbed pore water in systems characterized by very slow flow rates (Swartzendruber, 1961; Bear, 1972, pp. 127-8). Therefore, permeability coefficients measured in such systems using Darcy's law (eq. 4.9) - or those determined using the bulk flux (i.e. no tracer species of water) and Fick's first law (eq. 4.3) - should be simply called transport coefficients until the mechanism of mass transfer is known. (Note: when the D_{H_2O} ($T = 25^\circ$) exceeds the self diffusion coefficient of water at that temperature $1.5 \times 10^{-5} \text{ cm}^2 \text{ sec}^{-1}$, this implies that water may be moving dominantly by a viscous mechanism).

In order to compare the transport coefficients of water through serpentinites with those in compressed clays obtained from other experimental studies, it is necessary to determine the intrinsic permeabilities (k 's in darcys or cm^2) of the serpentine slices. This was done by substituting for the hydraulic gradient (P) in Darcy's law (eq. 4.9) the theoretical or potential osmotic pressure difference (eq. 4.8) produced by the water / serpentine slice / salt solution system (Kemper and Rollins, 1966). Because

Table 4.5. Intrinsic permeabilities (k 's) of partially serpentinized peridotites at 34°C in response to a pressure gradient equivalent to the calculated osmotic pressure, $\Delta\pi$, of a 6 molal NaCl solution.

Sample and Run No.	Pressure Gradient $\Delta\pi/x$	Flux of H_2O Q/ A.t	Intrinsic Permeability k
	bars cm^{-1}	$cm^3 cm^{-2} day^{-1}$ $\times 10^{-5}$	darcys
DA-611	1363	44.31	1. 2.76×10^{-12}
DA-621	1859.0	27.73	1.7 $\times 10^{-12}$
DA-911	1859.0	29.06	2. 1.49×10^{-12}
DA-411	1573.0	24.22	3. 1.31×10^{-12}
DA-311	1363.3	104.0	6.5 $\times 10^{-12}$
DA-321	1239.3	78.6 103.72	4.88 $\times 10^{-12}$ 7.11 $\times 10^{-12}$
Bay-11	1514.8	63.5 131.40	3.95 $\times 10^{-12}$ 7.36 $\times 10^{-12}$

Table 4.6. Intrinsic permeabilities (k 's) of totally serpentinized peridotites at 340°C in response to a pressure gradient equivalent to the calculated osmotic pressure, $\Delta\pi$, of a 6 molal NaCl solution.

Sample and Run No.	Pressure Gradient $\Delta\pi/x$	Flux of H ₂ O Q/A.t	Intrinsic Permeability k
	bars cm ⁻¹	cm ³ cm ⁻² day ⁻¹ $\times 10^{-3}$	darcys
DA-511	1278.1	1.84	1.14×10^{-11}
2		2.47	1.54×10^{-11}
4		1.96	1.5×10^{-11}
DC-521	929.5	0.68	4.25×10^{-12}
DC-532	1278.1	1.79	1.12×10^{-11}
DC-711	1278.1	0.92	1.2×10^{-11}
DC-733	1202.9	2.58	1.6×10^{-11}
DC-751	1460.7	2.20	1.37×10^{-11}
3		3.81	2.37×10^{-11}
DC-761	1460	3.30	2.06×10^{-11}
Liguria-11	1363	0.17	1.1×10^{-12}
Liguria-21	1202.9	0.79	4.95×10^{-12}

1 darcy = 9.87×10^{-9} cm²
or 9.66×10^{-4} cm sec⁻¹

the serpentine slices are not perfectly semipermeable (to salt ions), the transport coefficients (k 's) obtained may be as much as an order of magnitude too low (cf. Mauro, 1965; Fritz and Marine, 1983).

Tables 4.5 and 4.6 list the minimum intrinsic permeabilities calculated using this modified version of Darcy's law and the observed rates of water flow (converted from moles cm^{-3}) through the serpentine slices. In Figure 4.5 the measured average transport coefficients (D 's and k 's) are plotted against the density (to degree of serpentinization) of the samples; and are then compared with permeability coefficients measured in Na-bentonite, plotted as a function of its water-saturated density. Some variation with density is observed, although not to the extent seen in bentonite clays. Partially serpentinized peridotite slices with major cross-cutting veins (Bay and dA-3) have transport coefficients intermediate between that of the other samples. This suggests that the fundamental reason for the differences in the rates of salt and water transport between samples are not solely physical parameters related to the degree of serpentinization, but rather the details of the serpentinization process itself. The variable permeability clearly reflects differences in the geometry of void defects, produced because reaction stresses in a brittle medium are highly anisotropic on a local scale.

Figure 4.5

This graph illustrates the relationship between the measured transport coefficients of water and bulk density of serpentinized peridotites. A similar curve for sodium bentonite has been inserted for comparison. (The stippled area shows the range in permeability due to experimental scatter and variable pore salt contents). Open circles = partially serpentinized peridotites containing visible cross-cutting serpentine veins, triangles = partially serpentinized samples, solid circles = Ligurian serpentinites, and pentagons = completely serpentinized peridotites. Dashed line is indicated trend for samples without major veins.

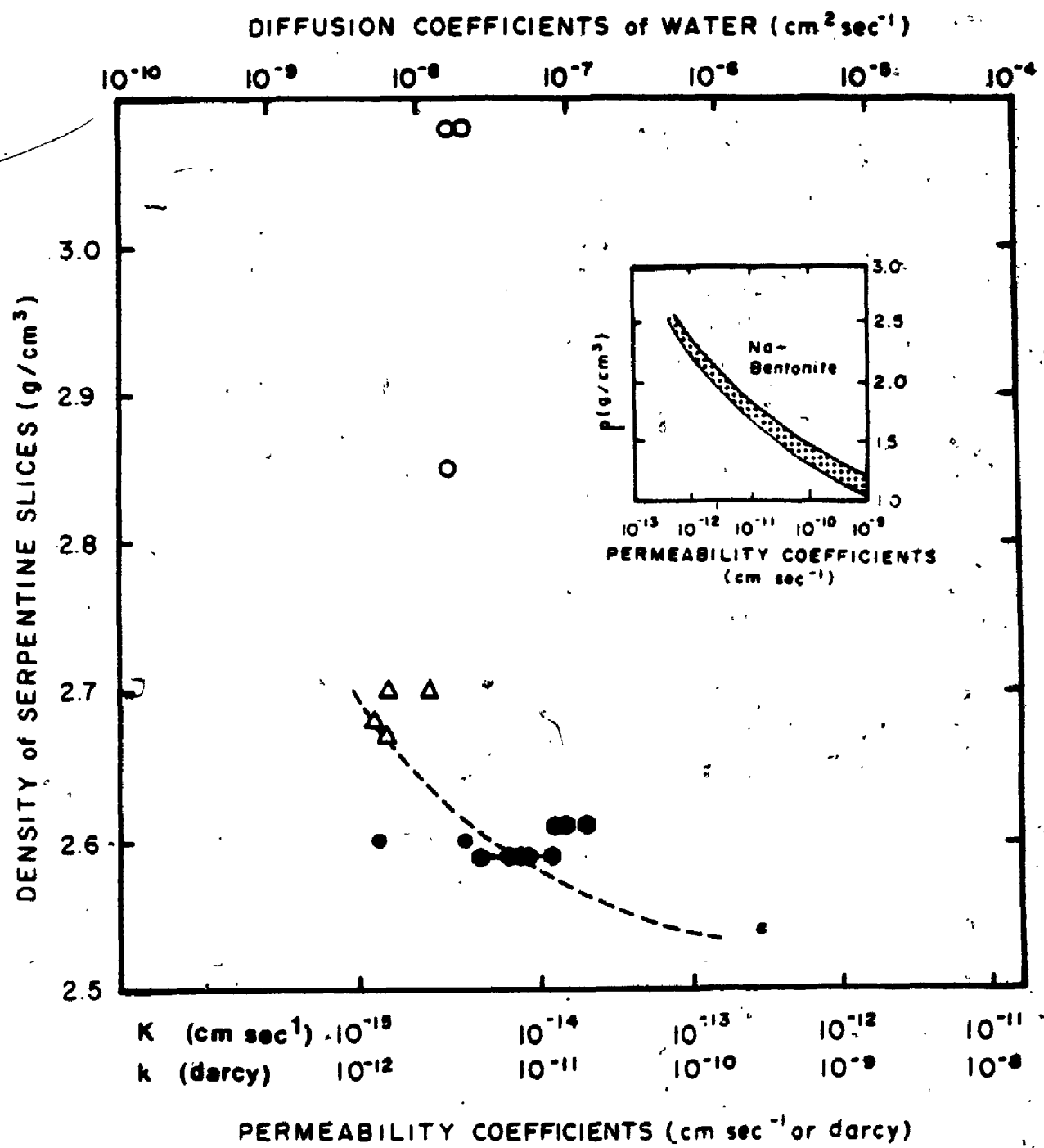


Table 4.7. Transport coefficients of water and ions in other low permeability materials.

Porous Material	Density (ρ) g cm^{-3}	Porosity %	Ion or H_2O $\text{cm}^2 \text{ sec}^{-1}$	Transport Coefficients k darcy
Serpentinitized Peridotites ¹	3.1 - 2.59	1.5 - 3	H_2O Cl^-	$10^{-8}-10^{-7}$ $(0.5-3) \times 10^{-9}$
Na-Bentonite ^{2,3} (Na-SO)	2.5 - 2.1	30 - 35	Cl^- , H_2O Cl^- , H_2O Cs^+ , Na^+	$(4-9) \times 10^{-8}$ 3×10^{-9} $(0.2-1) \times 10^{-10}$
Shales ⁴	2.09-2.1	21 - 24		$(1.6-11) \times 10^{-9}$
Concretes ⁵			Na^+ Cl^-	1×10^{-9} 4×10^{-10}
Zeolite, Heulandite ^{7,8} Chabazite ^{7,9}	2.2-2.1 2.1-2.05	35 47	H_2O H_2O Na^+	$10^{-8}-10^{-7}$ 1.3×10^{-7} $10^{-13}-10^{-12}$

(1) This study; transport coefficients determined under quasi-steady state conditions.

(2) Ericsson and Jacobsson (1981) and Kereinicks (1982); transient state ion diffusion obtained by concentration profile analysis except for Cl^- .

(3) $k(\text{H}_2\text{O})$ using hydraulic gradient; Push (1983).

(4) Kupper (1986b).

(5) Graf et al. (1965); hydraulic gradient.

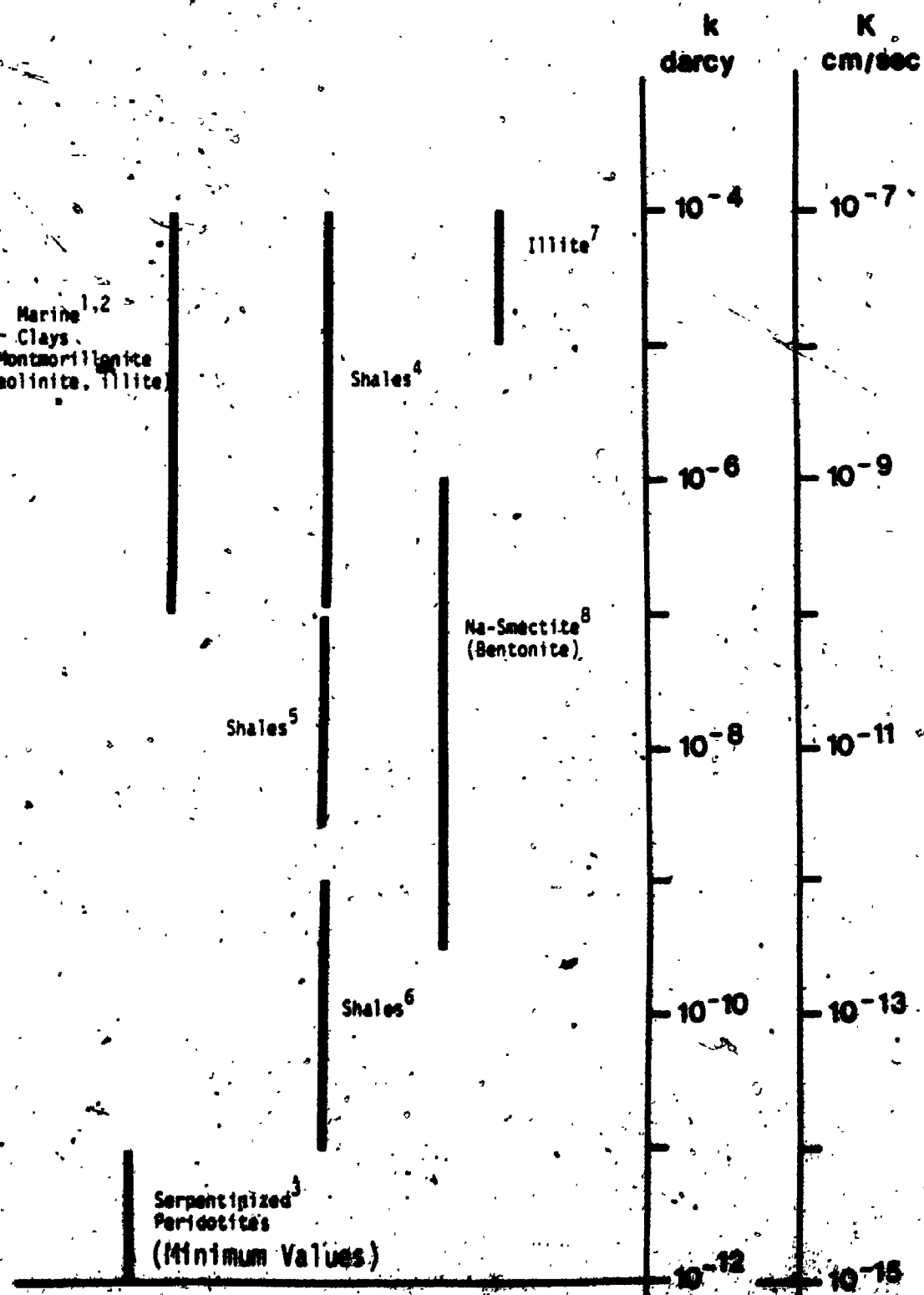
(6) Andersson et al. (1983); transient state measurements.

(7) Lerman (1979).

(8) Flanagan (1981); transient state measurements.

(2) Flanagan (1981); transient state measurements.

TABLE 4.8 The range in values of the intrinsic permeability (k) and hydraulic conductivity (K) coefficients in some unfractured porous media, including serpentinized peridotites.



1. Bryant et al., 1961
2. Fyeza and Cherry, 1979
3. This study (Values may be higher as the serpentine matrix is not perfectly semipermeable)

4. Fyeza and Cherry, 1979
5. Bryant, 1961
6. Bryant et al., 1965
7. Bryant et al., 1960

Tables 4.7 and 4.8 are a compilation of the transport coefficients of water and the measured ion diffusion coefficients respectively, obtained in different compressed clays and zeolites.

4.5 Summary and Conclusions

A serpentized peridotite can be considered as a semipermeable (though leaky), porous solid composed of an interconnected network of water filled voids, produced by plate buckling in the serpentine polymorph, lizardite. A thin slice of this rock placed in a diffusion (osmotic) cell substantially reduces the mass transport rate of the diffusing salt ions (Na^+ and Cl^-), while allowing a much faster rate of water transfer (i.e. by at least a factor of 30) in the reverse direction.

Effective porous system diffusion coefficients of water and sodium chloride determined in quasi-steady state serpentine systems, at room temperatures, were found to be on the order of 10^{-7} to $10^{-8} \text{ cm}^2 \text{ sec}^{-1}$, and 10^{-9} to $10^{-10} \text{ cm}^2 \text{ sec}^{-1}$, respectively. Calculated activation energies for the diffusion of water and salt suggest that D will increase by at least an order of magnitude for every 100°C rise in temperature (see Figure 4,4). The lower diffusivities, and hence rates of diffusion, of sodium chloride for the diffusion of this salt through the samples - in comparison to water - are due to an electrical reduction in

the mobility of these ions when entering or leaving the negatively charged serpentine slices, and possibly geometric effects. Salt filtration was quite variable because of the heterogeneity in the size of pores. Differences in the diffusivities of NaCl and H₂O between samples appear to reflect differences in the serpentinization process itself, rather than in the degree of serpentinization.

Similar transport coefficients (see Tables 4.7 and 4.8) have been reported for the migration of water and small non-interacting anions Cl⁻ and I⁻, and the alkali metal ions, Cs⁺ and Na⁺, in zeolites (Barrer, 1961; Letman, 1979; 10⁻⁸ to 10⁻⁷ cm² sec⁻¹) in a direction parallel to the layered structure and in highly compacted clays perpendicular to the orientation of the particles. Considering the large difference in the apparent porosity between the serpentine slices and the other porous media (about 5% - as compared to 20-30% for zeolites and compressed clays), the coefficients agree remarkably well with one another. They suggest that the average pore (i.e. defect) size in the serpentine veins is generally somewhat larger, but also quite variable.

A diffusion coefficient of water of 10⁻⁷ cm² sec⁻¹ is probably roughly equivalent to a quasi-intrinsic permeability coefficient of 10⁻¹⁰ to 10⁻¹¹ darcys, obtained using Darcy's law, and the theoretical osmotic pressure of the salt solution. What proportion of the mass transfer of

water through the serpentine slices is by viscous flow is not known, but if the diameter of the pores are on an order of 50-100x greater than that of a water molecule quasi-viscous flow may become significant. Especially when gradients are large and temperatures moderately high (100-300°C); i.e. at typical serpentinization temperatures. But if we consider the relatively small and variable size of the observed defects, and the effects of tortuosity, molecular mass transfer is probably the dominant transport mechanism for water in serpentinites under most conditions.

CHAPTER 5

THE DRIVING FORCE FOR SERPENTINIZATION

5.1. The Serpentine-Peridotite Interface

Consider the general problem, as shown in Figure 5.1, in which a crack (e.g. fault) connected to the seafloor has developed in a block of dry peridotite. At temperatures between 100°C and 400°C ($P_{H_2O} = P_{total}$) the rate of serpentinization is very rapid (Martin and Fyfe, 1970). Therefore if water is present a layer of serpentinized peridotite will immediately form along the margins of the crack, and the production of new serpentine at the peridotite-serpentine interface will depend on the diffusion rate of water through the existing serpentine reaction layer.

If the water penetration rate is slower than the reaction rate, the partial pressure of water, P_{H_2O} , at the reaction interface will be the equilibrium pressure of

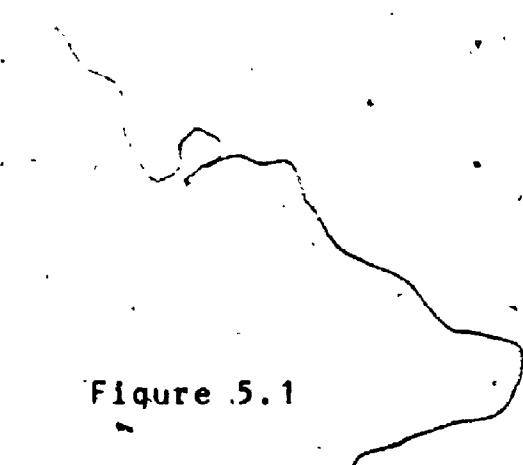
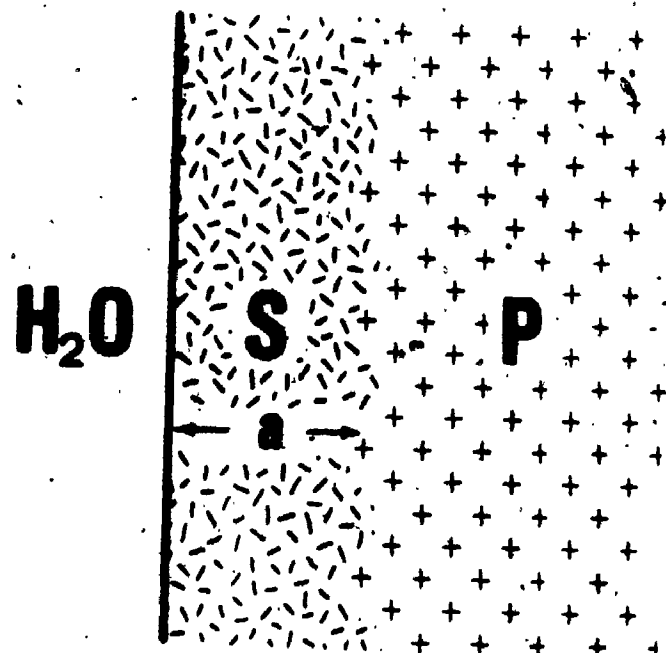
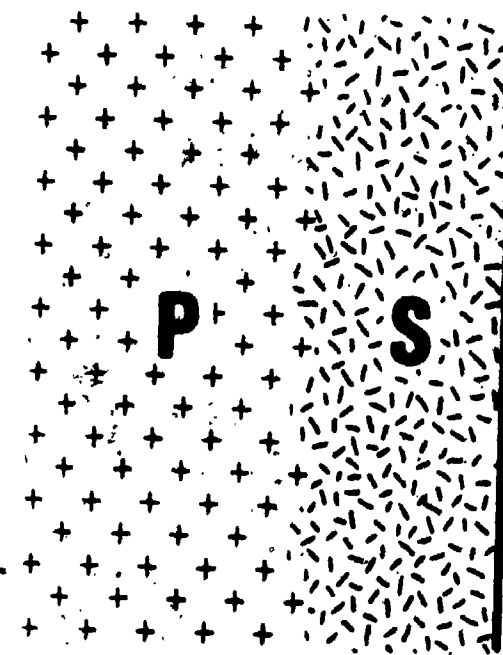


Figure 5.1

Schematic diagram showing the reaction environment along the margins of a crack, connected to the sea floor, that has developed in layer of peridotite. The reaction rate will be controlled by the rate of H_2O flow through reaction zone a.

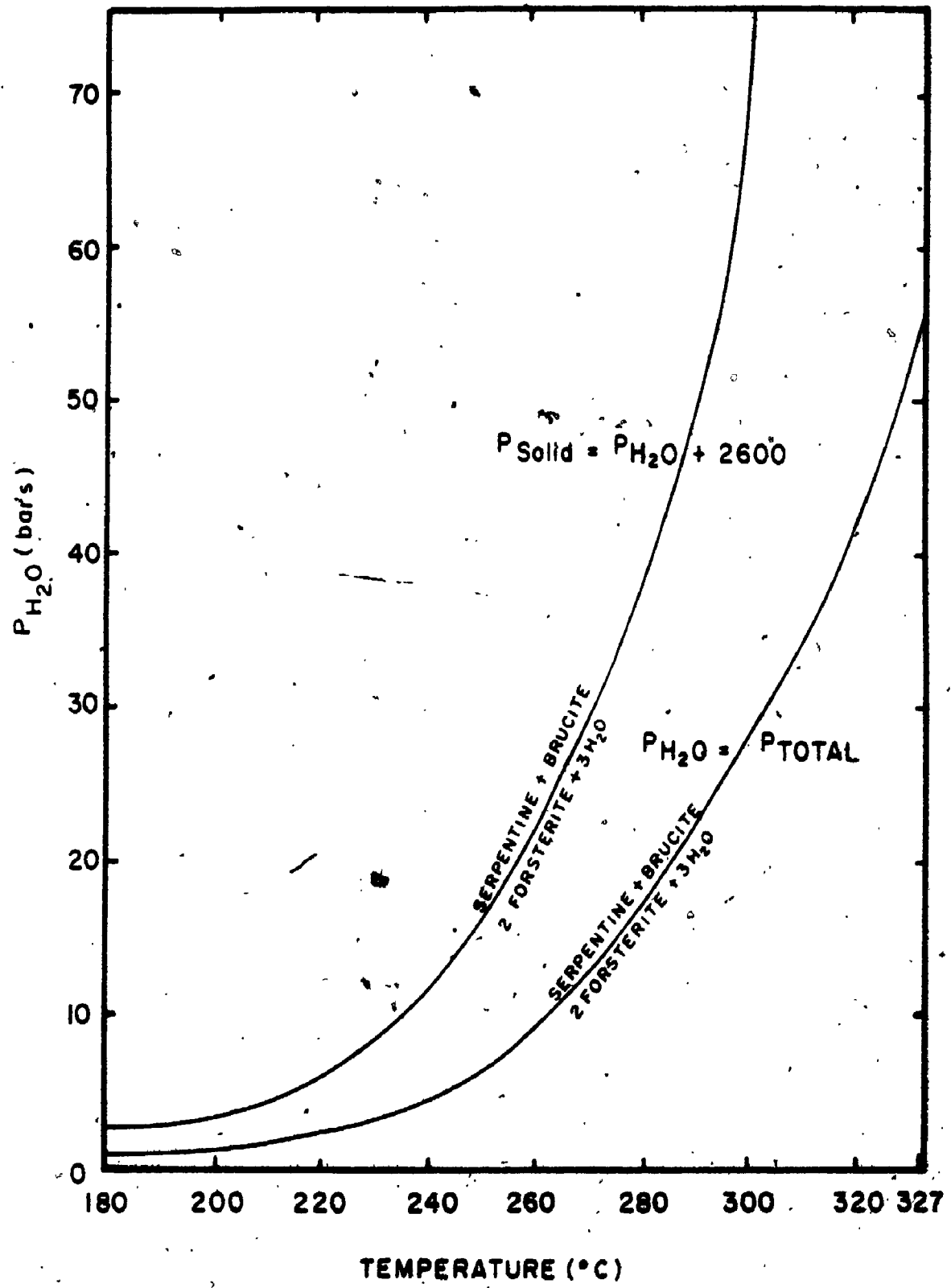


the particular serpentinization reaction. And, the magnitude of the fluid pressure in the macro-crack connected to the surface will be determined by the height of the fluid column in the crack (i.e. 100 bars/km). Since the system is open, the equilibrium vapor pressure curves must be recalculated for the case where the pressure on the solid is nonhydrostatic (i.e. $P_{H_2O} < P_{solid}$; see Fyfe, 1973). This correction lowers the equilibrium boundary, under steady state conditions, by about 500°C at depths of 5 to 8 kilometers in the crust. The reaction forsterite + water = serpentine + brucite is given as an example in Figure 5.2 (compare with Figure 2.1). The upper temperature limit of stability for serpentine would thus be about 4500°C ($P_{H_2O} < P_{solid}$, P_{H_2O} equilibrium = 1 kb; cf. Figure 2.1). When the a_{H_2O} is less than one the boundary will be shifted even more (see Brennan, 1983). At temperatures well below the upper stability limit of serpentine the equilibrium vapor pressure, as shown by the example in Figure 5.2, will be very low; only a few tens of bars at temperatures $\leq 3500^{\circ}\text{C}$ (c.f. Fyfe, 1958).

When the reaction is submarine, at typical depths (5-7 km) below the ocean floor water pressure gradients across a 1 centimeter thick layer of serpentine will be on the order of 1000 bars. The free energy change for a serpentinization reaction, given this new pressure of water, P_{H_2O} , in the crack, c, can now be written:

Figure 5.2

Vapor pressure-temperature diagram showing the shift in the boundary of the equilibrium vapor pressure curve, for the serpentine reaction serpentine + brucite = 2 Forsterite + $3H_2O$ when P_{total} is larger than P_{H_2O} , and is in a fixed ratio to P_{H_2O} . At temperatures below $280^{\circ}C$ the vapor pressure is very low (i.e. < 50 bars).



$$\Delta G_R(T_{eq.}, P_c) = \Delta G_R^\circ(T_{eq.}, P_{eq.}) - \int_{P_{eq}}^{P_c} V_{H_2O} dp \quad (5.1)$$

and as $\Delta G^\circ(T_{eq.}, P_{eq.}) = 0$,

the equation becomes,

$$\Delta G_R(T_{eq.}, P_c) = - \int_{P_{eq}}^{P_c} V_{H_2O} dp$$

$$\frac{f_{H_2O}(c)}{f_{H_2O}(eq.)} = - RT \ln f_{H_2O}(eq.) \quad (5.2)$$

where $f_{H_2O}(c)$ is the fugacity (or activity) of water in the crack at the new pressure, P_c , and $f_{H_2O}(eq.)$ and $T(eq.)$ are the equilibrium activity and temperature (° Kelvin) of water for the serpentinization reaction, respectively; and R is the gas constant = $1.987 \text{ cal mole}^{-1} (\text{OK})^{-1}$.

Because the system is open, there will be no equilibrium in the classical thermodynamic sense. Instead, if there is a continuous supply of water to the reaction interface, G^*_R will be strongly negative and the reaction will proceed spontaneously (and irreversibly) until all the reactants (e.g. olivine and pyroxene) have been consumed. The driving force for a serpentinization reaction is, therefore, the chemical potential (i.e. partial molal free energy) gradient of water across a reaction layer; i.e.

$$\frac{\Delta G_R}{x} = \frac{\Delta \mu_{H_2O}}{x} = \frac{-RT \ln \Delta f_{H_2O}}{x} \quad (5,3)$$

where $\Delta \mu_{H_2O}$ is the chemical potential difference of water, and x is the thickness of the serpentine reaction layer (cm). When P_{H_2O} in the macro-crack is about 1000 bars, and the equilibrium P_{H_2O} is on the order of 10 bars ($T = 300^\circ C$) (see Appendix II), the chemical potential gradient driving the diffusion of water through a layer of serpentine 1 centimeter thick will be on the order of -2000 calories per mole per centimeter.

In such a system a true steady state will never be reached, but if the change in the rate of production of new serpentine with time can be adequately described kinetically, the system may approach a quasi-stationary

condition. We shall assume that the rate of water diffusion through a continually expanding product layer of serpentine, and not an interface (nucleation, solution) process, is the rate controlling step in a serpentinization reaction (cf. Martin and Fyfe, 1970). The rate of change in the thickness, x , of a reaction layer (eg. serpentine), dx/dt (defined as the reaction velocity (Games, 1961), will be inversely proportional to the thickness of the layer. This is because the driving force for diffusion, the free energy gradient, is proportional to $1/x$; hence we can write,

$$\frac{dx}{dt} = \frac{k}{x} \quad (\text{cm sec}^{-1}) \quad (5.4)$$

(cf. Jost, 1961, pp. 340-2), where k is a rate constant with dimensions of $\text{cm}^2 \text{ sec}^{-1}$, that is proportional to the porous system diffusion coefficient of water, $D_w(T)$ multiplied by the difference in chemical potential of water, $\Delta\mu_{H_2O}(P, T)$ i.e. $k = D(\Delta\mu)/RT$ (see equation 4.4). Note $D/RT \cdot d\mu/dx$ is defined as the diffusional velocity (see section 4.2.1). Integrating the equation above gives the thickness of the layer, or the distance which the serpentine front has advanced, at a time, t :

$$x = k^{1/2} t^{1/2}$$

$$= \left(\frac{D}{RT} \Delta \mu_{H_2O} \right)^{1/2} t^{1/2}$$

$$= (\text{constant}) t^{1/2} \quad (5.5)$$

which is commonly called the parabolic rate law (cf., equation 4.7). This model assumes that the change in the free energy of water is linear; so the system is then quasi-stationary. Differentiating this equation with respect to distance as well as time (i.e. a partial derivative) would also result in a rate expression composed of a constant times $t^{1/2}$, but would not significantly improve the accuracy of the proposed linear model (cf. Drever, 1982, pp. 129-32).

At temperatures near 300°C, where the estimated value of D_{H_2O} is on the order of $10^{-4} \text{ cm}^2 \text{ sec}^{-1}$, water may penetrate serpentinized peridotites by quasi-viscous flow. Therefore, as discussed in Chapter 4, " D_{H_2O} " may not actually be a true diffusion coefficient. However, as long as the value of the "transport coefficient" has been fairly accurately measured, and the rate limiting reaction mechanism (eg. transport of water through a reaction layer with parabolic thickening of the product material) is known, mathematical models of the form given above should give reasonable kinetic information about the process itself - regardless of whether the rate constant used has been derived from Ficks first law or Darcy's law. The

diffusion coefficient D, derived from Fick's law, has been used in this study, because at moderate temperatures the transport of water in serpentinized peridotites is probably dominated by molecular mass transfer (ie. diffusion). This is a reasonable assumption considering the relatively small size of the void defects in serpentinized peridotites, and the magnitude of most of the temperature extrapolated diffusion coefficients. Still, it is possible that at temperatures close to the upper stability of serpentine and under conditions where ΔPH_2O is large, that quasi-viscous flow may become increasingly important. It is important to remember that a pressure gradient, or a chemical potential gradient, may produce a concentration (density) gradient which will drive a diffusive flux of water.

The thickness of a serpentinized peridotite layer (in meters), in which all the olivine and pyroxene have been converted to serpentine, is plotted as a function of time (years) in Figure 5.3 for different reaction temperatures (using the simplified parabolic equation $x^2 = 2Dt$).

The results presented in Fig. 5.2 and Table 5.1 show clearly that serpentinization is a rapid process; eg. at 300°C a layer of serpentine on the order of 1 kilometer will be formed in a block of peridotite in about 10^6 years. We can see that the volume of peridotite that will be hydrated during the life-span of, for example, a single continental-based hydrothermal event (3×10^4 to 3×10^5

Figure 5.3

Curves showing the distance, x , the reaction front advances versus time, t , for different values of $D_{H_2O}(T)$. These reaction distances were obtained using the simplified parabolic rate equation, $x = (2Dt)^{1/2}$.

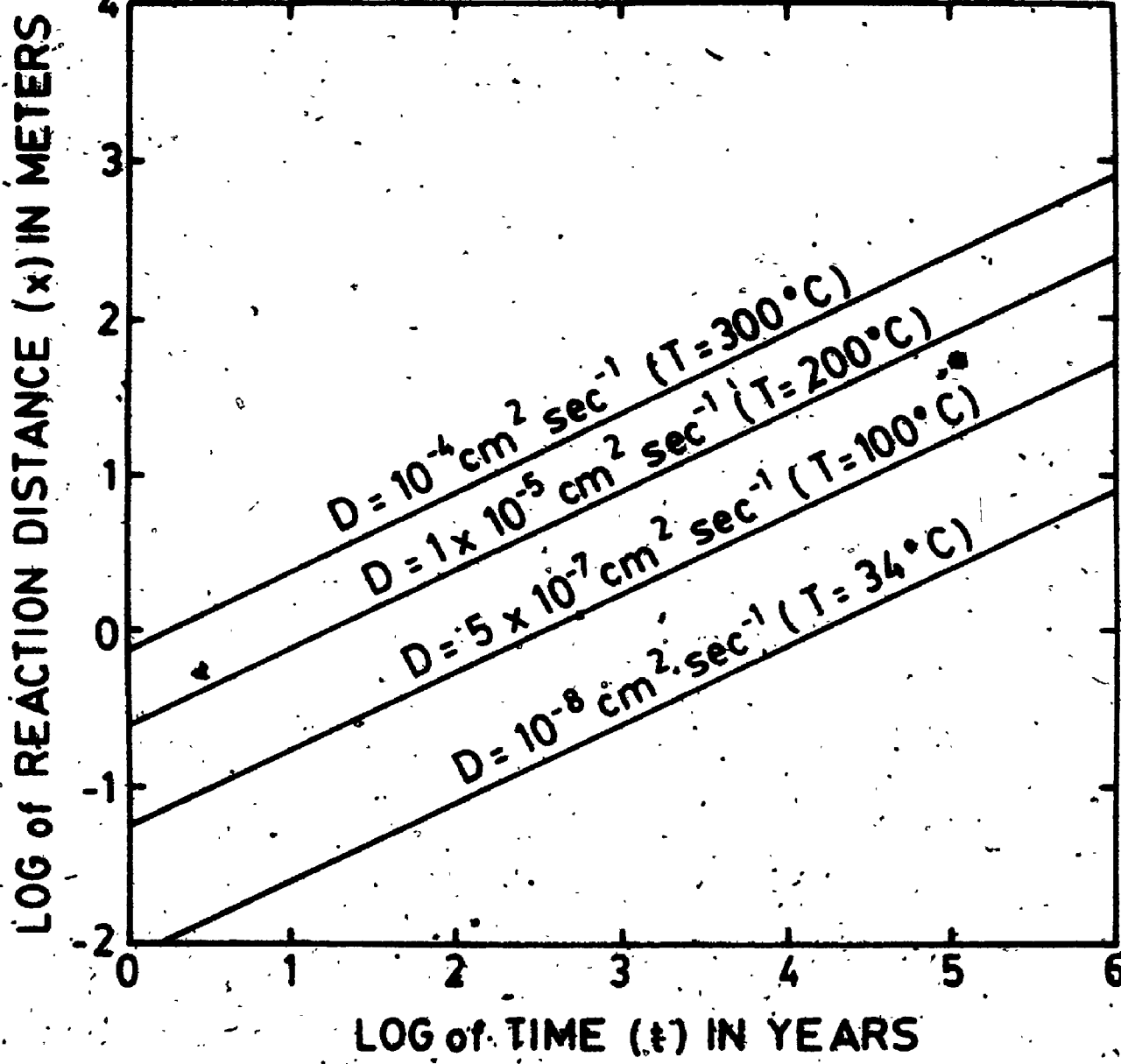


Table 5.1. Typical rates of serpentinization at moderate temperatures, obtained using the equation $x = (2Dt)^{1/2}$

T(°C)	D _{H₂O} (cm ² sec ⁻¹)	x(meters)	t(years)
34	10^{-8}		
100	5×10^{-7}	100	3×10^6
200	10^{-5}	100	1.5×10^5
300	10^{-4}	100	1×10^4

To completely serpentinize 1 km \approx 1 Ma at 300°C.

years; Ellis, 1979; Elder, 1976) is likely to be substantial when macro-cracks are spaced at distances of a few hundred meters or less.

The discussion, so far, has considered only the serpentinization that results when water is diffusing into a block of peridotite in a direction normal (i.e. x) to a vertical crack. Hot circulating water may, in fact, encounter a somewhat horizontal layer of peridotite at the crust-mantle interface and then begin forming a layer of serpentinized peridotite that increases slowly with age and shows lower seismic velocities (cf. Clague and Straley, 1977; Lewis and Snydsman, 1980). A serpentinized peridotite layer 1-2 kilometers thick is not unreasonable considering the estimated diffusion coefficients of water (see Figure 4.4) even if, as suggested by Lister (1980), the convective permeability necessary to create large Rayleigh numbers and vigorous convection extends only to the base of the gabbroic layer (i.e., to the base of layer 3).

5.2 A Semi-quantitative Analysis of the Forces and Fluxes

Coupled to Serpentinization

Coupled to a chemical potential gradient, that drives a diffusive flux of water and causes the reaction, is a chemically produced heat flux driven by the heat of hydration (the temperature gradient) and a flux of oxygenum to

driven by an effective pressure (stress) gradient-generated because of the large volume change of the reaction (see equations 1.1 and 1.2), i.e.

$$J_{H_2O} = - c RT \frac{D du}{dx} \text{ chemical flux (see eq. 4.4)}$$

$$q = K \frac{dT}{dx} \text{ heat flux} \quad (5.6)$$

$$P = \dot{\epsilon}(t) \frac{d\sigma}{dx} \text{ pressure flux} \quad (5.7)$$

where P is the pressure flux (dynes $\text{cm}^{-3} \text{ sec}^{-1}$), q is the heat flux ($\text{cal cm}^{-2} \text{ sec}^{-1}$), $\dot{\epsilon}$ is the volume strain rate ($\dot{\epsilon} = \Delta V/t$, where ΔV is the volume expansion of the solid phases due to serpentinization) in sec^{-1} , K is the coefficient of thermal conductivity ($\text{cal cm}^{-1} \text{ sec}^{-1} \text{ oc}^{-1}$), $d\sigma/dx$ is the stress gradient in $\text{dynes cm}^{-2} \text{ cm}^{-1}$, and dT/dx is the temperature gradient ($^{\circ}\text{C cm}^{-1}$).

At temperatures close to 3000°C the serpentinization reaction will generate an effective stress (i.e.

~~* $P_{swelling} \sim P_{load} = P_{effective}$ on the order of at least 5×10^8 dynes (see Table 3.2). The volume strain rates, $\dot{\epsilon}$, that will develop at the peridotite-serpentine interface in layers of serpentine 1 meter and 100 meters thick, assuming a volume change of 40% and reaction times of 10^7 seconds and 10^{12} seconds, are on the order of 10^{-6}~~

sec^{-1} (deformation will be fast) and $10^{-12} \text{ sec}^{-1}$ respectively (deformation is slow; cf. Price, 1975). These rates show that even without any detailed knowledge of the morphology of the cracks seen in serpentinites one is able to deduce that, in some cases, fracturing must cause high local strain rates to develop. These strain rates may in part be responsible for the microearthquakes reported near and away from ridge crests (Francis, 1981).

The volume change of the reaction, integrated over several million years, may cause a substantial increase in the elevation of seafloor topography. If most of the expansion is directed upwards - as is likely considering the crustal stress's distribution - in the time it takes to completely serpentinize a kilometer of peridotite (1 Ma) the crust will be raised about 400 meters. Opposing this is the slower thermal contraction of the ocean crust predicted by the square root of time law: $h = s(t)^{1/2}$ where h is the topographic height (km), s is the slope constant ($.39 \text{ km } (\text{m.y.})^{-1/2}$) (Lister, 1980).

Because serpentinization is highly exothermic (see equations 1.1 and 1.2), heat produced by the reaction may increase the rate of water diffusion, and if reaction rates are fast there is the additional possibility that the existing geothermal gradient (30°C km^{-1} based on an average q of 1.5 HFU) will be increased significantly. The

follows that given by Martin in 1970; which we believe, given the experimentally determined values of D_{H_2O} , can now be somewhat more accurately estimated.

Consider the serpentinization of 1 km³ of peridotite at a (Moho) depth of 8 km ($h_1 = 8 \times 10^5$ cm) below the sediment-seawater interface (a gradient of 30°C/km is assumed). The heat of hydration, H_R , in a peridotite (e.g. harzburgite) is roughly 200 calories per cm³ (see Fyfe and Lonsdale, 1981). If the time required to completely serpentinize 1 km (1×10^5 cm) of peridotite is on the order of 5×10^{13} sec (1.5×10^6 years) when $D_w = 10^{-4}$ cm² sec⁻¹ and $T = 2400^\circ\text{C}$, the heat flux, q^0 (cal s cm⁻² sec⁻¹), produced by the reaction (in the overlying crust, layer 1) when integrated over the reaction time, is:

$$q(1) = H_R/t$$

$$\text{so, } q(1) = \frac{200 \text{ cal/cm}^3}{10^{13} \text{ sec}} (10^5 \text{ cm})$$

$$= 4 \times 10^{-7} \text{ cal s cm}^{-2} \text{ sec}^{-1} \text{ (or 2 HFU).}$$

And the resulting heat flux q^* through the serpentine layer (i.e. into layer 1), will be,

$$\begin{aligned} q^* &= q(1) + q^0 \text{ (steady state conductive heat flux)} \\ &= (4 \times 10^{-7}) + (1.5 \times 10^{-6}) \\ &= 1.9 \times 10^{-6} \text{ cal cm}^{-2} \text{ sec}^{-1}. \end{aligned}$$

17

The immediate effect of the reaction is to change the normal steady state temperature distribution above the serpentine layer. The heat produced by the reaction diffuses to the surface slowly; the time, t , required for the heat to reach the surface - and establish a new quasi-steady state heat profile - is given by the equation (Verhoogen et al., 1970)

$$t = \frac{h^2}{\alpha} \text{ (seconds)},$$

where h is the depth to the heat source (cm), α (PT) is the thermal diffusivity ($\text{cm}^2 \text{ sec}^{-1}$). (Note $\alpha = k/c$, where c is the specific heat capacity in $\text{cal g}^{-1} \text{ }^\circ\text{C}^{-1}$.) If $\alpha = 5 \times 10^{-3} \text{ cm}^2 \text{ sec}^{-1}$ a time of 4 Ma is obtained. Considering the semi-quantitative nature of the calculation, it is constructive to assume a quasi-stationary temperature gradient has been reached when the serpentine front had advanced 1 km (i.e. q^* is now the new heat flux at the surface), and to calculate the rise in temperature at the top of the serpentine layer (T_{h_1} at $8 \times 10^5 \text{ km}$), and at the serpentine-peridotite interface (T_{h_2}). The temperature in layer 1 is given by the equation,

$$T_{h_1} = (q^*/K_1) x + T_0$$

therefore, $T_{h_1} = T_0 + \frac{1.9 \times 10^{-6}}{K} (8 \times 10^5)$

if K_1 , the thermal conductivity, is 5×10^{-3} cal $\text{cm}^{-1} \text{sec}^{-1}$ $^{\circ}\text{C}^{-1}$, and T_0 , the temperature at the surface = 0,

$$T_{h1} = 304^{\circ}\text{C}.$$

The heat of the reaction has caused the temperature to rise about 60°C , both in and immediately above the serpentine layer (i.e. assuming a geothermal gradient of $30^{\circ}\text{C km}^{-1}$). The temperature at the serpentine-peridotite interface, T_{h2} at a depth of 9 km is given by the equation,

$$q^* = K \frac{\Delta T}{h}$$

therefore, as $h = 1 \text{ km}$ ($1 \times 10^5 \text{ cm}$),

$$\Delta T = \frac{1.9 \times 10^{-6}}{5 \times 10^{-3}} (1 \times 10^5)$$

$$= 38^{\circ}\text{C}, \text{ and } T_{h2} \approx 342^{\circ}\text{C}$$

(cf. Martin, 1970, equation 20). If equilibrium is not reached until the serpentine layer is 2 km thick, $q^* = 1.7 \times 10^{-6} \text{ cal cm}^{-2} \text{ sec}^{-1}$, $T_{h1} = 272^{\circ}\text{C}$ and T_{h2} ($\approx 10 \text{ km}$) $\approx 340^{\circ}\text{C}$.

As the rate of the reaction is dependent on a number of variables, the former value is probably not unreasonable. The serpentinization of peridotite bodies at shallower depths in the crust - 1 or 2 km (at a reaction

temperature of 300°C) - would establish a quasi-steady state condition more rapidly with the surrounding rocks and would thus generate larger heat fluxes.

Observations on "strange" thermal springs near fossil sutures are common. It is possible that if peridotite slices are left in such regions, that abnormal heat fluxes may be generated by serpentinization (W. S. Fye, pers. comm.).

5.3 Limits on the Depth of Serpentinization in the Crust

5.3.1 The Lower Boundary

When the temperature rises above about 400°C ($P_{H_2O} < P_{total}$) the slope of the equilibrium P_{H_2O} curve - representing the upper stability limit of serpentine - becomes essentially vertical, P_{H_2O} increases rapidly and the reaction is soon stopped (i.e. $\Delta\mu_{H_2O} = 0$). The results of the swelling pressure calculations (Appendix II, Table 3.2) show that unless the fugacity of water, f_{H_2O} , is very low (< 50 bars, $T \leq 3500-4000^\circ C$) no effective ($P_{swelling} - P_{load} \leq 0$) swelling pressure stress is likely to develop at typical depths and fluid (P_{fluid}) pressures in the crust. But as long as there is a gradient in P_{H_2O} , water will continue to flow to the reaction site; it is easy to see that in this case the degree of serpentinization will be constrained by the volume of crack space provided by thermal contraction (see Epp and

Suyenaga, 1978). By rapidly reducing the difference in P_{H_2O} to zero in this P-T region, the temperature places a fairly rigid limit on the depth of serpentinization in the ocean or continental crust: i.e. about 10 km if the heat of hydration is included in the calculation (300°C/km gradient assumed).

5.3.2 The Upper Boundary

Normal metamorphic logic is that Pfluid is hydrostatic to depths of 5 km, $T = 1000^\circ C$, and $P_{H_2O} \approx 500$ bars in continental crust; just as in the seafloor crust peridotites can be expected to occur at moderate depths and be serpentinized.

At temperatures near 1000°C the rate of diffusion, as shown by the diffusion coefficient, will be too low to account for any substantial amount of serpentinization, unless cracks are spaced at distances of a few meters or less. For example, when $D = 5 \times 10^{-7} \text{ cm}^2 \text{ sec}$ ($T = 1000^\circ C$) and a reaction time of 10^3 and 10^4 years, the serpentine front will penetrate a distance of $x \approx 1.5$ meters and 5.6 meters, respectively.

Obducted peridotite slabs often exhibit an extensive, close spaced (meter scale) joint pattern (Hopson et al., 1981; Boudier and Coleman, 1981; Coleman, 1982, personal communication; this study). Considering the brittle behavior of serpentinized peridotites at low confining

pressures, which is coupled to residual volume stresses introduced by a possible earlier stage of higher temperature serpentinization, this deformation fabric is not at all surprising. The additional serpentinization of peridotites by meteoric water during emplacement is possible, of course, and is consistent with the stable isotope studies of Wenner and Taylor (1971, 1973, 1974).

At lower temperatures (i.e. 400°C) both hydration kinetics (nucleation?) and diffusion rates may become rate limiting (cf. Martin and Fye, 1970; Nesbitt and Bricker, 1978). This is a strong reason for doubting the conclusion of Barnes and O'Neill (1969) - that serpentinization is an on-going process at 250°C. Instead the aquifer chemistry may represent the faster dissolution of hydrous and anhydrous magnesium silicate minerals, along an open joint or shear crack system, as compared to the precipitation of the hydrous phases.

5.3.3 Summary and Conclusions

At temperatures between 1000°C and 4000°C ($P_{H_2O} < P_{total}$) the rate of advance of the reaction front driving serpentinization is controlled by the rate of water transport through an existing porous product layer of serpentinized material, itself a function of the bulk rock permeability, temperature and the intrinsic properties of the mass transfer of water in the porous medium itself.

At moderate depths (ie. > 5 km) in the crust there is a large potential, given the fluid pressure, P_{H_2O} (i.e. μ_{H_2O}), of a column of water in a crack connected to the surface, for either diffusive or quasi-viscous (Darcy-type) flow into fresh ultramafic rocks. It must be emphasized that it is the chemical reaction rate which is responsible for the large gradient in P_{H_2O} across the reaction interface.

Because the gradient in the chemical potential is a strong function of the thickness of the serpentinized layer and thus in crack spacing (and permeability), negative feedback will tend to slow down the rate of reaction as the reaction layer expands and the driving gradient decreases. In general, the faster the rate of water penetration the larger the heat flux - which will increase the rate of diffusion - and the higher the strain rate - which will tend to increase the rate of crack growth. One would also expect an oscillating growth of new cracks, and a temporary increase in permeability associated with the build-up of the swelling pressure stress (Fig. 5.4).

The serpentinization reaction consumes H_2O and generates a swelling pressure - as do clays (e.g. montmorillonites) with exchangeable interlayer cations - because the chemical potential of water, μ_{H_2O} ($= RT \ln \frac{P_{H_2O}}{P_0}$ at low total pressures), at the reaction interface is low in comparison to that of the

33
OF / DE

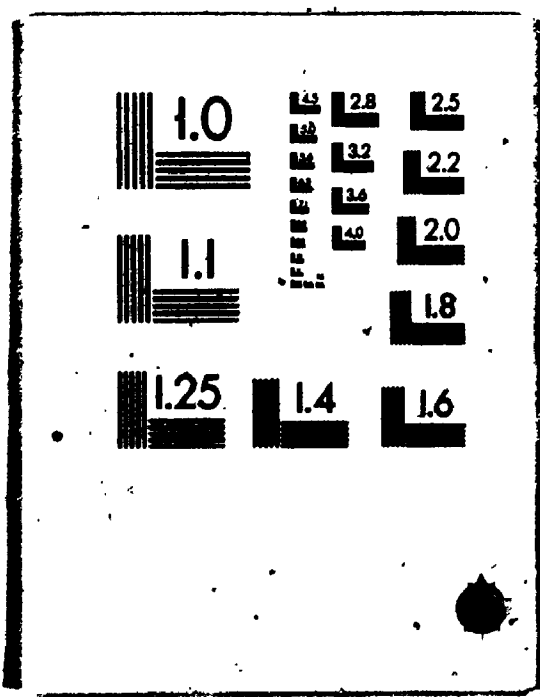
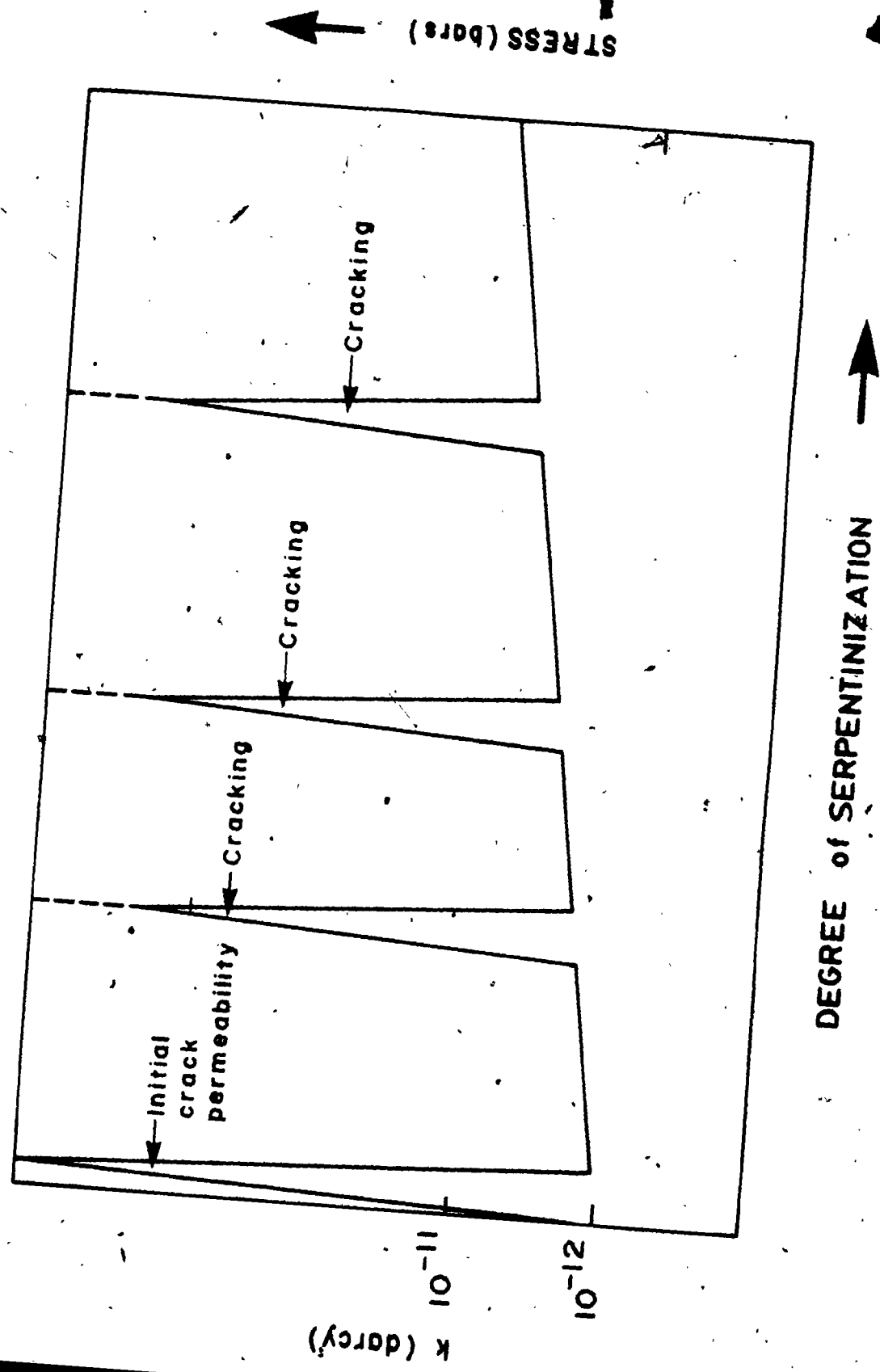


Figure 5.4

Diagram showing possible permeability fluctuations due to episodic cracking during serpentinization. Following crack formation, slower reaction rebuilds the stress to generate new cracks.



fluid solvent ($\text{aq.} \mu\text{H}_2\text{O}$) in the surrounding environment. As a result a large difference in $P_{\text{H}_2\text{O}}$ is produced. Therefore, in order for the reaction system to regain equilibrium with the fluid entering the system hydration must occur and the rock must swell. If this swelling pressure stress exceeds the lithostatic pressure being applied to the solid phases, the rock will crack, not once, but repeatedly.

Ultimately temperature is rate controlling, as the equilibrium (reaction) $P_{\text{H}_2\text{O}}$, transport coefficient, and the reaction kinetics are all strongly temperature dependent.

CHAPTER 6

SUMMARY AND CONCLUSIONS

It appears that water can penetrate serpentinized peridotites at appreciable rates by diffusing through defects caused by the buckling of the platy serpentine mineral, lizardite. However, under conditions where the temperatures are moderately high and the water pressure gradients are large the movement may be by slow Darcy flow. Diffusion coefficients on the order of 10^{-8} to 10^{-4} $\text{cm}^2 \text{ sec}^{-1}$ must be anticipated over temperatures from 30-300°C, respectively, inside the serpentine stability region. Using the simplified parabolic rate law, $x = (2Dt)^{1/2}$, such coefficients imply a mean penetration distance (x) through serpentinized peridotite in the range of 1-80 cm a^{-1} . Given the large PH_2O gradient produced by the reaction (i.e. PH_2O external - P_{eq} . interface), this process will cause large volume strains coupled to the flow of heat and water and reaction rates. Blocks of

peridotite undergoing rapid hydration may generate large volume strains which under most conditions will cause this massive portion of the rock to deform by a brittle mechanism, although at high confining pressures ($P > 1 \text{ kb}$), perhaps developed in part by volume expansion itself, serpentinites may deform plastically (ductilly) (Raleigh and Patterson, 1965). As the swelling pressures of this process are on the order of a kilobar, crack growth will be a continuous process. This is in accord with the complex array of cross-cutting microfractures ubiquitous to serpentinites on all scales. The reaction clearly will not be dependent on the continual removal of magnesium and silica by circulating fluids, for which there is no geochemical evidence.

Hydration will proceed more rapidly along intra- and inter-granular microfractures than perpendicular to cracks, but with a linear crack density of about 50 cracks/cm, observed in peridotites from the Philippines, most of the rock will be prone to attack at similar rates. It is also clear that if ultramafics occur at shallow depths in the ocean crust, vertical strains may cause apparent diapiric rise and exposure of small serpentinite bodies. An upward rate of movement of 1 mm/yr predicted by Bonatti (1976, see also Bonatti and Hamlyn, 1981) is quite reasonable.

Salt filtration depends on the cation exchange capacity of minerals other than serpentine, the porosity,

the solute concentration of the fluid in the crack, and streaming potentials generated by the fluid flow itself. More field work is needed to determine if very high salinity fluids will be produced (see Vanko and Batiza, 1982) by membrane filtration, but the experimental results presented in this study suggest that serpentinized peridotites behave somewhat semipermeably to salt ions (eg. Na^+ , Cl^-). If flow rates are very slow - and this must be a critical parameter - ions may have difficulty entering the rock during serpentinization, and as a consequence locally circulating fluids may become enriched in salt ions - especially Cl^- . To preserve electrical neutrality, either oxyhalides must precipitate or metal species must be leached from the surrounding rock.

According to Lister (1974, 1980, 1981), once active cracking penetration, and therefore also the "active" phase of hydrothermal circulation (with a life span of millions of years), ceases due to the combined effects of chemical alteration - e.g. serpentinization and/or static fatigue - , heat conduction from below will continue to drive a "passive" hydrothermal system..

During this stage, water circulating to the base of the ocean crust may lead to the moderately rapid hydration of the upper mantle, making serpentinization an integral part of ocean floor hydrothermal circulation and metamorphism. If the bulk permeability of the overlying crust

remains high enough for fluid to convect through the lower oceanic crust, the ocean crust may thicken gradually with age due to serpentization (Lewis and Snydsman, 1980; Mutter and Kempner, 1983). This will provide the additional seafloor heat flow and elevation not predicted by the $(\text{age})^{1/2}$ model (see Anderson and Skilbeck, 1981).

Although the permeability necessary for convection must gradually decrease with age as cracks are sealed, the evidence indicates strongly that convection - of which an increased proportion may be closed-system to recirculated flow - continues for tens of millions of years (i.e. >100 km from the ridge crest) (Davis and Lister, 1977; Anderson et al., 1979; Lister, 1981). Note, that while near ridge basalts show patchy alteration, in ophiolites the alteration is often pervasive.

One of the basic difficulties of making any definitive conclusion concerning the extent of metamorphism of lower crustal material is that our understanding of the structure beneath ridges is still incomplete (see report by Fye and Macdonald, 1984). If new lithosphere, in the form of seamounts, ridges, volcanoes, and blocks flows into fracture zones, as suggested by Smoot (1983), individual layers may be absent or thinner than normal oceanic crust, making them more accessible to attack by seawater. The complexity of normal oceanic crust is now being recognized in ophiolites (Lewis, 1983). It must also be recognized that the obduc-

tion of oceanic crust is a relatively rare process, and as such the metamorphism observed in ophiolites may not be completely representative of "typical" ocean floor processes (Coleman, 1983).

When macro-cracks are spaced on a scale of meters, as they are at Coto - because of the thermal contraction in the dykes cubic kilometers of peridotite may be totally serpentinized in a few thousand years. The extent and distribution of serpentinized peridotites, as well as the degree of serpentinization within the Zambales ophiolite, Philippines, may be typical of that forming beneath many modern island arcs or oceanic islands, whereas those exposed in the Ligurian ophiolite and Bay of Islands ophiolite may be characteristic of similar processes occurring within transform faults (Cortesogno et al., 1981), and in ocean crust and upper mantle with a more normal sea-floor spreading tectonic history (Casey et al., 1983; Karson, 1983), respectively. Ultramafic rocks dredged from the equatorial Mid-Atlantic Ridge by Bonatti et al. (1971), Aumento and Loubat (1971) and Dmitriev et al. (1971) contain microstructures, indicative of high local volume strains, that are very similar to those observed in the land based ophiolites discussed in this study (see above).

This study clearly shows that serpentinization is a rapid and continuous process in seafloor and deep groundwater environments. The reaction is controlled only by the

availability of water to ultramafic rocks through their cover. As the reaction consumes on the order of 5×10^{11} liters of water per km^3 of rock, serpentinized peridotites may represent a large sink for water in the ocean crust. Thus, during either the hydration or dehydration process, ultramafic rocks will produce some very special dynamic and chemical effects. Since peridotites are a dominant component of the earth's crust, these processes need to be considered more fully.

APPENDIX I

SUMMARY OF ANALYTICAL TECHNIQUES

I-1. Whole rock geochemistry

Ten major-oxides (Na_2O , SiO_2 , TiO_2 , $\text{-Al}_2\text{O}_3$, Fe_2O_3 , MnO , MgO , CaO , K_2O and P_2O_5) were determined by X-ray fluorescence using a Philips PW-1450 Automatic Sequential Spectrometer. The standard monitor used was FS94, supplied by R.W. Norrish (CSIRO, Australia). Except for Na_2O and LOI (volatiles, e.g. H_2O), the analyses were performed according to the fusion techniques of Norrish and Hutton (1969). Na_2O was analysed using pressed pellets; and loss on ignition (LOI) - i.e. H_2O - was calculated by determining the weight loss after roasting powdered samples of the rock for 2 hrs at 1100°C . This may include about 2 percent by weight of sorbed water (Hess and Otalora, 1964).

The results indicate that major element determinations are generally accurate to within 2-5% of the amount present, except for MgO , which in Mg-rich rocks (i.e. peridotites), may err by as much as 5-10%.

I-2. Electron microprobe mineral analyses

Mineral chemical analyses were obtained from 25 mm diameter polished thin sections coated with carbon, using a Materials Analysis Company model 400 electron microprobe equipped with three diffractometers and Krisel automation. The equipment was operated at 15 kv, and with a sample current of 25 nA. The following standards were used: bronzite for Mg, Si, and Fe; kaersutite for Al and Ti; diopside for Ca; orthoclase for K; albite for Na; chromite for Cr; phodonite for Mn; and biotite for Cl. The precision of replicate analysis indicates that the results are accurate to within \pm 1 to 2% for the major elements and up to \pm 10% for the minor elements.

I-3. Identification of the serpentine minerals, including brucite

A combination of optical (see Wicks and Whittaker, 1977), electron microscopic (see Cressy, 1979) and X-ray diffraction techniques are necessary for the accurate determination of the different serpentine minerals (i.e. antigorite, chrysotile, lizardite) and their proportions (see Mumpton and Thompson, 1973).

X-ray diffraction

Standard X-ray diffraction patterns of finely-powdered rock samples were obtained using a Rigaku/"Geigerflex"

X-ray diffractometer system; D/Max series. While this method is useful in determining if any serpentine minerals (including brucite) are present, it is not very diagnostic with regards to their actual identification (cf. Whittaker and Zussman, 1956).

However, by using a microbeam X-ray diffraction camera selected areas of a thin section can be removed, photographed, and compared with the optical (eg. textural) properties observed under the petrographic (and scanning electron microscope). Ten representative sections were studied - under the guidance of F. J. Wicks at the Royal Ontario Museum in Toronto - with a Norelco microbeam camera according to the methods of Wicks and Zussman (1975).

1-4. Density

The densities, ρ , of the serpentized peridotites were determined according to Archimedes' Principle; i.e. $\rho = WA \cdot L / WA - WL$, where L is the density of the liquid (eg. de-ionized water), WA is the weight of the solid sample in air, and WL is the weight of the solid when immersed in the liquid (Wilson, 1972). The density of a dry peridotite is taken as 3.25 g/cm^3 and that of a completely serpentized peridotite $\leq 2.55 \text{ g/cm}^3$ (Hess, 1964; Page, 1967).

1-5. Weight percent magnetite

The magnetite content was determined by measuring the

magnetic susceptibility - using a Bison Susceptibility Meter, Model 3103 - of powdered whole rock samples (of equal volume) against known standards. The results should be considered as semi-quantitative, as differences in grain - i.e. domain - sizes related to the crystallization of magnetite during serpentinization will produce a somewhat variable magnetic susceptibility curve. This effect is not completely removed by crushing and sieving the sample.

I-6. Effective porosity

The effective porosity was determined by drying the serpentine slices used in the experiments in an oven for 2 weeks at 110°C, and then measuring the weight loss; so: wt. H₂O lost (g) divided by (density of H₂O (g/cm³)) x volume of sample (cm³) = cm³ of liquid per cm³ of sample. When multiplied by 100 it is equivalent to the effective porosity; defined as the percentage of interconnected pore spaces in the total volume of rock.

APPENDIX II

THERMODYNAMIC CALCULATIONS, INCLUDING THE CONCENTRATIVE PROPERTIES OF AQUEOUS SALT SOLUTIONS

II-1. P-T diagrams

A) The vapor-pressure curve for the reaction serpentine + brucite = forsterite + H₂O, where P_{H₂O} = P_{total} under conditions where P_{H₂O} is low (i.e., < 100 bars) can be determined using the following thermodynamic relationships (see Fyfe et al., 1958; Fyfe, 1973).

$$(1) \left(\frac{\partial G}{\partial P} \right)_T = V$$

$$(2) \left(\frac{\partial G}{\partial T} \right)_P = -S$$

It is assumed that at low pressures the gas phase may be treated as essentially ideal; so the Gibbs free energy,

$$\Delta G_R = -RT \ln P_{H_2O}$$

and that for most reactions the change in entropy, $S \approx$ constant with T at moderate T's.

B) To correct the above curve for conditions where the pressure on the solids is non-hydrostatic (i.e. P on solids $\gg P_{\text{gas}}$, so $P_{H_2O} < P_{\text{total}}$), the new Gibbs free energy of reaction G^* under these conditions becomes,

$$\Delta G_{\text{Reaction}} = \Delta G_R^\circ + \int_{P_{\text{eq}}}^{P_{\text{solid}}} V_{\text{solids}} \, dP + \int_{P_{\text{eq}}}^{P_{H_2O}} V_{H_2O} \, dP = 0$$

(see Fyfe, 1973), where P_{eq} is the equilibrium vapor pressure under conditions where $P_{H_2O} = P_{\text{total}}$, P_{solid} is the lithostatic pressure being applied to the solids, and P_{H_2O} is the new equilibrium vapor pressure where $P_{H_2O} < P_{\text{total}}$.

Values for the entropy (ΔS_T°), the molar volume (ΔV_{solids}), and the Gibbs free energy of formation (ΔG_T°) were taken from Robie et al. (1979). The standard state is the stated temperature and 1 bar.

II-2. Swelling pressures

The swelling pressure, P_s , of the reaction is defined

as the total pressure needed to stop hydration, given a particular fluid pressure, $P_{\text{hydrostatic}} = P_{\text{H}_2\text{O}}$ in a crack. Let us assume that the reaction has reached equilibrium with a pressure P_s being applied by a piston, at a given T , and $P_{\text{H}_2\text{O}}$ in the environment. Therefore, the thermodynamic question that must be answered is: what load pressure, P_s , must be put on the piston to stop the reaction = pressure (or stress) the process can generate, ($T, P_{\text{H}_2\text{O}}$)? i.e.

$$\Delta G_R = \int_{P_{\text{eq}}}^{P_s} \Delta V_{\text{Solids}} dp - \int_{P_{\text{eq}}}^{P_{\text{H}_2\text{O}}} V_{\text{H}_2\text{O}} dp = 0$$

therefore,

$$\Delta V_{\text{Solids}} \Delta P_s = \int_{P_{\text{eq}}}^{P_{\text{H}_2\text{O}}} V_{\text{H}_2\text{O}} dp$$

where P_{eq} is the equilibrium vapor pressure at a given temperature (calculated in II-IB) and V is the change in the volume of the solid phases in cm^3 . The right hand side of the above equation can be calculated using values of $(G-H_o)_T, p$ of H_2O given in Sharp (1962), or using the fugacities of H_2O from Helgeson (1974) or Burnham et al. (1969). (Note: values of $(G-H_o)$ must be converted to cm^3

bars.)

II-3. Concentrative properties of aqueous solutions

The molal concentrations (moles kg⁻¹) of NaCl (Cs) and H₂O (Cw) in the various experimental salt solutions were taken from the Handbook of Physics and Chemistry (1973 by Wolf et al.). The solubility of salt in water at a given temperature is listed in Mellor's (see Briscoe et al., 1961).

Values of the solubility of sucrose (cane sugar), C₁₂H₂₂O₁₁ are listed in Seidel (1917, p. 693). The activity of water in a saturated sucrose solution is given by Robinson and Stokes (1965).

The activities of water (a_{H₂O}) in different NaCl solutions - used in the calculation of osmotic pressures - are listed in Robinson and Stokes (1965).

APPENDIX III

**REPRESENTATIVE MICROPROBE ANALYSES FROM THE ZAMBALES
OPHIOLITE COMPLEX, PHILIPPINES**

Table III-1a. Representative microprobe analyses of partially serpentinized olivines and pyroxenes and serpentinite veins from Acohe Mine area.

Analysis No.	Sample No. H-8 (Mesh textured serpentinite)										(Veln) 10 10
	1	2	3	4	5	6	7	8	9		
SiO ₂	36.29	41.67	41.13	40.46	41.65	34.52	37.57	37.34	20.24		40.30
TiO ₂	0.0	0.0	0.0	0.01	0.0	0.0	0.0	0.0	0.0		0.0
Al ₂ O ₃	0.66	0.0	0.0	0.0	0.0	0.0	0.0	0.0	0.0		0.0
FeO	5.49	2.51	2.93	2.84	1.91	7.38	5.15	5.52	9.78		1.04
MnO	0.0	0.09	0.0	0.0	0.02	0.0	0.03	0.03	0.08		0.04
MgO	38.96	41.05	40.78	40.69	41.16	40.56	41.36	41.00			45.50
CaO	0.0	0.01	0.01	0.02	0.0	0.0	0.0	0.06	0.02		0.0
NiO	0.19	0.0	0.0	0.0	0.0	0.05	0.0	0.14	0.07		0.0
Cr ₂ O ₃	0.07	0.0	0.14	0.23	0.04	0.0	0.24	0.01	0.05		0.18
K ₂ O	0.01	0.02	0.0	0.0	0.06	0.03	0.05	0.0	0.02		0.01
Na ₂ O	0.0	0.0	0.0	0.0	0.0	0.03	1.64	0.0	0.0		0.0
Total	81.69	85.35	84.98	84.25	84.84	82.54	84.44	85.75	75.76		83.66

Table III-1a (continued)

Analysis No.	Sample No. H-B				
	(Vein) 11	(Vein) 12	(Vein) 13	(Vein) 14	(Vein) 15
SiO ₂	41.86	40.63	41.29	40.36	40.39
TiO ₂	0.0	0.0	0.0	0.0	0.0
Al ₂ O ₃	0.0	0.0	1.59	0.33	0.0
FeO	1.12	7.80	1.04	2.92	3.15
MnO	0.0	0.01	0.14	0.08	0.11
MgO	42.40	37.41	39.98	41.06	40.27
CaO	0.0	0.0	0.0	0.0	0.04
NiO	0.0	0.0	0.0	0.18	0.01
Cr ₂ O ₃	0.16	0.0	0.06	0.07	0.10
K ₂ O	0.0	0.03	0.01	0.06	0.02
Na ₂ O	0.0	0.0	0.0	0.0	0.0
Cl					
Total	85.55	85.89	84.12	85.05	84.06
					86.13

Analyses (a) 1, 4, 6-8, 9 (shows signs of secondary alteration?), 14 and 15 mesh textured lizardite + brucite + chrysotile; (b) 2, 3 and 5 sill-p-fibre chrysotile; (c) 10-13 and 16 lizardite + brucite + chrysotile in complex vein.

Table III-1b

Sample No. DA-6.
(Mesh textured serpent line)

Analyzed No.	1	2	3	4	5	6	7	8	9	10
SiO ₂	36.28	36.34	33.93	32.61	34.32	35.09	35.52	35.79	33.79	33.66
TiO ₂	0.00	0.00	0.00	0.04	0.01	0.06	0.0	0.02	0.04	3.00
Al ₂ O ₃	0.00	0.00	0.00	0.00	0.00	0.0	0.0	0.0	0.0	0.0
FeO	5.35	3.82	7.09	5.93	6.52	6.36	6.31	5.27	7.85	6.50
MnO	0.07	0.23	0.45	0.20	0.11	0.28	0.0	0.17	0.0	0.08
MgO	41.88	40.05	42.54	41.60	41.62	42.43	40.24	42.44	41.93	41.95
CaO	0.01	0.00	0.00	0.04	0.01	0.07	0.03	0.0	0.0	0.0
Na ₂ O	0.22	0.07	0.13	0.16	0.11	0.53	0.47	0.31	0.11	0.0
Cr ₂ O ₃	0.11	0.35	0.11	0.00	0.00	0.0	0.0	0.0	0.0	0.0
Na ₂ O	0.44	1.49	0.97	0.00	0.04	0.0	0.0	0.0	0.0	0.0
Cl	0.46	0.11	0.09	0.00	0.17	0.0	0.02	0.04	0.0	0.0
K ₂ O	0.0	0.01	0.03	0.02	0.03	0.0	0.0	0.0	0.10	0.11
Total	84.83	82.47	85.33	80.61	82.93	84.81	82.58	84.03	83.82	85.31

Table III-1b (continued)

		Sample No. DA-6				
Analysis	No.	11	12	13	14	15
SiO ₂		34.23	33.26	34.07	36.06	36.58
TiO ₂		0.04	0.0	0.0	0.0	0.0
Al ₂ O ₃		0.00	0.0	0.0	0.0	0.02
FeO		8.03	6.30	7.04	8.39	6.54
MnO		0.02	0.0	0.0	0.01	0.0
MgO		41.84	41.77	40.91	41.39	41.98
CaO		0.0	0.05	0.0	0.03	0.03
NiO		0.28	0.0	0.0	0.02	0.0
Cr ₂ O ₃		0.0	0.0	0.07	0.09	0.03
Na ₂ O		0.0	0.0	0.0	0.0	1.08
Cl		0.0	0.09	0.29		
K ₂ O		0.05	0.04	0.0	0.10	0.02
Total		84.48	81.52	82.37	86.08	86.27

Analyses 1-15, mesh rims of lizardite-II and brucite.

Table III-1c

		Sample No. DA-9 (Mesh textured serpentine)						
Analysis No.	1	2	3	4	5	6	7	8
SiO ₂	35.19	25.44	27.88	40.57	35.16	25.79	33.19	34.05
TiO ₂	0.02	0.0	0.0	0.0	0.06	0.0	0.0	0.0
Al ₂ O ₃	0.0	0.0	0.0	0.0	0.0	0.0	0.0	0.0
FeO	5.58	10.80	5.13	4.43	6.71	7.96	6.86	7.03
MnO	0.0	0.0	0.0	0.0	0.0	0.0	0.0	0.0
HgO	40.88	40.55	40.16	40.22	41.29	41.72	41.39	41.25
CaO	0.0	0.0	0.0	0.0	0.0	0.0	0.0	0.0
MnO	0.0	0.0	0.0	0.11	0.0	0.27	0.19	0.0
Cr ₂ O ₃	0.02	0.07	0.07	0.0	0.0	0.0	0.19	0.0
K ₂ O	0.01	0.0	0.0	0.08	0.0	0.0	0.06	0.0
Na ₂ O	0.0	0.0	0.0	0.0	0.0	0.0	0.0	0.0
Cl	0.09	0.06	0.05	0.05	0.01	0.09	0.28	0.44
Total	81.72	76.91	73.30	85.46	83.23	75.83	82.10	82.77

Analyses 1-9, lizardite-II + brucite in mesh rims.

Table III-1d

Sample No. W9-82 (Complexly banded serpentine vein)										
Analysis No.	1	2	3	4	5	6	7	8	9	10
SiO ₂	36.38	35.83	36.64	39.86	37.12	40.07	34.51	38.77	37.86	39.54
TiO ₂	0.0	0.0	0.04	0.0	0.02	0.0	0.0	0.0	0.0	0.0
Al ₂ O ₃	4.20	5.44	1.88	0.11	0.44	0.11	0.18	0.20	0.34	2.55
FeO	7.53	8.82	5.77	6.15	8.64	6.37	7.58	6.10	7.74	8.69
MnO	0.05	0.24	0.05	0.0	0.0	0.08	0.08	0.14	0.16	0.05
MgO	36.86	37.31	36.98	38.56	36.68	38.29	41.27	37.59	39.50	40.72
CaO	0.10	0.0	0.02	0.0	0.01	0.04	0.0	0.0	0.0	0.0
NiO	0.21	0.0	0.0	0.04	0.06	0.18	0.09	0.12	0.14	0.28
Cr ₂ O ₃	0.51	0.46	0.42	0.04	0.28	0.14	0.04	0.04	0.22	0.01
K ₂ O	0.06	0.06	0.02	0.04	0.0	0.04	0.0	0.05	0.02	0.01
Na ₂ O	0.36	0.27	0.0	0.04	0.0	0.0	0.91	0.0	0.0	0.0
Total	86.26	88.43	81.83	84.83	83.25	85.32	84.04	83.01	85.98	91.85

Table III-1d (continued)

Sample No. H9-82										
Analysis No.	11	12	13	14	15	16	17	18	19	20
S102	38.72	34.83	40.04	40.50	39.45	39.90	39.60	36.64	39.87	39.49
TiO ₂	0.08	0.0	0.0	0.0	0.0	0.0	0.0	0.0	0.0	0.0
Al ₂ O ₃	1.13	4.76	0.17	0.05	0.82	0.71	0.43	0.64	0.53	0.58
FeO	5.85	8.57	6.91	5.71	6.44	7.22	6.02	5.39	4.99	6.23
MnO	0.09	0.08	0.0	0.20	0.13	0.10	0.02	0.13	0.0	0.11
MgO	37.88	36.66	37.73	46.61	37.15	37.76	38.70	36.34	38.21	38.32
CaO	0.02	0.0	0.03	0.0	0.04	0.0	0.05	0.0	0.01	0.01
NiO	0.0	0.23	0.0	0.0	0.07	0.18	0.11	0.05	0.24	0.46
Cr ₂ O ₃	0.54	0.14	0.08	0.0	0.54	0.14	0.13	0.09	0.03	0.18
K ₂ O	0.0	0.03	0.10	0.03	0.0	0.05	0.0	0.03	0.0	0.0
Na ₂ O	0.02	0.0	0.16	0.16	0.0	0.0	0.0	0.0	0.0	0.20
Total	84.32	85.30	85.21	93.26	84.64	86.06	85.05	79.29	83.88	85.58

Table III-1d (continued)

Analysis No.	Sample No. Hg-82								
	21	22	23	24	25	26	27	28	29
SiO ₂	35.39	39.87	39.07	38.98	36.06	39.47	34.69	40.00	39.99
TiO ₂	0.0	0.0	0.0	0.0	0.0	0.0	0.0	0.0	0.0
Al ₂ O ₃	0.63	0.45	0.61	0.62	0.03	2.27	1.67	1.16	0.84
FeO	6.23	5.89	6.19	5.86	5.68	13.32	5.82	10.64	7.18
MnO	0.21	0.05	0.09	0.0	0.0	0.28	0.14	0.01	0.10
MgO	38.60	38.36	37.64	38.23	38.94	32.27	36.00	33.99	38.88
CaO	0.07	0.0	0.01	0.0	0.02	0.01	0.15	0.51	0.0
NiO	1.11	0.35	0.09	0.23	0.0	0.0	0.25	0.0	0.0
Cr ₂ O ₃	0.0	0.09	0.14	0.0	0.14	0.17	0.19	0.15	0.09
K ₂ O	0.04	0.01	0.06	0.05	0.05	0.06	0.02	0.05	0.08
Na ₂ O	0.0	0.0	0.0	0.0	0.0	0.35	0.07	0.0	0.0
Total	82.28	85.07	83.97	81.42	88.20	78.92	86.51	87.16	85.60

Table III-1d (continued)

Analysis No.	Sample No. H9-82							
	31	32	33	34	35	36	37	38
SiO ₂	39.26	37.05	38.46	39.68	33.70	38.45	40.48	40.75
TiO ₂	0.0	0.0	0.0	0.0	0.0	0.0	0.02	0.0
Al ₂ O ₃	0.07	1.24	0.73	3.49	0.10	2.59	0.50	0.64
FeO	7.51	8.64	8.20	6.70	6.98	7.68	6.79	6.51
MnO	0.08	0.05	0.09	0.06	0.13	0.22	0.10	0.01
MgO	40.29	38.96	39.52	40.34	43.22	38.20	37.67	39.27
CaO	0.0	0.0	0.0	0.0	0.0	0.02	0.02	0.11
NiO	0.14	0.18	0.15	0.08	0.12	0.0	0.09	0.01
Cr ₂ O ₃	0.13	0.0	0.08	0.09	0.14	0.74	0.16	0.05
K ₂ O	0.01	0.0	0.02	0.02	0.0	0.0	0.11	0.02
Na ₂ O	0.16	0.0	0.04	0.20	0.05	0.0	0.05	0.0
Total	87.65	86.13	87.28	90.66	84.43	87.90	85.88	87.36
								86.52
								83.43

Analyses of lizardite + brucite + chrysotile: (a) 1-4, 6-8, 13-18, 24, 25 and 40 in complex cross-cutting vein; (b) 5, 9, 11 and 27 (after pyroxene), 30, 31, 34 (after pyroxene), 35, mesh rims (edges) of above vein; (c) 19, 23, 29, 38 (after pyroxene) 39 yellowish high relief mesh rims along edge of vein; (d) 26 and 32 (after pyroxene), 33 reddish high relief (prisms) in vein above; (e) 10 (after pyroxene) 12, 28 (after pyroxene) yellowish, and 37 (yellowish) mesh rims (veinlets) away from vein; (f) 20-22 dendritic (Ni-Fe-S?) filaments and associated serpentine; (g) 36, pyroxene bastite.

Table III-1e

Analysis No.	Sample No. DA-3 (Serpentine veins)						
	1	2	3	4	5	6	7
SiO ₂	41.48	30.81	40.72	39.62	35.51	40.65	36.43
Al ₂ O ₃	0.40	0.63	1.40	0.14	0.09	2.05	0.04
FeO	7.39	7.75	8.62	6.57	7.59	5.59	7.12
MnO	0.23	0.07	0.0	0.0	0.09	0.08	0.03
MgO	46.78	43.10	37.02	39.71	41.37	37.78	41.57
CaO	0.13	0.04	0.16	0.03	0.05	0.11	0.11
NiO	0.0	0.0	0.0	0.0	0.40	0.07	0.04
Cr ₂ O ₃	0.12	0.0	0.31	0.0	0.0	0.0	0.0
Na ₂ O	0.0	0.0	0.0	0.0	0.0	0.0	0.0
Cl	0.16	0.03	0.86	0.02	0.12	0.21	0.10

Analyses 107 lizardite + brucite in ribbon-textured vein.

Table III-2a. Representative microprobe analyses of completely serpentinized olivines and pyroxenes from the Coto Mine area.

Analysis No.	Sample No. C-31 (Chrysotile veins/hourglass textured serpentine)									
	1	2	3	4	5	6	7	8	9	10
SiO ₂	41.16	42.07	41.34	41.29	43.46	44.16	42.89	43.54	41.71	36.86
TiO ₂	0.0	0.0	0.0	0.01	0.0	0.0	0.0	0.0	0.0	0.0
Al ₂ O ₃	0.05	1.59	0.05	0.02	0.46	0.27	0.48	0.05	0.89	1.31
FeO	2.47	3.18	2.76	2.55	1.66	1.91	1.97	1.76	4.12	4.24
MnO	0.0	0.0	0.0	0.03	0.0	0.0	0.0	0.0	0.13	0.0
MgO	40.72	39.28	39.79	40.03	40.40	40.21	39.73	42.06	36.14	36.83
CaO	0.0	0.07	0.0	0.0	0.0	0.0	0.03	0.0	0.06	0.07
NiO	0.16	0.23	0.25	0.31	0.05	0.0	0.0	0.0	0.51	0.50
Cr ₂ O ₃	0.07	0.27	0.08	0.05	0.24	0.0	0.07	0.20	0.53	0.49
K ₂ O	0.02	0.0	0.0	0.02	0.05	0.02	0.02	0.0	0.04	0.03
Na ₂ O	0.0	0.0	0.0	0.0	0.0	0.0	0.02	0.0	0.0	0.0
Total	84.64	86.69	84.27	84.30	86.33	86.57	85.20	87.62	84.13	80.33

Analyses (a) mesh textured serpentine. 1, 2 (bastite), 3-4, and 9-10 (bastites). (b) 5-8 cross-fiber chrysotile in vein.

Table III-2b

Sample No. 909-1
(Mesh textured serpentine)

Analysis No.	1	2	3	4	5	6	7	8	9	10
SiO ₂	40.03	38.21	41.37	39.03	40.64	40.06	37.32	38.84	38.74	39.71
Al ₂ O ₃	0.39	0.09	0.20	0.82	0.17	0.33	0.20	0.51	0.68	0.31
FeO	2.98	1.92	1.66	2.27	1.55	1.58	3.59	3.89	2.99	3.28
MnO	0.04	0.07	0.02	0.03	0.08	0.11	0.27	0.08	0.14	0.20
MgO	39.81	39.65	40.96	39.64	40.70	40.59	38.99	39.71	39.28	39.64
CaO	0.02	0.11	0.07	0.03	0.04	0.02	0.05	0.04	0.02	0.0
NiO	0.0	0.0	0.68	0.0	0.09	0.54	0.05	0.23	0.29	0.25
Cr ₂ O ₃	0.0	0.0	0.0	0.37	0.0	0.0	0.0	0.0	0.0	0.0
Na ₂ O	0.0	0.31	0.13	0.07	0.17	0.03	0.30	0.34	0.96	0.59
Cl	0.15	0.16	0.18	0.17	0.02	0.04	0.09	0.14	0.19	0.22
Total	83.42	80.52	85.27	82.42	83.47	83.29	80.87	83.79	83.29	84.20

Analysis (a) 1-3, and 5-10 are lizardite + brucite + chrysotile in mesh textured serpentine.
(b) 4 - bastite.

Table III-2c

Analysis No.	Sample No. III-X (Chrysotile veins/hourglass textured serpentinite)					
	1	2	3	4	5	6
SiO ₂	42.65	31.79	42.99	38.48	40.34	38.38
TiO ₂	0.0	0.0	0.0	0.0	0.22	0.0
Al ₂ O ₃	0.0	0.0	0.0	0.0	0.0	0.0
FeO	2.41	4.41	0.87	2.36	1.67	2.13
MnO	0.05	0.08	0.16	0.04	0.0	0.23
MgO	41.56	51.16	42.39	42.31	44.47	44.83
CaO	0.0	0.0	0.0	0.0	0.0	0.0
NiO	0.17	0.0	0.0	0.0	0.0	0.0
Cr ₂ O ₃	0.13	0.11	0.14	0.15	0.18	0.04
K ₂ O	0.08	0.0	0.06	0.02	0.07	0.0
Na ₂ O	0.0	0.0	0.0	0.0	0.0	0.0
Total	87.06	87.55	86.61	83.36	86.95	85.60

Analyses (a) 1, 2, 4-6 - chrysotile + brucite in cross-fibre veins.

(b) 3 - lizardite + brucite + chrysotile in hourglass textures.

Table 111-2d

Analysis No.	Sample No. DC-5 (Mesh textured serpent line)									
	1	2	3	4	5	6	7	8	9	10
SiO ₂	34.43	34.39	34.61	35.80	34.54	34.80	40.63	40.70	37.21	36.75
TiO ₂	0.05	0.0	0.0	0.0	0.04	0.0	0.0	0.0	0.0	0.0
Al ₂ O ₃	1.16	1.23	1.17	1.23	1.41	1.14	0.0	0.0	1.11	1.06
FeO	3.95	3.98	3.97	3.28	3.20	3.37	1.84	2.41	2.79	2.68
MnO	0.21	0.11	0.0	0.0	0.0	0.0	0.0	0.0	0.0	0.0
MgO	38.53	39.71	39.02	36.81	38.00	38.68	41.75	41.69	38.55	38.65
CaO	0.0	0.0	0.0	0.0	0.0	0.0	0.0	0.0	0.0	0.0
NiO	0.09	0.48	0.07	0.0	0.0	0.07	0.0	0.0	0.0	0.0
Cr ₂ O ₃	0.56	0.52	0.50	0.60	0.74	0.72	0.0	0.23	0.87	0.95
K ₂ O	0.0	0.0	0.0	0.0	0.0	0.0	-0.02	0.0	0.01	0.0
Na ₂ O	0.0	0.0	0.0	0.0	0.0	0.0	0.0	0.0	0.0	0.0
Cl	0.20	0.33	0.13	0.23	0.22	0.45	0.12	0.09	0.46	0.23
Total	79.18	80.77	79.46	77.95	78.16	79.22	84.37	85.13	81.00	80.30

Table III-2d (continued)

Analysis No.	Sample No. DC-5				
	11	12	13	14	15
SiO ₂	40.07	35.38	40.07	36.23	36.16
TiO ₂	0.0	0.0	0.0	0.0	0.0
Al ₂ O ₃	0.0	0.96	0.0	1.02	1.27
FeO	2.60	3.75	2.14	3.66	3.73
MnO	0.0	0.0	0.0	0.0	0.0
MgO	40.17	39.27	39.86	39.39	39.18
CaO	0.0	0.0	0.0	0.0	0.0
Na ₂ O	0.0	0.0	0.0	0.0	0.0
Cr ₂ O ₃	0.21	0.70	0.0	0.75	0.61
K ₂ O	0.0	0.0	0.0	0.0	0.0
Na ₂ O	0.0	0.0	0.0	0.0	0.13
Cl	0.15	0.25	0.22	0.29	0.44
Total	83.20	80.31	82.29	81.33	81.53

Analyses (a) 1-5, 6, 9, 10, 12, 14 and 15 - lizardite + chrysotile in bastites.
 (b) 7, 8, 11 and 13 - lizardite - It + brucite + chrysotile in mesh (including ribbon) and hourglass textures.

APPENDIX IV

REPRESENTATIVE WHOLE-ROCK (XRF) ANALYSES FROM THE ZAMBALES
OPHIOLITE COMPLEX, PHILIPPINES

Table IV-1. Representative major element analyses of serpentinitized peridotites from the Acoche Mine area, recalculated to 100% anhydrous.

Sample No.	A-2-30	A-2	A-2a	A-2c	DA-6	DA-4	DA-9	DA-3
SiO ₂	44.47	40.49	39.79	45.65	40.07	39.98	40.83	45.70
TiO ₂	0.02	0.02	0.02	0.04	0.02	0.02	0.02	0.06
Al ₂ O ₃	1.02	0.19	0.19	1.44	0.09	0.16	0.10	2.46
FeO*	7.47	8.19	8.10	10.94	8.72	8.93	8.36	6.86
MnO	0.14	0.35	0.16	0.14	0.16	0.16	0.15	0.12
MgO	45.62	50.53	51.58	41.57	50.91	50.63	50.36	41.96
CaO	1.22	0.17	0.13	0.05	0.10	0.10	0.16	2.75
K ₂ O	0.0	0.0	0.0	0.14	0.0	0.0	0.0	0.03
P ₂ O ₅	0.0	0.0	0.0	0.0	0.0	0.0	0.0	0.03
BaO	0.0	0.0	0.0	0.0	0.0	0.0	0.0	0.0
Na ₂ O	0.0	0.0	0.0	0.0	0.0	0.0	0.0	0.0
H ₂ O	10.42	13.00	13.70	13.13	11.56	12.70	12.60	6.07
Total	99.96	99.94	99.97	99.97	100.07	99.98	99.98	99.90
Mg/Si	1.02	1.24	1.28	0.91	1.27	1.25	1.23	0.92
Percent*								
Serpentinitized	70	86	81	100	80	83	84	20
Rock type	H	D	D	D	b	b	H	

*The Percent Serpentinitized was determined by density measurements (Appendix I-4).

Table IV-1 (continued)

Sample No.	DA-1	LFVINTA	K1-65A	A-1250	A8-194	A-3	J4-110	Kd-56	H9-82	H9-82(cr)
SiO ₂	40.17	44.29	39.18	42.00	40.39	43.08	40.37	40.25	44.19	39.73
TiO ₂	0.02	0.04	0.03	0.02	0.03	0.03	0.02	0.01	0.04	0.03
Al ₂ O ₃	0.26	1.18	0.60	0.94	0.98	0.42	0.25	0.15	1.13	0.34
FeO*	6.74	7.38	9.52	8.46	7.86	9.34	7.71	8.11	7.71	7.79
MnO	0.12	0.14	0.14	0.16	0.15	0.17	0.15	0.06	0.15	0.14
MgO	52.40	45.47	50.27	45.56	50.09	44.13	51.28	51.19	44.82	51.89
CaO	0.27	1.55	0.22	2.81	0.13	2.90	0.19	0.11	1.92	0.05
K ₂ O	0.0	0.0	0.0	0.01	0.36	0.01	0.0	0.0	0.01	0.0
P ₂ O ₅	0.0	0.0	0.0	0.0	0.0	0.0	0.0	0.0	0.0	0.0
BaO	0.0	0.0	0.0	0.0	0.0	0.0	0.0	0.0	0.0	0.0
Na ₂ O	0.0	0.0	0.0	0.0	0.0	0.0	0.0	0.0	0.0	0.0
H ₂ O	16.76	6.06	12.37	10.75	14.00	13.97	11.84	16.23	4.90	15.48
Total	99.98	100.05	99.96	99.98	99.99	99.98	99.97	99.98	99.97	99.97
Mg/Si	1.3	1.03	1.28	1.08	1.24	1.03	1.26	1.27	1.01	1.3
Percent Serpentinitized	92	36	82	65	81	100	78	100	28	62
Rock Type	σ	H	H	H?	H?	D	D	H	H	CHROMITITE

*) Total iron given as FeO.

**) H = harzburgite
D = dunite

Table IV-2. Major element analyses of serpentinized peridotites from the Coto Mine area,
recalculated to 100% anhydrous.

Sample No.	C-111	C-35	W-2-11	DC-5	DC-7	C-21	C-31	C-5	CW-850
S102	40.25	45.30	45.30	40.20	43.24	42.79	45.79	44.55	40.57
T102	0.04	0.03	0.10	0.02	0.02	0.06	0.01	0.02	0.02
Al2O ₃	0.45	0.90	0.51	1.20	0.42	7.09	0.52	0.53	1.21
FeO	8.14	10.00	7.77	8.29	7.41	6.66	7.55	7.40	8.09
MnO	0.14	0.14	0.11	0.14	0.13	0.25	0.06	0.13	0.13
MgO	50.96	43.60	46.12	50.13	48.73	42.91	46.05	47.09	49.96
CaO	0.0	0.01	0.02	0.0	0.03	0.21	0.0	0.26	0.0
K ₂ O	0.01	0.0	0.05	0.0	0.0	0.0	0.0	0.0	0.0
P ₂ O ₅	0.0	0.0	0.0	0.0	0.0	0.0	0.0	0.0	0.0
BaO	0.0	0.0	0.0	0.0	0.0	0.0	0.0	0.0	0.0
Na ₂ O	0.0	0.0	0.0	0.0	0.0	0.0	0.0	0.0	0.0
H ₂ O	22.78	14.84	12.97	14.99	14.12	21.64	13.30	13.70	14.86
Total	99.99	99.98	99.98	99.98	99.98	99.95	99.98	99.98	99.98
Mg/Si	1.26	0.96	1.02	1.24	1.11	1.00	1.00	1.05	1.23
Percent Serpentinized	96	100	100	92	95	-	97	93	100
Rock Type	D	H	D	H	D	D	D	D	D

Table IV-2 (continued)

Sample No.	909-5
SiO ₂	44.38
TiO ₂	0.0
Al ₂ O ₃	0.35
FeO	9.66
MnO	0.12
MgO	45.47
CaO	0.0
K ₂ O	0.0
P ₂ O ₅	0.0
BaO	0.0
Na ₂ O	0.0
H ₂ O	10.41
Total	99.98
Mg/SI	1.02
Percent Serpentinized	95
Rock type	H

1) Total iron given as FeO.

2) H - harzburgite

D - dunite

3) H₂O = 101

APPENDIX V

SUMMARY OF THE PHYSICAL AND CHEMICAL PROPERTIES OF THE
SERPENTINE SLICES USED IN THE EXPERIMENTS

Table V - 1. Summary of solution concentrations, run temperatures, and the physical properties of the serpentine slices used in the experiments.

Sample No.	Run No.	Run Temperature °C	Concentration of NaCl Solution in Cell B moles kg ⁻¹	Sample Thickness (X) mm	Density gm ⁻³	Percent Serpentinized	% Porosity* cm ³ cm ⁻³ x 100
DC-51	1	34	6	3.2	2.59	95	2-3
	2	34	6				
	3	34	2				
	4	34	6				
DC-52	1	34	6				
DC-53	2	34	2				
	1	34	6				
	2	34	6				
DC-71	1	40	6				
	2	34	6				
	3	25	6				
	4	24	6				
DC-72	1	34	2				
DC-73	2	34	2				
	3	34	2				
	4	40	2				
	1	24	2				
DC-74	2	25	6				
	3	34	6				
	4	40	6				
	1	24	6				
DC-75	1	34	6				

Table V-1 (continued)

Reference No.	Run No.	Run Temperature °C	Concentration of NaCl Solution in Cell B moles kg ⁻¹	Sample Thickness (x) mm	Density g m ⁻³	Percent Serpentinized	% Porosity*
				cm ³ cm ⁻³ × 100			
DC-76	1	34	2	4	2.8		
	2	34	3	6			
	3	34	3	6			
Liguria-1	1	34	2	6	3.0	92	
-2	1	34	6	3.4			
-2	2	34	4				
DA-61	1	34	6				
DA-62	1	25	6				
	2	24	6				
	3	40	6				
DA-91	1	34	6				
	2	24	6				
	3	40	6				
DA-41	1	34	6				
DA-31	1	34	6				
DA-32	1	34	6				
Bay-11	1	34	6				
				2.7	80	1.5	
				2.2	2.67	84	
				3.0	2.68	83	
				6	3.1-3.025	20-30	
				6	2.86	60	
				6	2.7		

Total = 38

*The porosity given is a representative value for a particular sample type (i.e. partial or completely serpentinized sample).

Table V-2. The mineralogy and textures of the serpentinite slices used in the diffusion experiments.

Sample No.	Igneous Rock Name	Serpentine Textures and Mineralogy
1) dA-4	Dunite (<10% opx)	Mesh lizardite-II + brucite Same
2) dA-9		Same
3) dA-6		Same
4) dA-3	Harzburgite (15-30% opx)	* 1) Mesh lizardite-II + brucite 2) Cross-cutting veins composed of complexly banded (II to fracture) lizardite
5) dC-7	Dunite	*Mesh, hourglass and ribbon-textured lizardite-II + brucite + chrysotile Same
6) dC-5		Harzburgite Same
7) Urigia I.	Harzburgite	Same
8) Bay of Islands	Harzburgite (30% opx)	1) Mesh lizardite-II 2) Cross-cutting veins filled with complexly banded lizardite

*Cross-cutting fractures in dC-5 and dC-7 are "filled" with ribbon-textured serpentinite and magnetite.

APPENDIX VI

**A SUMMARY OF THE ADDITIONAL AVERAGE FLUXES AND DIFFUSION
COEFFICIENTS MEASURED FOR THE TRANSPORT OF H₂O AND NaCl
THROUGH SERPENTINIZED PERIDOTITES**

Table VI-1. Fluxes and diffusivities of water and salt through serpentinized peridotites' at temperatures from 25 to 400°C in response to different NaCl concentrations.

Sample and Run No.	Time days	Average Flux of water moles cm^{-2} day $\times 10^{-6}$	$D_{\text{H}_2\text{O}}$	Time days	Average Flux of Salt moles cm^{-2} day $\times 10^{-6}$	D_{salt}	$D_{\text{H}_2\text{O}}$ D_{salt}
<u>250°C - 2 molal NaCl</u>							
DC-722	(30)	24.59	4×10^{-8}	(100)	8.39	1.5×10^{-8}	2.66
<u>- Saturated Sucrose</u>							
DC-741	(30)	54.91	9.52×10^{-8}				
<u>- 6 molal NaCl</u>							
DC-732	(29)	99.03	5.4×10^{-8}	(30)	3.8	2.2×10^{-9}	24.5
DA-61	(23)	3.68	2×10^{-9}	(30)	0.017	1.1×10^{-11}	101.62
<u>340°C - 2 molal NaCl</u>							
DC-513	(58)	30.9	5.7×10^{-8}				
DC-522	(49)	26.4	6.7×10^{-8}	(52)	0.96	2.2×10^{-9}	30.45
DC-721	Flux of water erratic						
DC-723	(38)	28.43	4×10^{-8}				

Table VI-1 (continued)

Sample and Run No.	Time days	Average Flux of water moles cm^{-2} day $\times 10^{-6}$	$D_{\text{H}_2\text{O}}$ $\text{cm}^2 \text{ sec}^{-1}$	Time days	Average Flux of Salt moles cm^{-2} day $\times 10^{-6}$	D_{Salt} $\text{cm}^2 \text{ sec}^{-1}$	$D_{\text{H}_2\text{O}}$ D_{Salt}
DC-731	(83)	5.904	1×10^{-8} (85)		2.76	4.8×10^{-9}	2.08
DC-763	(25)	115.68	1.67×10^{-7} (74)		4.69	7.6×10^{-9}	24.60
			- 3 molal NaCl				
DC-762	(11)	162.43	1.75×10^{-7} (12)		5.84	6.3×10^{-9}	27.76
			- Sat. Sucrose				
DC-742	(30)	58.16	1×10^{-7}				
DC-752	(11)	168.48	2.6×10^{-7} (12)		6.66	5.4×10^{-9}	24.07
			- 400C - Sat. Sucrose				
DC-743	(33)	40.65	3.5×10^{-8}				
			- 6 molal NaCl				
DC-533	(33)	140.64	8.68×10^{-8} (23)		4.21	2.6×10^{-9}	
DC-7242	(2)	76.9	7.75×10^{-8} (33)		11.8	6.8×10^{-9}	11.39
DA-63	(33)	38.64	1.64×10^{-8} (23)		1.64	7×10^{-10}	23.42
			- 2 molal NaCl				
DC-7242	(2)	38.4	6.4×10^{-8} (33)		1.54	2.6×10^{-9}	24.61

{2} Reverse flow of salt and water observed.

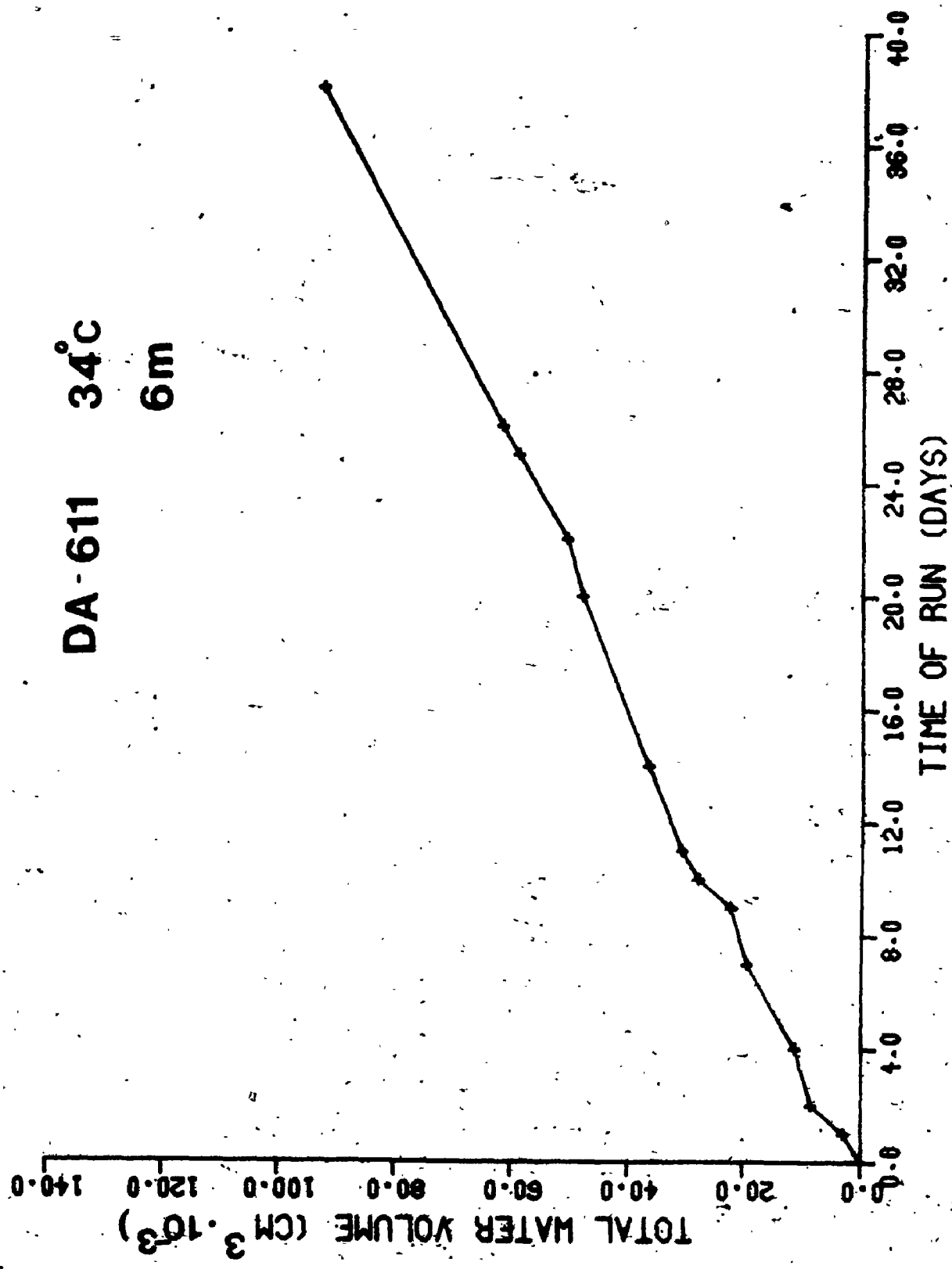
APPENDIX VII

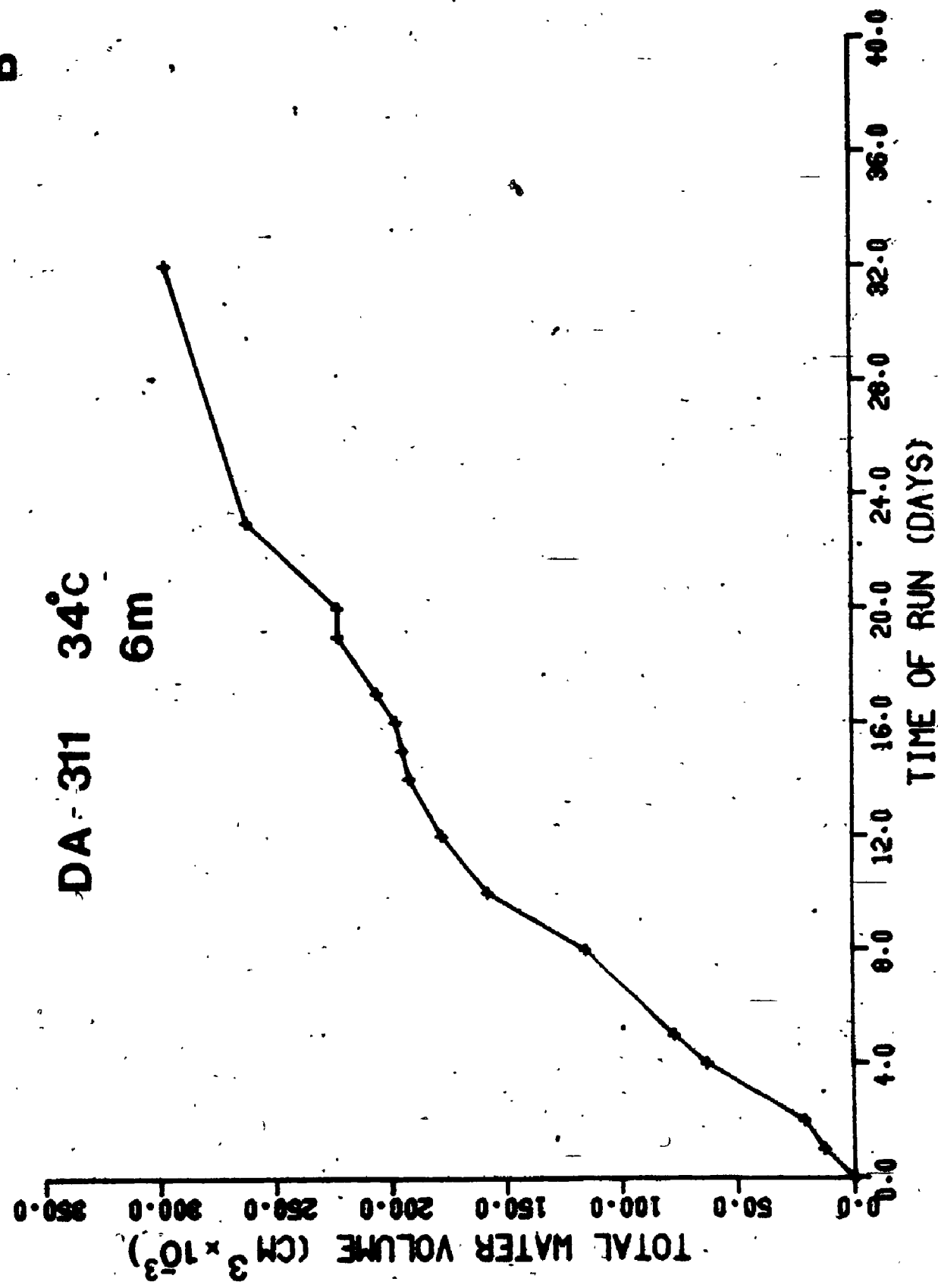
**REPRESENTATIVE FIGURES SHOWING THE TOTAL VOLUME OF WATER
TRANSPORTED ACROSS A SLICE AS A FUNCTION OF TIME**

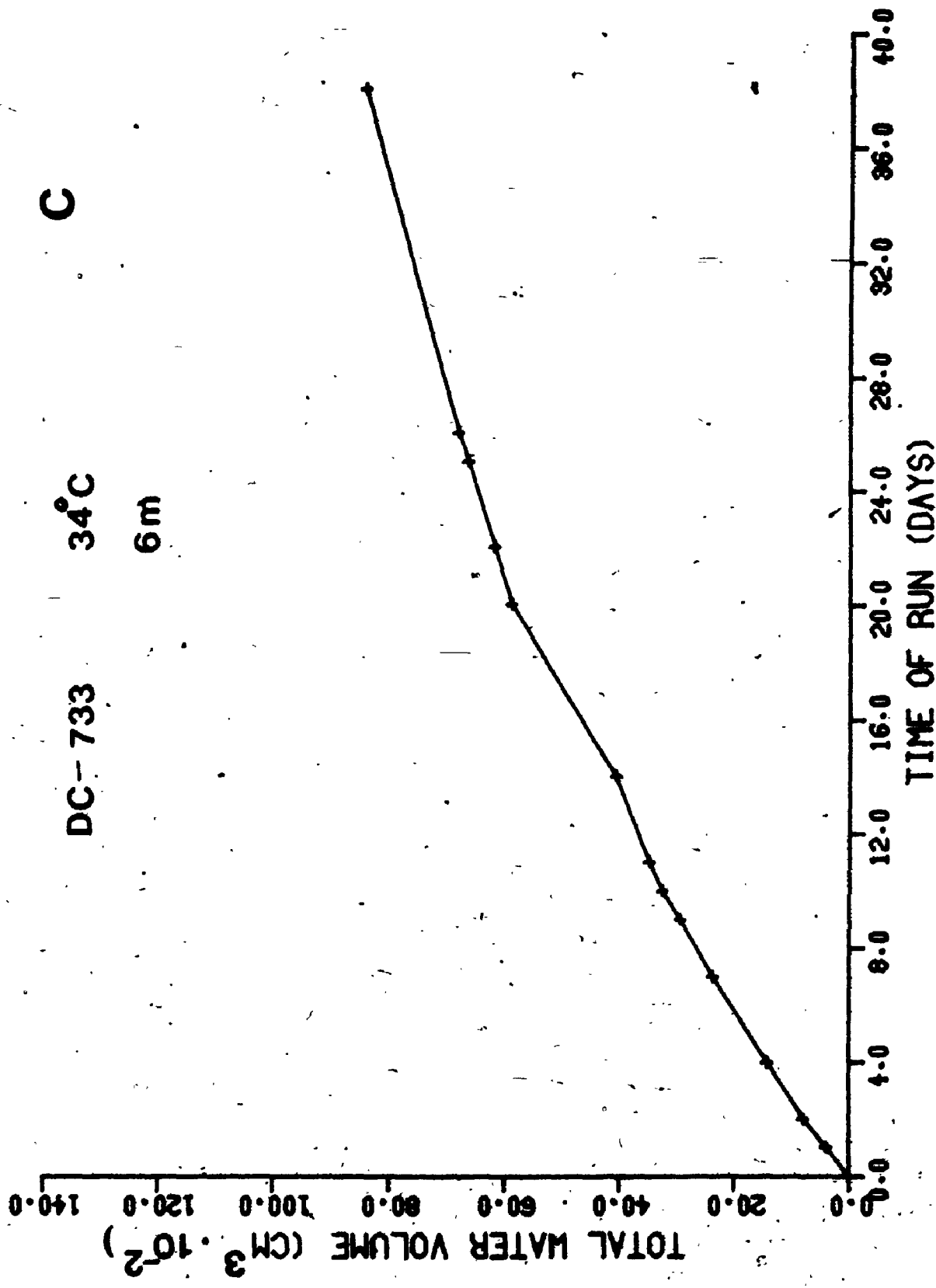
Figure VII-1A to J

Representative plots showing the total volume of water observed flowing through the slices as a function of time. This value was averaged and then converted to moles in order to calculate the fluxes and diffusion coefficients listed in Tables 4.1 to 4.4. The heading contains the sample number, the run number and the temperature under which the run was conducted, followed (underneath) by the solution concentration (in molal units).

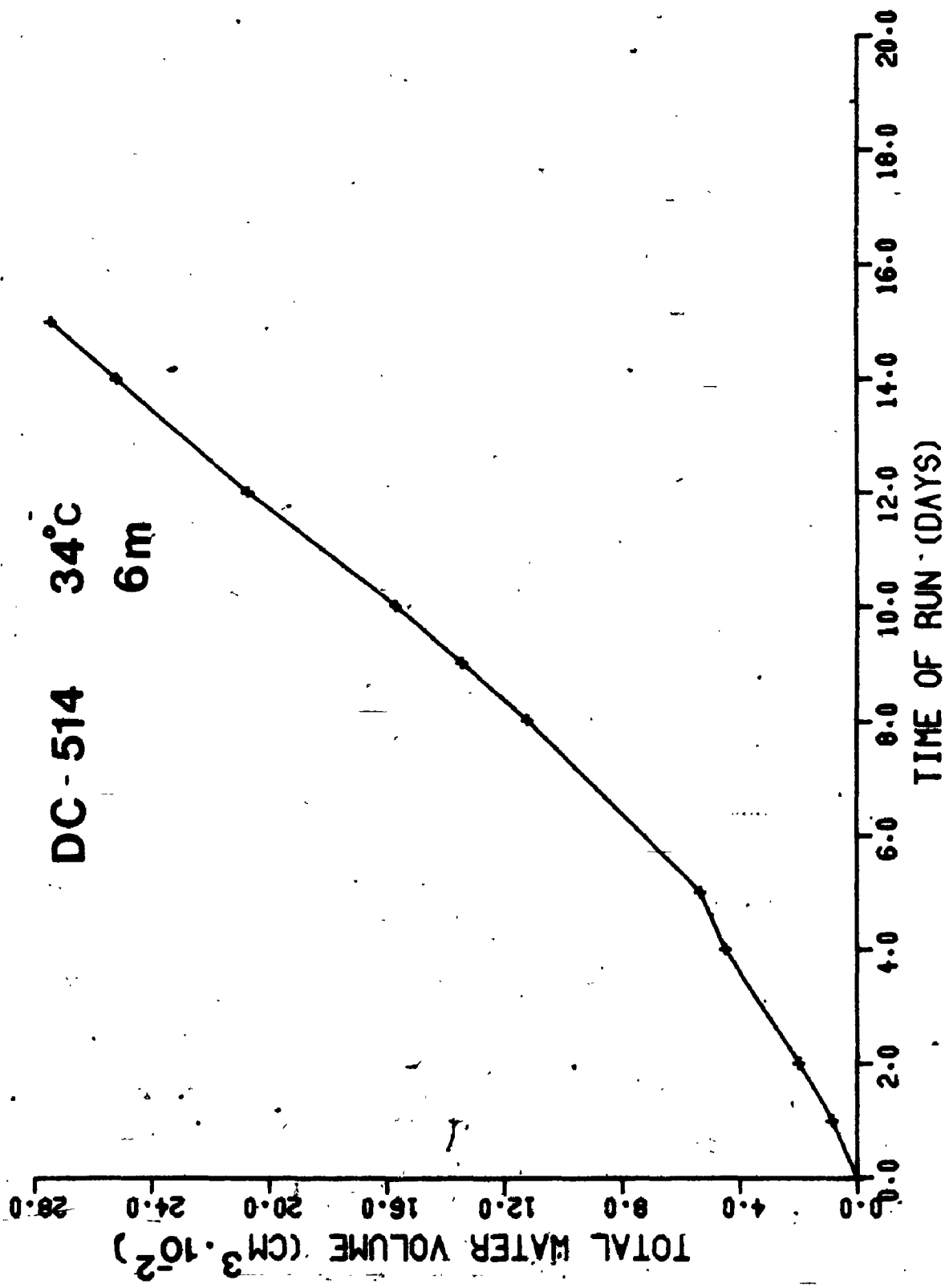
A

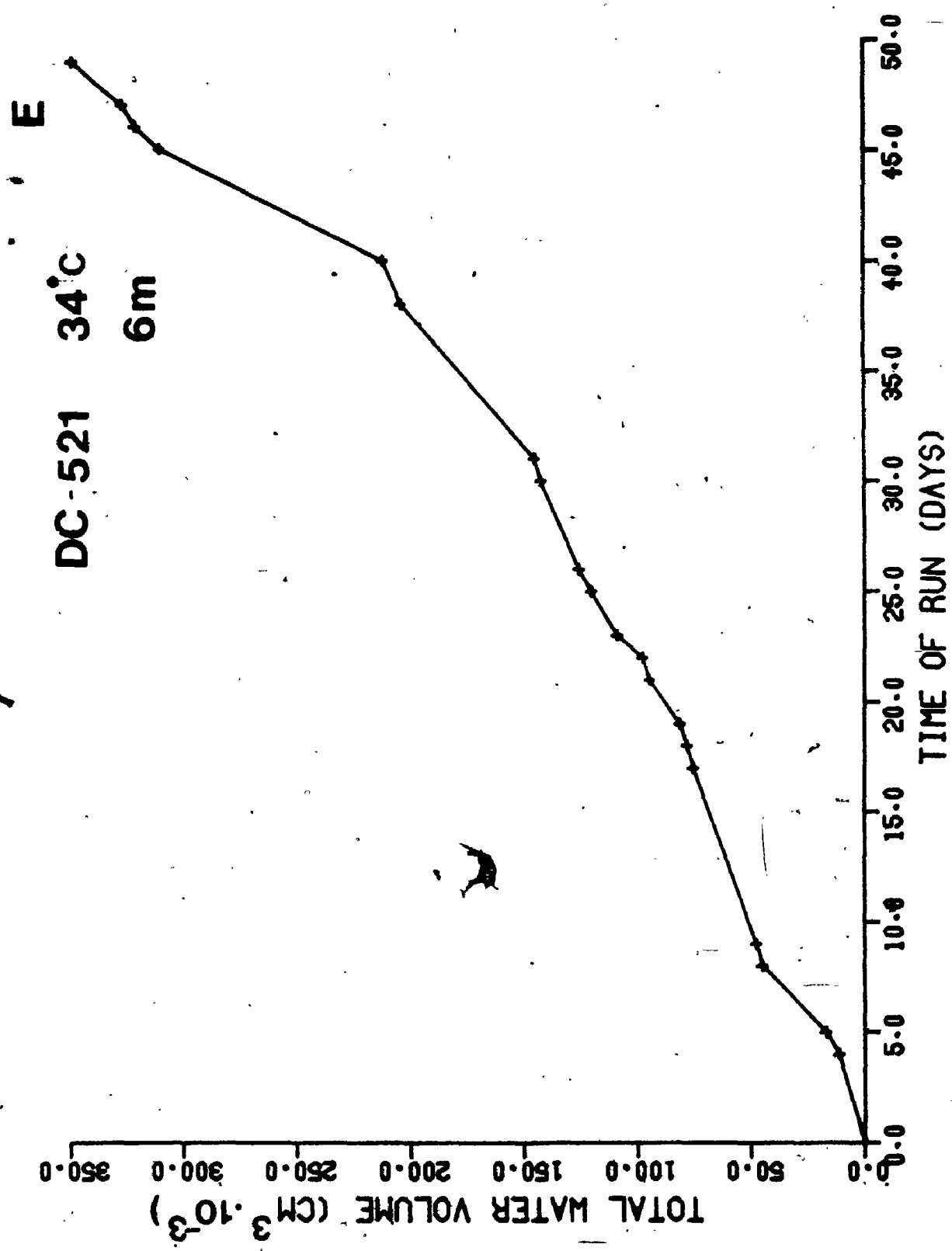


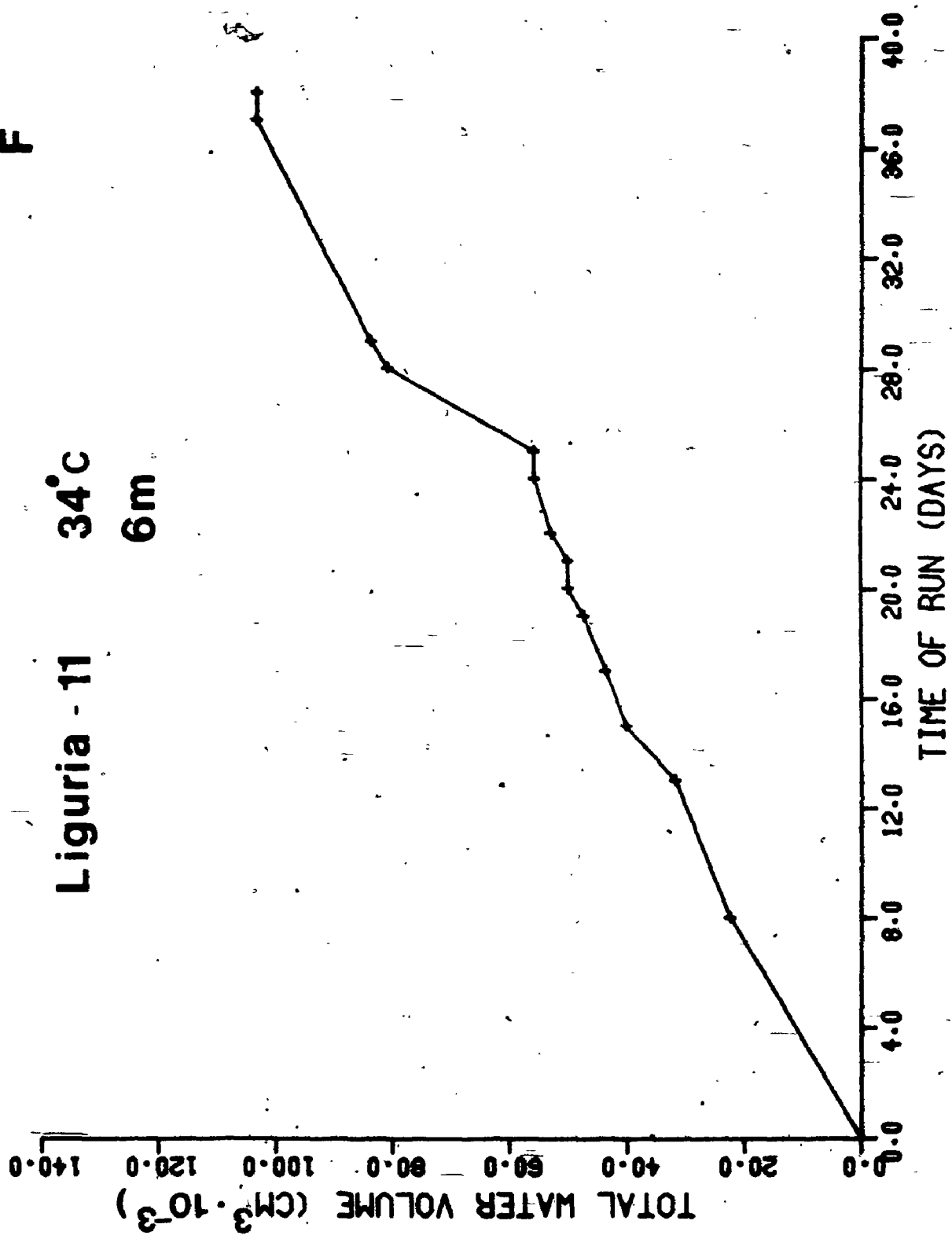
B

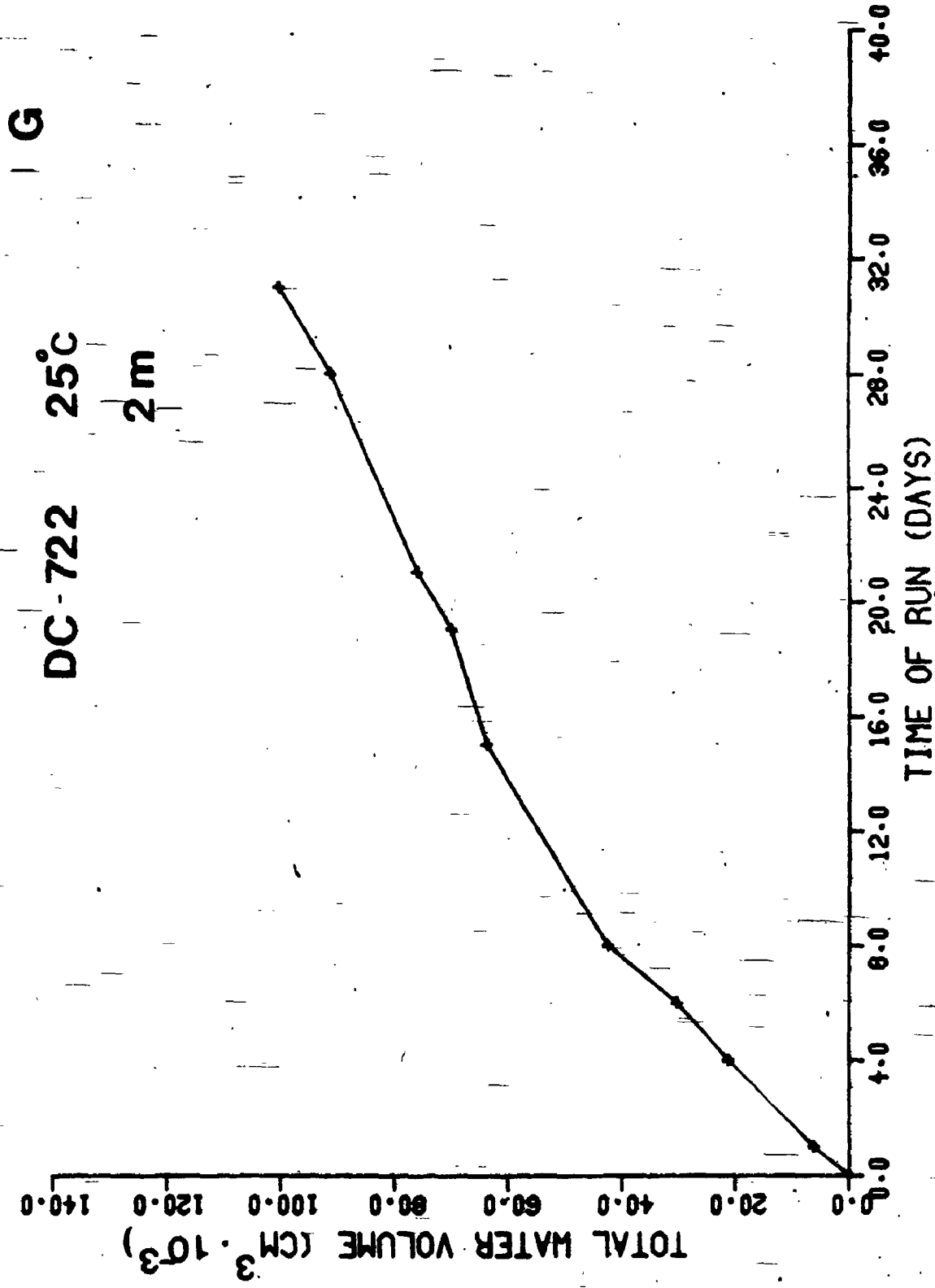


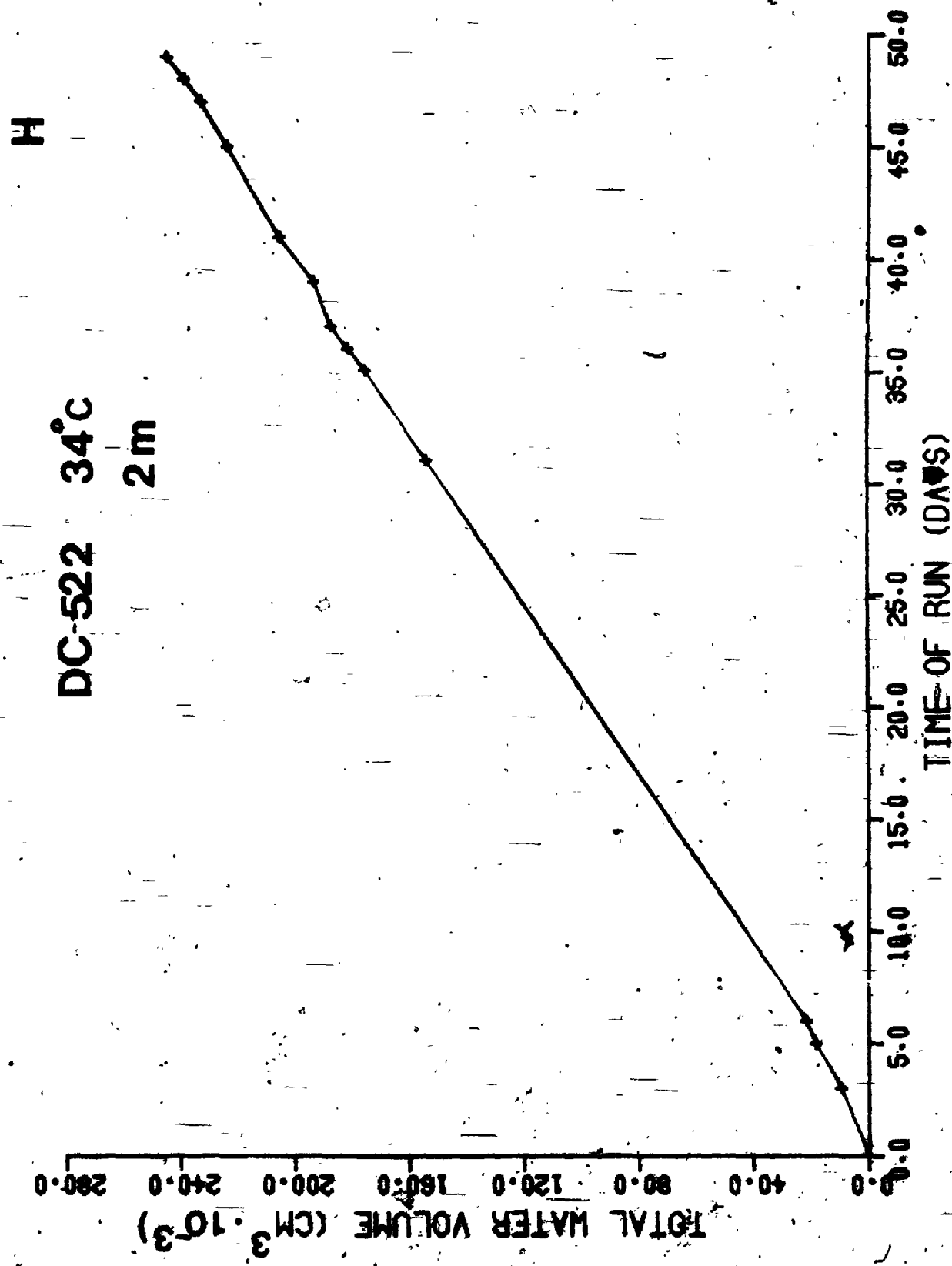
D

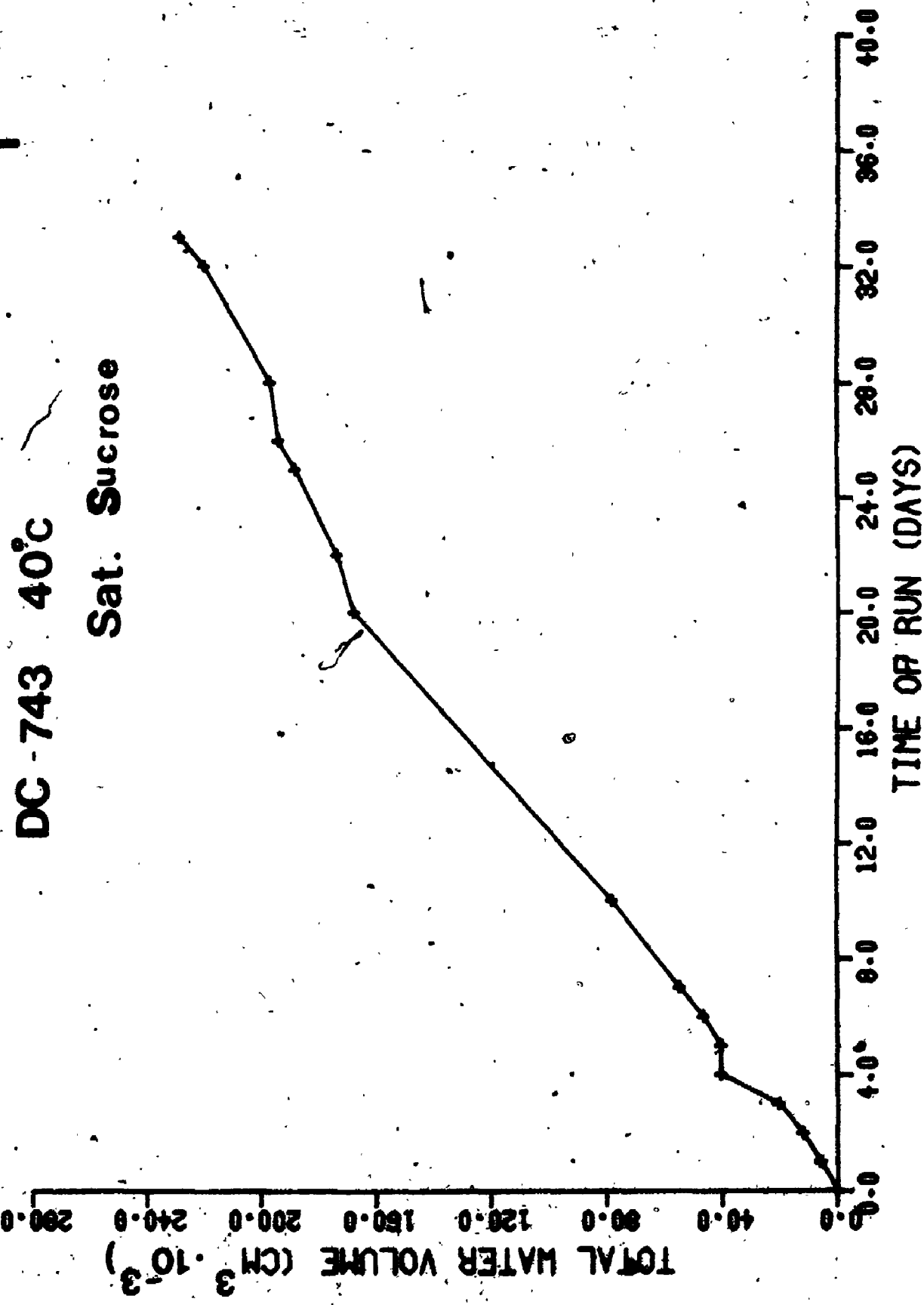


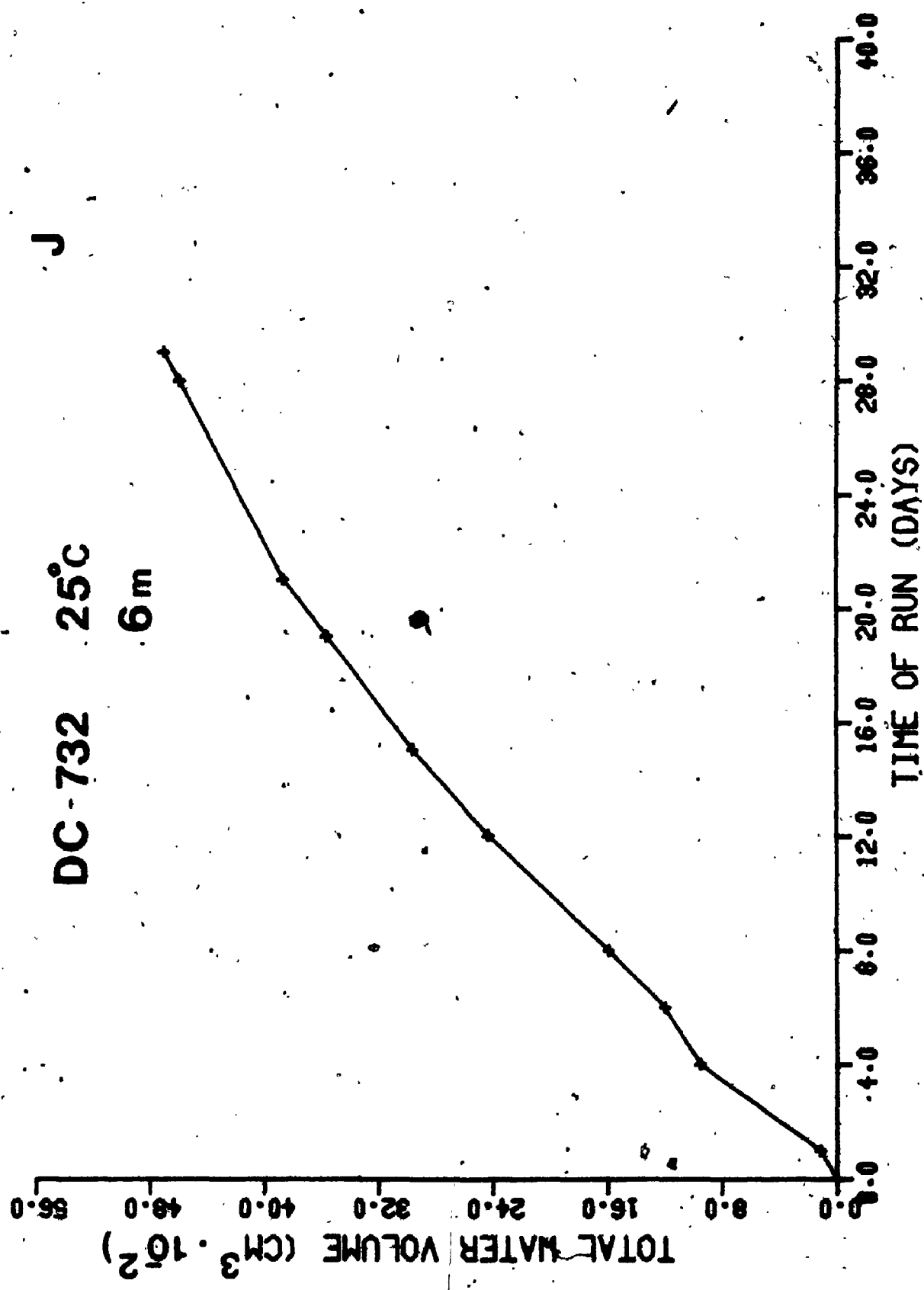












APPENDIX VIII

DESCRIPTION OF SERPENTINE TEXTURES AND MINERALOGY IN
SERPENTINIZED PERIDOTITES COLLECTED FROM THE LIGURIAN
OPHIOLITE SUITE, ITALY, AND THE BAY OF ISLANDS OPHIOLITE
COMPLEX IN NEWFOUNDLAND

VIII-1 Liguria, Italy

VIII-2 Bay of Islands, Newfoundland

VIII-1 Serpentinites from Liguria, Italy

In hand-specimen, serpentinized (90-100%) peridotites from Liguria (collected by W.S. Fyfe and F. Barriga near Sestrilevante, East Liguria) are a distinctive bluish-green. This color is typical of serpentinites which are heavily serpentinized (i.e. water/rock ratios high) and are not extensively subaerially weathered. Some remnant pyroxene is still visible.

In thin section, the slice is chaotically fractured and veined - i.e. intense uni-directional strain deformation is indicated. Ribbon and mesh textures, composed primarily of lizardite-IT (as indicated by microbeam diffraction), dominate. Minor slip-fibre chrysotile is also observed.) X-ray diffraction showed that no, or very little, brucite was present. Most of the iron in the rock is concentrated in veins as magnetite (which as well as the lack of brucite (Fe rich) increases the color noted above).

VIII-2 Serpentinized Peridotites from Bay of Island

Sample No. NA-71-19 (60% serpentinized) - from the collection of W.R. Church, studied by Riccio (1976) - used in the present diffusion experiments is typical of other serpentinized (harzburgite) peridotites collected from this area.

In hand specimen, serpentinized peridotites from the

Bay of Islands massif appear greenish-grey. Specimens are variably serpentinized (see Table 1) and display an extensive network of cross-cutting veins.

In thin section the serpentine veins are characteristically complexly banded, and appear to have split crystals of olivine apart. Grains of olivine are typically shattered and filled with a mosaic of microveinlets of serpentine. The dominant serpentine mineral, as shown by microbeam X-ray diffraction, is lizardite-IT. Brucite was detected by XRD.

Similar textured serpentinized peridotites have been dredged from the walls of fracture zones in the equatorial Mid-Atlantic Ridge by Bonatti et al. (1971).

REFERENCES

- Alabaster, T., Pearce, J. A. and Malpas, J. (1982). The volcanic stratigraphy and petrogenesis of the Oman ophiolite complex. *Contrib. Mineral. Petrol.* 81: 168-183.
- Amato, F. L. (1965). Stratigraphic paleontology in the Philippines. *Philipp. Geol.* 20: 121-140.
- Anderson, O. L. and Grew, P. C. (1977). Stress corrosion theory of crack propagation with applications to geophysics. *Rev. of Geophys. and Space Phys.* 15(1): 77-104.
- Anderson, R. N. (1981). Surprises from the Glomar Challenger. *Nature* 293: 261-262.
- Anderson, R. N. and Skilbeck, J. N. (1981). Oceanic heat flow. In *The Sea*, vol. 7, *The Oceanic Lithosphere*. Edited by C. Emiliani. Wiley Interscience, New York, p. 489-524.
- Andersson, K., Torstenfelt, B. and Allard, B. (1983). Sorption and diffusion studies of Cs and I in concrete. KBS Technical Report, 83-13, Stockholm, Sweden, 20 p.
- Ashby, M. F. and Verral, R. (1977). Micromechanisms of flow and fracture, and their relevance to the rheology of the upper mantle. Cambridge University, report CUED/C - Mat/TR30: 40 p.
- Aumento, F. (1969). Geological investigations, Mid-Atlantic Ridge. *Geol. Surv. Canada. Rept. Activ.* Paper 69-1 pt. A: 253-257.
- Aumento, F. (1969). Serpentine mineralogy of ultrabasic intrusions in Canada and on the Mid-Atlantic Ridge. *Geol. Surv. Can. Spec. Paper* 69-53: 1-67.
- Aumento, F. and Loubat, H. (1971). The Mid-Atlantic Ridge near 45°N. XVI. Serpentinized ultramafic intrusions. *Can. J. Earth Sci.* 8: 631-663.
- Bacuta, G. C. (1978). Geology of some alpine-type chromite deposits in the Philippines. Bureau of Mines Rept., Manila, Philippines.

- Bailey, S. W. (1969). Polytypism of trioctahedral 1:1 layer silicates. *Clays Clay Minerals* 17: 355-371.
- Barber, D. J. (1970). Thin foils of non-metals made for electron microscopy by sputter-etching. *J. Mat. Sci.* 5: 1-8.
- Barrer, R. M. (1941). Diffusion in and Through Solids. Cambridge Univ. Press.
- Barnes, I. and O'Neil, J. R. (1969). The relationship between fluids in some fresh Alpine-type ultramafics and possible modern serpentinization, Western U.S. *Bull. Geol. Soc. Am.* 80: 1947-1960.
- Barnes, I., La Marche, V. C. Jr. and Himmelberg, G. R. (1967). Geochemical evidence of present-day serpentinization. *Science* 56: 830-832.
- Barnes, I., O'Neil, J. R. and Trescases, J. J. (1978). Present day serpentinization in New Caledonia, Oman and Yugoslavia. *Geochim. Cosmochim. Acta* 42: 144-145.
- Barnes, I., Rapp, J. B. and O'Neil, J. R. (1972). Metamorphic assemblages and the direction of flow of metamorphic fluids in four instances of serpentinization. *Contrib. Mineral. Petrol.* 35: 263-276.
- Barrer, R. M. (1982). Hydrothermal Chemistry of Zeolites. Acad. Press, New York, 360 p.
- Bates, T. F. (1959). Morphology and crystal chemistry of 1:1 layer lattice silicates. *Amer. Mineral.* 44: 79-115.
- Bear, J. (1972). The Dynamics of Fluids in Porous Media. American Elsevier, New York.
- Ben-Avraham, Z. A., Nur, A. and Jones, D. (1982). The emplacement of ophiolites by collision. *J. Geophys. Res.* 87: 3861-3867.
- Benson, W. N. (1926). The tectonic conditions accompanying the intrusion of basic and ultrabasic igneous rocks. *U.S. Nat. Acad. Sci. Mem.* 1: 1-90.
- Bieniawski, Z. T. (1967). Mechanism of brittle fracture of rock. *Int. J. Rock Mech. Min. Sci.* 4: 407-423.
- Bloch, S. and Hoffmann, A. W. (1978). Magnesium metasomatism during hydrothermal alteration of new-ocean crust. *Geology* 6: 275-277.

- Bonatti, E. (1968). Ultramafic rocks from the Mid-Atlantic Ridge. *Nature, Lond.* 219: 363.
- Bonatti, E. (1978). Vertical tectonism in oceanic fracture zones. *Earth Planet. Sci. Lett.* 37: 369-79.
- Bonatti, E. and Hamlyn, P. R. (1981). Oceanic ultramafic rocks. In *The Sea, The Oceanic Lithosphere*. Edited by C. Emiliani. Wiley-Interscience, New York, 7, 489-524 p.
- Bonatti, E., Honnorez, J. and Ferrara, G. (1971). Peridotite-gabbro-basalt complex from the equatorial Mid-Atlantic Ridge. *Phil. Trans. Roy. Soc. Lond.* A268: 385-402.
- Bosshard, E. and MacFarlane, D. J. (1970). Crustal structure of the Western Canary Islands from seismic refraction and gravity data. *J. Geophys. Res.* 75(26): 4901-4918.
- Bottinga, Y. and Steinmetz, L. (1979). A geophysical, geochemical, petrological model of the sub-oceanic lithosphere. *Tectonophysics* 55: 311-347.
- Boudier, F. and Coleman, R. G. (1981). Cross section through the peridotite in the Samail ophiolite, south-eastern Oman Mountains. *J. Geophys. Res.* 86: 2573-2592.
- Bowen, N. L. and Tuttle, O. F. (1949). The system MgO-SiO₂-H₂O. *Geol. Soc. Am. Bull.* 60: 439-460.
- Bowin, C. O., Nalwalk, A. J. and Hersey, J. B. (1966). Serpentinized peridotite from the north wall of the Puerto Rico Trench. *Geol. Soc. Am. Bull.* 77: 257-270.
- Brace, W. F. and Bombelakis, E. G. (1963). A note on brittle crack growth in compression. *J. Geophys. Res.* 71(6): 3790.
- Brennan, P. V. (1983). The Petrology and Petrogenesis of Selected Ultramafic Rocks in Eastern Australia. Ph.D. thesis. La Trobe Univ., Australia.
- Brindley, G. W. (1967). Nomenclature, geometry of ideal layers, bonding. In *Short Course Lecture Notes on Layer Silicates*. Amer. Geol. Inst.
- Brindley, G. W. (1981). Structures and chemical compositions of clay minerals. In *Short Course in Clays and The Resource Geologist*. Edited by F. J.

- Longstaffe. Min. Assoc. of Canada, 7, Calgary, 1-21
P.
- Brindley, G. W. and Zussman, J. (1957). A structural study
of the thermal transformation of serpentine minerals
to forsterite. Amer. Mineral. 42: 461-474.
- Briscoe, H.V.A. et al. (1962). Mellor's Comprehensive
Treatise on Inorganic and Theoretical Chemistry. II
(Supplement), Longmans, Green and Co., London.
- Bryant, W. R., Bennett, R. H. and katherman, C. E. (1981).
Shear strength, consolidation, porosity, and perme-
ability of oceanic sediments. In The Sea, The Oceanic
Lithosphere, vol. 7. Edited by C. Emiliani. New
York, Wiley-Interscience, 1555-1616.
- Bryner, L. (1967). Geology of the Barlo Mine, and
vicinity, Dasol, Pangasinan Province, Luzon,
Philippines. Rep. Invest. 60. Philippine Bureau
Mines, Manila.
- Bullard, E. C., Maxwell, A. E. and Revelle, R. (1956).
Heat flow through the deep sea floor. Advances in
Geophys. 3: 153-181.
- Burham, C. W., Holloway, J. R. and Davis, N. F. (1969).
Thermodynamic properties of water to 1000°C and 10,000
bars. The Geological Soc. of America Special Paper
132, 96 p.
- Campbell, I. H. (1975). Direct evidence of present-day
serpentinization in the Jimberlana Intrusion, Western
Australia. Geol. Mag. 112: 77-80.
- Cande, S. C. and Kent, D. V. (1976). Constraints composed
by the slope of magnetic anomalies on the magnetic
source. J. Geophys. Res. 81: 4157-4162.
- Cardwell, R. K., Isacks, B. L. and Karig, D. E. (1980).
The spatial distribution of earthquakes, focal
mechanism solutions, and subducted lithosphere in the
Philippine and northeastern Indonesian islands. In
The Tectonic and Geological Evolution of Southeast
Asian Seas and Islands. Edited by Hayes, D. E.
Geophys. Monog. Ser. 23, Washington, D.C., p. 1-23.
- Caruso, L. J. and Chernosky Jr., J. V. (1979). The
stability of lizardite. Can. Min. 17: 757-769.
- Casey, J. F., Karson, J. A., Eithon, D., Rosencrantz, E.
and Titus, M. (1983). Reconstruction of the geometry

- of accretion during formation of the Bay of Islands ophiolite complex. *Offioliti* 8(2): 264-265.
- Cendero, A. (1969). The volcano-plutonic complex of La Gomera (Canary Islands). *Bull. Volcanol.* 34(2): 537-561.
- Chernosky, J. V. Jr. (1975). Aggregate refractive indices and unit cell parameters of synthetic serpentine in the system MgO-Al₂O₃-SiO₂-H₂O. *Am. Mineral.* 60: 200-208.
- Chidester, A. H. (1962). Petrology and geochemistry of selected talc-bearing ultramafic rocks and adjacent country rocks in north-central Vermont. *U.S. Geol. Surv. Prof. Pap.* 345.
- Chidester, A. H. (1968). Evolution of the ultramafic complexes of northwestern New England. In *Studies of Appalachian Geology*. Edited by Zen, E-an and others. New York, Interscience Pubs., Inc., 343-354 p.
- Christensen, N. I. and Salisbury, M. H. (1975). Structure and constitution of the lower oceanic crust. *Rev. Geophys. Space Phys.*, 13: 57-86.
- Church, W. R. (1972). Ophiolite: its definition, origin as oceanic crust, and mode of emplacement in orogenic belts, with special reference to the Appalachians. Canada Dept. Energy, Mines and Resources, Earth Physics Br. Publ. 42: 71-85.
- Clague, D. A. and Straley, P. F. (1977). Petrologic nature of the oceanic Moho. *Geology* 5: 133-136.
- Clark, A. L. and Greenwood, W. R. (1972). Petrographic evidence of volume increase related to serpentinitization, Union Bay, Alaska. *U.S. Geol. Surv. Prof. Pap.* 800C, C21-C27.
- Cogulu, E. and Laurent, R. (1984). Mineralogical and chemical variations in chrysotile veins and peridotite host-rocks from the asbestos belt of southern Quebec. *Can. Mineral.* 22: 173-183.
- Coleman, R. G. (1966). New Zealand serpentinites and associated metasomatic rocks. *New Zealand Geol. Surv. Bull.* 76: 102 p.
- Coleman, R. G. (1971). Petrologic and geophysical nature of serpentinites. *Bull. Geol. Soc. Amer.* 82: 897-918.

- Coleman, R. G. (1977). *Ophiolites*. Berlin, Springer-Verlag, 229 p.
- Coleman, R. G. (1983). Preaccretion tectonics and metamorphism of ophiolites. A special issue on 'Ophiolites: Oceanic Tectonics and Metamorphism'. *Ophioliti* (suppl. to 8), Florence, p. 18.
- Coleman, R. G. and Irwin, P. I. (1977). Philippine Sea Ophiolites. *Geotimes*: 23-24.
- Coleman, R. G. and Keith, T. E. (1971). A chemical study of serpentinization - Burro Mountain, California. *J. Petrol.* 12: 311-328.
- Coleman, R. G. and Peterman, Z. E. (1975). Oceanic plagiogranite. *J. Geophys. Res.* 80: 1099-1108.
- Condie, K. C. and Madison, J. (1969). Composition and volume change accompanying progressive serpentinization of dunites from Webster-Addie ultramafic body, N.C. *Am. Mineral.* 54: 1173-1179.
- Cooke, H. C. (1937). Thetford, Disraeli, and eastern half of Warwick map areas. *Geol. Surv. Canada Mem.* 211.
- Coplen, T. B. and Hanshaw, B. B. (1973). Ultrafiltration by a compacted clay membrane - I. Oxygen and hydrogen isotopic fractionation. *Geochem. Cosmochim. Acta* 37: 2295-2310.
- Cortesogno, L., Galbiati, B. and Principi, G. (1981). Descrizione dettagliata di alcuni caratteristici affioramenti di brecce serpentinitiche della Liguria Orientale ed interpretazione in chiave geodinamica. *Ophioliti* 6(1): 47-76.
- Crank, J. (1956). *The Mathematics of Diffusion*. Oxford Univ. Press, 347 p.
- Cressy, B. A. (1979). Electron microscopy of serpentinite textures. *Can. Mineral.* 17: 757-769.
- Cressy, B. A. and Zussman, J. (1976). Electron microscopy of serpentinite textures. *Can. Mineral.* 14: 307-313.
- Cruz, M., Jacobs, J. and Fripiat, J. J. (1972). The nature of the cohesion energy in kaolin minerals. *Intern. Clay Conf.*, Madrid., 35-43 p.
- Davis, E. E. and Lister, C.R.B. (1977). Heat flow measured over the Juan de Fuca ridge: evidence for widespread

- hydrothermal circulation in a highly heat transportative crust. *J. Geophys. Res.* 82: 4845-4860.
- de Beer, J. H. and Gough, D. I. (1980). Conductive structures in southernmost Africa: a magnetometer array study. *Geophys. J.R. astr. Soc.* 63: 479-495.
- de Beer, J. H., van Zijl, J. S. and Gough, D. I. (1982). The Southern Cape Conductive Belt: Its composition, origin and tectonic significance. In press.
- Denbigh, K. (1981). *The Principles of Chemical Equilibrium*. Cambridge Univ. Press, Cambridge, 494 p.
- Dewey, J. F. (1976). Ophiolite obduction. *Tectonophysics* 31: 93-120.
- Dietz, R. S. (1961). Continent and ocean basin evolution by spreading of the sea floor. *Nature* 190: 854-857.
- Dietz, R. S. (1963). Alpine serpentinites as oceanic rind fragments. *Geol. Soc. Am. Bull.* 74: 947-952.
- Diment, W. D. (1964). Thermal conductivity of serpentinites from Mayaguez, Puerto Rico, and other localities. In *Study of Serpentinite: The AMOSC core hole near Mayaguez, P.R.* Nat. Acad. Sci.-Nat. Res. Council Publ. 1188: 92-106.
- Dixon, J. B. (1977). Kaolinite and serpentine group minerals. In *Minerals in Soil Environments*. Edited by J. B. Dixon and S. B. Weed. Soil Sci. Soc. of America. Madison, Wisconsin, 357-403 p.
- Drevor, J. I. (1982). *The Geochemistry of Natural Waters*. Prentice-Hall Inc., New Jersey, 388 p.
- du Rietz, T. (1935). Peridotites, serpentines, and soapstones of northern Sweden. *Geol. Foren. Stockholm Forch* 57: 133-260.
- Dullien, F.A.L. (1979). *Porous Media: Fluid Transport and Pore Structure*. Acad. Press, New York, 396 p.
- Dungan, M. A. (1977). Metastability in serpentine-olivine equilibria. *Am. Mineral.* 62: 1018-1029.
- Dungan, M. A. (1979). A microprobe study of antigorite and some serpentine pseudomorphs. *Can. Mineral.* 17: 771-784.

- Durbin, R. P. (1960). Osmotic flow across permeable cellulose membranes. *J. Gen. Physiol.* 44: 315-326.
- Dutt, G. R. and Low, P. F. (1962). Diffusion of alkali chlorides in clay-water systems. *Soil Sci. Soc. Amer. Proc.* 23: 233-240.
- Early, J. W. (1958). On chloride in serpentinized dunite. *Am. Min.* 43: 148-155.
- Elder, J. (1965). Physical processes in geothermal areas. In *Terrestrial heat flow*. Edited by W.H.K. Lee. Am. Geophys. Union, Washington, D.C., p. 211.
- Elder, J. (1976). *The Bowels of the Earth*: Oxford. Oxford University Press, 222 p.
- Elder, J. W. (1978). Model of hydrothermal ore genesis. In *Volcanic Processes in Ore Genesis*. The Institute of Mining and Metallurgy and The Geological Soc. of London, 4-12 p.
- Ellis, A. J. (1968). Natural hydrothermal systems and experimental hot water/rock interaction: Reactions with NaCl solutions and trace metal extraction. *Geochim. Cosmochim. Acta* 32: 1356-1363.
- Ellis, A. J. (1970). Chemical processes in hydrothermal systems - a review. In *Proc. Symp. Hydrogeochemistry and Biogeochemistry*, Vol. 1. Washington, D.C. The Clarke Co., 1-20 p.
- Ellis, A. J. (1971). Magnesium ion concentrations in the presence of magnesium chlorite, calcite, carbon dioxide, quartz. *Am. J. Sci.* 271: 481-489.
- Ellis, A. J. (1979). Explored geothermal systems. In *Geochemistry of hydrothermal ore deposits*, 2nd ed. Edited by H. L. Barnes. Holt, Rinehart and Winston, p. 632-683.
- Epp, D. and Suyenaga, W. (1978). Thermal contraction and alteration of the oceanic crust. *Geology* 6: 726-728.
- Erickson, T. E. and Jacobsson, A. (1981). Ion diffusion in compacted sodium and calcium bentogites. KBS Technical Report, 81-12, Stockholm, Sweden.
- Evans, A. G. (1972). A method for evaluating the time-dependent failure characteristics of brittle materials and its applications to polycrystalline alumina. *J. Mater. Sci.* 7: 1137-1146.

- Evans, B. W. (1977). Metamorphism of alpine-peridotite and serpentinite. *Ann. Rev. Earth Planet. Sci.* 5: 397-447.
- Evans, B. W. (1977). Metamorphism of alpine peridotite and serpentinite. *Ann. Rev. Earth Planet. Sci.* 5: 397-447.
- Evans, B. W. and Trommsdorff, V. (1970). Regional metamorphism of ultramafic rocks in the Central Alps: Paragenesis in the system CaO-MgO-SiO₂-H₂O. *Schweiz. Mineral. Petrogr. Mitt.* 50: 481-492.
- Evans, B. W., Johannes, W., Oterdoom, H. and Trommsdorff, V. (1976). Stability of chrysotile and antigorite in the serpentine multisystem. *Schweiz. Mineral. Petrogr. Mitt.* 56: 79-93.
- Federal Institute for Geosciences and Raw Materials, Hannover (1978). Chrome. Repts. on Raw-Material by County. XV. Philippines. Sect. 3.13. Translated by D. Vitaliano of the U.S. Geol. Surv. (1980). From Bandesanstalt für Geowissenschaften und Rebstoff, Hannover. Rohstoffwirtschaftliche Länderberichte, XV, Philippinen..
- Fernandez, N. M. (1960). Notes on the geology and chromite deposits of the Zambales Range. *Philipp. Geol.* 14: 1-8.
- Fick, A. (1855). Ueber diffusion. *Ann. Phys. (Leipzig)* 170: 59-86.
- Fox, P. J. and Stroup, J. B. (1981). The Plutonic Foundation of the Ocean Crust. In *The Sea, The Oceanic Lithosphere*. Edited by C. Emilian. Wiley-Interscience, N.Y., 7, p. 119-218.
- Francis, G. H. (1956). The serpentinite mass Glen Urquhart, Inverness-shire, Scotland. *Amer. J. Sci.* 254: 201-226.
- Francis, T.J.G. (1981). Serpentinization faults and their role in the tectonics of slow spreading ridges. *J. Geophys. Res.* 86: 11616-11622.
- Freeze, R. A. and Cherry, J. A. (1979). *Groundwater*. Prentice Hall, Englewood Cliffs, N.J., 604 p.
- Fritz, S. J. and Marine, W. I. (1983). Experimental support for a predictive osmotic model of clay membranes. *Geochim. Cosmochim. Acta.* 47: 1515-1522.

Fuller, M., McCabe, R., Williams, I. S., Almasco, J., Encina, R. Y., Zanoria, A. S. and Wolfe, J. A. (1983). Paleomagnetism of Luzon. In The Tectonic and Geologic Evolution of Southeast Asian Seas and Islands. Part 2. Edited by D. E. Hayes. Geophys. Mono. 27, 79-94 p.

Fyfe, W. S. (1958). A further attempt to determine the vapour pressure of brucite. Am. J. Sci. 256: 729-732.

Fyfe, W. S. (1964). Geochemistry of Solids: An Introduction. McGraw-Hill, Inc., 199 p.

Fyfe, W. S. (1973). Dehydration reactions. A. A. Petrol. Geologists 57: 190-197.

Fyfe, W. S. (1974). Heats of chemical reactions and submarine heat production. Geophys. J. R. Astron. Soc. 37: 213-215.

Fyfe, W. S. and Lonsdale, P. (1981). Ocean floor hydrothermal activity. In The Sea, The Oceanic Lithosphere, vol. 7. Edited by C. Emiliani. New York, Wiley-Interscience, p. 589-638.

Fyfe, W. S., Price, N. J. and Thompson, A. B. (1978). Fluids in the Earth's Crust. Elsevier, Amsterdam, 383 p.

Fyfe, W. S., Turner, F. J. and Verhoogen, J. (1958). Metamorphic reactions and metamorphic facies. Geol. Soc. Am. Mem. 73: 259 p.

Gass, I. G. (1968). Is the Troodos massif of Cyprus a fragment of Mesozoic ocean floor? Nature 220: 39-42.

Gass, I. G. and Masson-Smith, D. (1963). The geology and gravity anomalies of the Troodos massif, Cyprus. Phil. Trans. Roy. Soc. Lond. A255: 417-467.

Gass, I. G. (1976). Origin and emplacement of ophiolites. In Volcanic Processes in Ore Genesis: The Instit. of Mining and Metallurgy, London, p. 4-12.

Geary, E. E. and Kay, R. W. (1983). Petrological and geochemical documentation of ocean floor metamorphism in the Zambales ophiolite, Philippines. In The Tectonic and Geologic Evolution of Southeast Asian Seas and Islands. Part 2. Edited by D. E. Hayes. Geophys. Mono. 27, 139-156 p.

- Gerlach, D. C., Ave Lallement, H. and Leeman, W. P. (1981). An island arc origin for the Canyon Mountain ophiolite complex, E. Oregon, U.S.A. *E. P. Sci. Letters* 53: 255-265.
- Gervasio, F. C. (1974). Ore deposits of the Philippines mobile belt. *J. Geol. Soc. Philippines*, XXV (3).
- Giese, R. F. (1973). Interlayer bonding in kaolinite, dickite, and nacrite. *Clays and Clay Minerals* 21: 145-149.
- Giese, R. F. (1980). Hydroxyl orientations and interlayer bonding in amesite. *Clays and Clay Minerals* 28: 81-86.
- Gillary, F. H. (1959). The X-ray study of synthetic Mg-Al serpentinites and chlorites. *Amer. Mineral.* 44: 719-728.
- Gomes, W. (1961). Definition of rate constant and activation energy in solid state reactions. *Nature* 192: 865.
- Goslin, J., Benzart, R., Francheteau, J. and Le Pinchon, X. (1972). Thickening of the oceanic layer in the Pacific Ocean. *Mar. Geophys. Res.* 1: 418-427.
- Gough, D. I. (1981). Magnetometer arrays and geodynamics. In *Evolution of the Earth's Crust*. Edited by R. J. O'Connell and W. S. Fyfe. *Geod. Ser.* 5: 87-95.
- Graf, D. L., Friedman, I. and Meents, W. F. (1965). The origin of saline formation waters. II. Isotopic fractionation by shale micropore systems. *Illinois State Geol. Surv. Circ.* 393, 32 p.
- Green, D. H. (1961). Ultramafic breccias from the Musa Valley, eastern Papua. *Geol. Mag.* 98: 1-26.
- Green, D. H. (1964). The petrogenesis of the high-temperature peridotite intrusion in the lizard area, Cornwall. *J. Petrol.* 5: 134-188.
- Green, D. H. (1984). Genesis of Morb. "ophiolitic" basalts, and boninites. In *Workshop in Experimental Geochemistry*. Monash Univ., Australia, 4 p.
- Gregory, R. T. and Taylor, H. P. Jr. (1981). An oxygen isotope profile in a section of Cretaceous ocean crust, Samail Ophiolite, Oman: Evidence for ^{180}O buffering of the oceans by deep (>5 km) seawater.

- hydrothermal circulation of mid-ocean ridges. J. Geophys. Res. 86: 2737-2755.
- Hajash, A. Jr. (1975). Hydrothermal processes along mid-ocean ridges: an experimental investigation. Contrib. Mineral. Petrol. 53: 205-226.
- Hamburger, M. W., Cardwell, K. and Isacks, B. L. (1983). Seismotectonics of the Northern Philippine island arc. In The Tectonic and Geologic Evolution of Southeast Asian Seas and Islands. Part 2. Edited by D. E. Hayes. Geophys. Mono. 27, 1-22 p.
- Hammel, H. T. and Scholander, P. F. (1976). Osmosis and Tensile Solvent. Springer-Verlag, New York, 133 p.
- Handin, J. (1964). Strength at high confining pressure and temperature of serpentinite from Mayaguez, Puerto Rico. In Study of Serpentinite. Edited by C. A. Burke. Nat. Acad. Sci.-Nat. Res. Publ. 1188.
- Hanshaw, B. B. and Coplen, T. B. (1973). Ultrafiltration by a compacted clay membrane - II. Sodium ion exclusion at various ionic strengths. Geochem. Cosmochim. Acta 37: 2311-2327.
- Harker, A. (1935). Petrology for Students. Cambridge, AT The University Press, London, England, 300 p.
- Harrison, . (1981). Magnetism of the oceanic crust. In The Sea, The Oceanic Lithosphere. Edited by C. Emiliani. Wiley-Interscience, N.Y., 7, p. 219-237.
- Hawkins, J. W. (1979). Geology of marginal basins and their significance to the origin of ophiolites. In Ophiolites, Proc. of Intern. Sympos. on Ophiolites, Cyprus. Edited by A. Panayitou. Geol. Surv. Dept. Nicosia, Cyprus, 224-254 p.
- Hawkins, J. W. and Evans, C. A. (1983). Geology of the Zambales Range, Luzon, Philippine Islands: Ophiolite derived from an island-arc back basin pair. In The Tectonic and Geologic Evolution of Southeast Asian Seas and Islands. Part 2. Edited by D. E. Hayes. Geophys. Mono. 27, 95-123 p.
- Hayashi, H. (1978). Semiquantitative chemical analysis of asbestos fibers and clay minerals with an analytical electron microscope. Clays and Clay Min. 26: 181-188.
- Helfferich, F. (1962). Ion Exchange. McGraw-Hill, New York, 624 p.

- Helgeson, H. C. and Kirkham, D. H. (1974). Theoretical prediction of the thermodynamic behaviour of aqueous electrolytes at high pressures and temperatures: I. Summary of the thermodynamic/electrostatic properties of the solvent. Am. J. Sci. 274: 1089-1198.
- Hemley, J. J., Montoya, J. W., Christ, C. L. and Hostetler, P. B. (1977a). Mineral equilibria in the MgO-SiO₂-H₂O system: I. Talc-chrysotile-forsterite-brucite stability relations. Am. J. Sci. 277: 322-351.
- Hemley, J. J., Montoya, J. W., Shaw, D. R. and Luce, R. W. (1977b). Mineral equilibria in the MgO-SiO₂-H₂O system: II. Talc-antigorite-forsterite-anthophyllite-enstatite stability relations and some geologic implications in the system. Am. J. Sci. 277: 353-383.
- Herzen, R. von (1959). Heat flow from the southern Pacific. Nature 183: 882-883.
- Hess, H. H. (1954). Geological hypotheses and the Earth's crust under the oceans. Roy. Soc. London, Proc., A. 222: 341-348.
- Hess, H. H. (1954). Serpentinites, orogeny, and epeirogeny. In Crust of the Earth. Edited by A. Poldervaart. Geol. Soc. of Am. Spec. Paper 62, 762 p.
- Hess, H. H. (1962). History of ocean basins. In Petrologic Studies. A volume to honor A. F. Buddington. Edited by A. Engel, H. L. James and B. F. Leonard. Geol. Soc. Amer. Buddington vol.: 599-622.
- Hess, H. H. and Otalora, G. (1964). Mineralogical and chemical composition of the Mayaguez serpentinite cores. In Study of Serpentinite. Edited by C. A. Burke. Nat. Acad. Sci.-Nat. Res. Coun. Publ. 1188: 152-168.
- Hillig, W. S. and Charles, R. J. (1965). Surfaces, strain-dependent reactions and strength. In High Strength Materials. Edited by V. F. Zachey. John Wiley and Sons, N.Y., p. 682-705.
- Himmelberg, G. R. and Loney, R. A. (1980). Petrology of ultramafic and gabbroic rocks of the Canyon Mountain ophiolite, Oregon. Amer. J. Sci. 280-A: 232-268. Materials. Edited by V. F. Zachey. John Wiley, New York, 682-705 p.

- Honnerez, J. and Kirst, P. (1975). Petrology of rodingites from the equatorial Mid-Atlantic fracture zones and their geotectonic significance. *Contrib. Mineral. Petrol.* 49: 233-257.
- Hopson, C. A., Coleman, R. G., Gregory, R. T., Pallister, J. S. and Bailey, E. H. (1981). Geologic section through the Samail ophiolite and associated rocks along a Muskat-Ibra transect, southeastern Oman mountains. *J. Geophys. Res.* 86: 2527-2544.
- Hostetler, P. B., Coleman, R. G., Mumpton, F. A. and Evans, B. W. (1966). Brucite in Alpine serpentinites. *Am. Mineral.* 51: 75-98.
- Hubbert, K. M. and Rubey, W. W. (1959). Role of fluid pressure in mechanics of overthrust faulting. *Bull. Geol. Soc. America* 70: 115-166.
- Hussong, D. M. and Uyeda, S. (1982). Tectonic processes and the history of the Mariana Arc: A synthesis of the results of DSDP Leg 60. *Initial Reports of the DSDP*, LX: 909-929.
- Iishi, K. and Saito, M. (1973). Synthesis of antigorite. *Amer. Mineral.* 58: 915-919.
- Ito, E., Harris, D. M. and Anderson, A. T. (1983). Alteration of oceanic crust and geologic cycling of chlorine and water. *Geochem. Cosmochim. Acta* 47: 1613-1624.
- Jahns, H. R. (1967). Serpentinites of the Roxbury District, Vermont. In *Ultramafic and Related Rocks*. Edited by P. J. Wyllie. John Wiley and Sons Inc., New York, 137-167 p.
- Johannes, W. (1968). Experimental investigations of the reaction forsterite + water = serpentine + brucite. *Contrib. Mineral. Petrol.* 19: 309-315.
- Jost, W. (1960). *Diffusion in Solids, Liquids, and Gases*. Acad. Press, New York, 558 p.
- Kanamori, H. (1977). The energy release in great earthquakes. *J. Geophys. Res.* 80: 2981-2987.
- Kemper, W. D. and Evans, N. A. (1963). Movement of water as effected by free energy and pressure gradients. III. Restriction of solutes by membranes. *Soil Sci. Amer. Proc.* 27: 485-490.

- Kemper, W. D. and Evans, N. A. (1963). Movement of water as effected by free energy and pressure gradients: III. Restriction of solutes by membranes. *Soil Sci.* Soc. Am. Proc. 27: 485-490.
- Kemper, W. D. and Maasland, D. E. (1964). Reduction in salt content of solution on passing through thin films adjacent to charged surfaces. *Soil Sci. Soc. Amer. Proc.* 28: 318-323.
- Kemper, W. D. and Rollins, J. B. (1966). Osmotic efficiency coefficients across compacted clays. *Soil Sci. Soc. Amer. Proc.* 59: 529-534.
- Kemper, W. D. and van Schaik, J. C. (1966). Diffusion of salts in clay-water systems. *Soil Sci. Soc. Amer. Proc.* 30: 534-540.
- Kempner, W. C. and Gettrust, J. F. (1983). Ophiolites, synthetic seismograms and ocean crustal structure: 3. An aging model for ocean crust. In *Oceanic Lithosphere: Origin, Structure and Dynamics*. Edited by G. F. Sharman. *Tectonophysics*, in press.
- Kerr, R. A. (1983). Ophiolites: Windows on which ocean crust? *Science* 219: 1307-1309.
- Kohls, D. W. and Rodda, J. L. (1967). Iowaite, a new magnesium hydroxide-ferric oxychloride from the Precambrian of Iowa. *Am. Mineral.* 52: 1261-1271.
- Kohls, D. W. and Rodda, J. L. (1967). Iowaite, a new hydrous magnesium hydroxide-ferric oxychloride from the Precambrian of Iowa. *Am. Min.* 52: 1261-1271.
- Kuniyoshi, S. and Liou, J. G. (1976). Contact metamorphism of the Karmutsen volcanics, Vancouver Island, British Columbia. *J. Petrol.* 17: 73-99.
- Kunze, G. (1956). Die gewellte struktur des Antigorits: 1. *Z. Kristallogr.* 108: 82-107.
- Lambe, T. W. and Whitman, R. V. (1976). *Soil Mechanics*. John Wiley and Sons, N.Y., 553 p.
- Laurent, R. (1975). Petrology of the alpine-type serpentinites of Asbestos and Thetford Mines, Quebec. *Schweiz. Mineral. Petrog. Mitt.* 55: 431-455.
- Lerman, A. (1979). *Geochemical Processes*. Wiley-Interscience, New York, 481 p.

- Lewis, B.T.R. (1983). The process of formation of ocean crust. *Science* 220: 151-157.
- Lewis, B.T.R. and Snydsman, W. E. (1977). Evidence for a low velocity layer at the base of the oceanic crust. *Nature* 266: 340-344.
- Lewis, G. N., Randall, M., Pitzer, K. S. and Brewer, L. (1961). *Thermodynamics*. McGraw-Hill, New York, 722 p.
- Li, Y.-H. and Gregory, S. (19). Diffusion of ions in sea water and deep-sea sediments. *Geochem. Cosmochim. Acta* 38: 703-714.
- Liou, J. G. and Ernst, W. G. (1979). Oceanic ridge metamorphism of the East Taiwan ophiolite. *Contrib. Mineral. Petrol.* 68: 335-348.
- Lister, C.R.B. (1974). On the penetration of water into hot rocks. *Geophys. J. R. Abstr. Soc.* 39: 465-509.
- Lister, C.R.B. (1980). Qualitative models of spreading-center processes, including hydrothermal penetration. In Subduction zones, mid-ocean ridges, oceanic trenches and geodynamics. Edited by S. Uyeda. *Tectonophysics* 37: 203-218.
- Lister, C.R.B. (1981a). "Active" and "passive" hydrothermal systems in the oceanic crust: predicted physical conditions. In The Dynamic Environment of the Ocean Floor (Heath, Lexington, Mass.) (in press).
- Lister, C.R.B. (1981b). Rock and water histories during sub-ocean hydrothermal events. *Oceanologica Acta*, Proc. 26th Int. Geol. Congress, Paris, p. 41-46.
- Lockwood, J. P. (1971). Sedimentary and gravity-slide emplacement of serpentinite. *Geol. Soc. Am. Bull.* 82: 919-936.
- Lockwood, J. P. (1973). Possible mechanisms for the emplacement of alpine-type serpentinite. *G.S.A. Memoir* 132: 273-287.
- Loney, R. A., Himmelberg, G. R. and Coleman, R. G. (1971). Structure and petrology of the alpine-type peridotite at Burro Mountain, California, U.S.A. *J. Petrol.* 12: 245-309.
- Torrimer, J. W. (1979). Osmosis. In Applied Fibre Science. Edited by F. Happey. Academic Press, New York, 71-102 p.

- Low, P. F. (1976). Viscosity of interlayer water in montmorillonite. *Soil Sci. Soc. Amer. Proc.* 40: 500-504.
- Manheim, F. T. (1970). The diffusion of ions in unconsolidated sediments. *Earth Planet. Sci. Lett.* 9: 307-309.
- Margaritz, M. and Taylor, H. P. (1974). Oxygen and hydrogen isotope studies of serpentinization in the Troodos complex, Cyprus. *Earth Planet. Sci. Lett.* 23: 8-14.
- Martin, B. (1968). Some theoretical and experimental observations on rates of hydration in the system MgO-SiO₂-H₂O. Ph.D. thesis, Manchester Univ., London, England, 109 p.
- Martin, B. and Fyfe, W. S. (1970). Some experimental and theoretical observations on the kinetics of hydration reactions with particular reference to serpentinization. *Chem. Geol.* 6: 185-195.
- Martin, R. J. (1972). Time-dependent crack growth in quartz and its application to the creep of rocks. *J. Geophys. Res.* 77: 1406.
- Martin, R. J. and Durham, W. B. (1975). Mechanisms of crack growth in quartz and its application to the creep of rocks. *J. Geophys. Res.* 80: 4837-4844.
- Matsubayashi, O. (1983). Heat flow measurements in the Central Pacific Basin, and their implications. In *Oceanic Lithosphere: Origin, Structure and Dynamics*. Edited by G. F. Sharman. *Tectonophysics*, in press.
- Mauro, A. (1965). Osmotic flow in a rigid porous membrane. *Science* 149: 867-869.
- Mellini, M. (1982). The crystal structure of lizardite IT: hydrogen bonds and polytypism. *Amer. Mineral.* 67: 587-598.
- Nelson, W. G. and Thompson, G. (1970). Layered basic complex in oceanic crust, Romanche Fracture Zone, Atlantic Ocean. *Science* 168: 817.
- Nelson, W. G., Jarosewitch, E., Bowen, V. T. and Thompson, G. (1967). St. Peter and St. Paul rocks: A high-temperature mantle-derived intrusion. *Science* 155: 1532-35.

- Middleton, A. P. and Whittaker, E.J.W. (1976). The structure of Povlen-type chrysotile. *Can. Mineral.* 17: 301-306.
- Misawa, T., Hashimoto, K. and Shimodaira, S. (1974). The mechanism of formation of iron oxide and ortho-hydroxides in aqueous solutions at room temperature. *Corrosion Science* 14: 131-149.
- Miyashiro, A. (1973). The Troodos ophiolite complex was probably formed in an island arc. *Earth Planet. Sci. Lett.* 19: 218-224.
- Miyashiro, A., Shido, F. and Ewing, M. (1969). Composition and origin of serpentinites from the Mid-Atlantic Ridge near 24° and 30° north latitude. *Contr. Min. Petrol.* 23: 117-127.
- Miyashiro, A., Shido, F. and Ewing, M. (1969). Composition and origin of serpentinites from the Mid-Atlantic Ridge near 24° and 30° north latitude. *Contrib. Mineral. Petrol.* 23: 117-127.
- Mokady, R. S. and Low, P. F. (1968). Simultaneous transport of salt and water through clays: I. Transport Mechanisms. *Soil Sci.* 105: 112-131.
- Moody, J. B. (1976). An experimental study on the serpentinization of iron-bearing olivines. *Can. Mineral.* 14: 462-478.
- Moore, E. M. (1969). Petrology and structure of the Vourinos ophiolite complex, northern Greece. *Geol. Soc. Amer. Spec. Paper* 118, 74 p.
- Moore, E. M. and Vine, F. J. (1971). The Troodos massif, Cyprus, and other ophiolites as oceanic crust, evaluation and implications. *Phil. Trans. Roy. Soc. Lond.* 268: 443-466.
- Mottl, M. J. and Seyfried, W. E. (1980). Sub-seafloor hydrothermal systems rock-vs. seawater-dominated. In *Seafloor Spreading Centers: Hydrothermal Systems*. Edited by P. A. Rona and R. P. Lowell. Dowden, Hutchinson and Ross, Stroudsburg, p. 66-82.
- Moutte, J. (1979). Le Massif De Tiebaghi, Nouvelle Caledonie et ses Gites de Chromite. Ph.D. thesis. L'Ecole Nationale Supérieure des Mines de Paris. 160 p.

- Mumpton, F. A. (1971). Natural zeolites. In Mineralogy and geology of natural zeolites. Edited by F. A. Mumpton. Min. Soc. of Amer. 4, 1-17 p.
- Mumpton, F. A. and Thompson, C. S. (1975). Mineralogy and origin of the Coalinga asbestos deposit. Clays Clay Minerals 23: 134-143.
- Murray, J. W. (1979). Iron oxides. In Mineralogical Soc. of Amer. Short Course Notes on Marine Minerals. Edited by R. Burns, Vol. 6, p. 47-98.
- Mutter, J. C., Buhl, P., Alsop, J., Detrick, R., Stoffa, P. L., Diebold, H. B., Hinz, K. and Phillips, J. (1983). Two ship multichannel seismic transect across 200 my. of oceanic crust in the central north Atlantic. In Oceanic Lithosphere: Origin, Structure and Dynamics. Edited by G. F. Sharman. Tectonophysics, in press.
- Nelson, B. W. and Roy, R. (1958). Synthesis of the chlorites and their structural and chemical constitution. Amer. Mineral. 43: 707-725.
- Neretnieks, I. (1982). Diffusivities of some dissolved constituents in compacted wet bentonite-MX80 and the impact on radionuclide migration in the buffer. KBS Technical Report, 82-27, Stockholm, Sweden.
- Nesbitt, H. W. and Bricker, O. P. (1978). Low temperature alteration processes affecting ultramafic bodies. Geochim. Cosmochim. Acta 42: 403-409.
- Nicolas, A., Giradeau, J., Marcoux, J., Dupre, B., Xibin, W., Yougong, C., Haixiang, Z. and Xuechang, X. (1981). The Xigaze ophiolite (Tibet): a peculiar oceanic lithosphere. Nature 294: 414-417.
- Nigrini, A. (1969). Prediction of ionic fluxes in rock alteration processes at elevated temperatures. Ph.D. thesis, Northwestern Univ., Evanston, Ill., 83 p.
- Nitsch, K. H. (1971). Stabilitätsbeziehungen von prehnit und pumpellyit-haltigen pargenesen. Contrib. Mineral. Petrol. 30: 240-260.
- Nur, A. (1983). Accreted terranes. Rev. Geophys. and Space Physics 21(8): 1779-1785.
- O'Hara, M. J. (1967). Mineral facies in ultrabasic rocks. In Ultramafic and Related Rocks. Edited by P. J. Wyllie. John Wiley & Sons, New York, 464 p.

- Oxburgh, E. R. (1972). Flake tectonics and continental collision. *Nature* 239: 202-204.
- Page, N. J. (1967). Serpentinitization at Burro Mountain, California. *Contrib. Mineral. Petrol.* 14: 321-342.
- Page, N. J. (1967). Serpentinitization considered as a constant volume metasomatic process: a discussion. *Am. Mineral.* 52: 545-548.
- Page, N. J. (1968). Serpentinitization in a sheared serpentinite lens, Tiburon Peninsula, California. *U.S. Geol. Surv. Prof. Paper* 600-B: 21-28.
- Pannetier, G. and Souchay, P. (1967). Chemical Kinetics. Elsevier.
- Parker, R. L. and Oldenburg, D. W. (1973). Thermal model of ocean ridges. *Nature* 242: 137-139.
- Parsons, B. and Sclater, J. G. (1977). An analysis of the variation of ocean floor bathymetry and heat flow with age. *J. Geophys. Res.* 78: 7786-7787.
- Patterson, R. (1970). An Introduction to Ion Exchange. Heyden and Sons Ltd., 109 p.
- Phelps, D. and Ave Lallentant, H. G. (1980). The Sparta ophiolite complex, northeast Oregon: a plutonic equivalent to low K₂O island-arc volcanism. *Amer. J. Sci.* 280-A: 345-358.
- Phillips, A. H. and Hess, H. H. (1936). Metamorphic differentiation at contacts between serpentine and siliceous country rocks. *Am. Mineral.* 21: 333-362.
- Poty, B., Holland, H. D. and Boresik, M. -(1972). Solution mineral equilibria in the system MgO-SiO₂-H₂O-MgCl₂ at 500°C and 1 kbar. *Geochem. Cosmochim. Acta* 36: 1101-1113.
- Price, N. J. (1975). Rates of deformation. *J. Geol. Soc. London* 131: 553-575.
- Pritchard, H. M. (1979). A petrographic study of the processes of serpentinitization in ophiolites and in the ocean crust. *Contrib. Mineral. Petrol.* 68: 231-241.
- Prothero, W. A. and Reid, I. D. (1982). Microearthquakes on the East Pacific Rise at 21°N and Rivera Fracture Zone. *J. Geophys. Res.* 87: 8509-8518.

- Pundsack, F. L. (1956). The properties of asbestos. II. The density and structure of chrysotile. *J. Phys. Chem.* 60: 361-364.
- Purdy, G. M. (1983). The homogeneity of ocean crust. In *Oceanic Lithosphere: Origin, Structure and Dynamics*. Edited by G. F. Sharman. *Tectonophysics*, in press.
- Push, R. (1983). Use of clays as buffers in radioactive repositories. KBS Technical Report, 83-46, Stockholm, Sweden, 79 p.
- Quon, S. H. and Ehlers, E. G. (1963). Rocks of northern part of Mid-Atlantic Ridge. *Geol. Soc. Am. Bull.* 74: 1-8.
- Radoslovich, E. W. (1962). The cell dimensions and symmetry of layer-lattice silicates. II. Regression relations. *Amer. Mineral.* 47: 617-636.
- Raitt, R. W. (1956). Seismic refraction studies of the Pacific Ocean Basin. *Geol. Soc. Amer. Bull.* 67: 1623-1640.
- Raleigh, C. B. and Patterson, M. S. (1965). Experimental deformation of serpentinite and its tectonic implications. *J. Geophys. Res.* 70: 3965-3985.
- Ramsey, J. G. (1980). The crack-seal mechanism of rock deformation. *Nature* 284: 135-139.
- Ribando, R. J., Torrance, K. E. and Turcotte, D. L. (1976). Numerical models for hydrothermal circulation in the oceanic crust. *J. Geophys. Res.* 81: 3007-3012.
- Riccio, L. (1976). Stratigraphy and Petrology of the Peridotite-Gabbro Component of the Western Newfoundland Ophiolites. Univ. of Western Ontario, Ph.D. thesis, 265 p.
- Richter, D. and Simmons, G. (1977). Microcracks in crustal igneous rocks: Microscopy. In *The Earth's Crust*. Edited by A. F. Spilhaus. *Geophys. Mon. Series* 20. Am. Geophys. Uncon. 149-180 p.
- Ringwood, A. E. (1982). Phase transformations and differentiation in subducted lithosphere: Implications for mantle dynamics, basalt petrogenesis, and crustal evolution. *J. Geology* 90: 611-643.
- Riordan, P. H. (1955). The genesis of asbestos in ultra-basic rocks. *Econ. Geol.* 50: 67-81.

Robie, R. A., Hemingway, B. S. and Fisher, J. R. (1977). Thermodynamic properties of minerals and related substances at 298.150K and one bar (10^5 pascals) pressure, and at higher temperatures. U.S. Geol. Surv. Bull. 1259, 1256 p.

Robinson, R. S. and Stokes, R. H. (1965). Electrolyte Solutions. London; Butterworths, 571 p.

Rodgers, K. A. (1975). A comparison of the geology of the Papuan and New Caledonian ultramafic belts. Jour. Geol. 83: 47-60.

Ross, C. S., Foster, M. D. and Myers, A. T. (1954). Origin of dunites and olivine rich inclusions in basaltic rocks. Am. Min. 39: 693-737.

Rossmann, D. L. (1964). Chromite deposits of the north-central Zambales Range, Luzon, Philippines. U.S. Geol. Surv. Open File Rep. 65.

Roy, D. M. and Roy, R. (1954). An experimental study of the formation and properties of synthetic serpentines and related layer silicate minerals. Amer. Mineral. 39: 959-975.

Rucklidge, J. C. and Patterson, G. C. (1977). The role of chlorine in serpentinization. Contrib. Mineral. Petrol. 65: 39-44.

Rucklidge, J. C. and Zussman, J. (1965). The crystal structure of the serpentine mineral, lizardite, $Mg_3Si_2O_5(OH)_4$. Acta Cryst. 19: 381-389.

Sanford, R. F. (1982). Growth of ultramafic reaction zones in greenschist to amphibolite facies metamorphism. A. J. Sci. 282: 543-616.

Saunders, A. D., Tarney, J., Marsh, N. G. and Wood, D. A. (1979). In Ophiolites, Proc. of Intern. Sympos. on Ophiolites, Cyprus. Edited by A. Panayitou. Nicosia, Cyprus, 193-204 p.

Scarf, C. M. and Wyllie, P. J. (1967). Serpentine dehydration curves and their bearing on serpentinite deformation in orogenesis. Nature 215: 945-6.

Scheidegger, A. E. (1960). The Physics of Flow Through Porous Media. Univ. of Toronto Press, Toronto, Canada.

Scholz, C. H. (1972). Static fatigue of quartz. J. Geophys. Res. 77: 2104-2114.

- Schweller, W. J., Karig, D. E. and Bachman, S. B. (1983). Ophiolite setting and emplacement history of the Zambales ophiolite, Luzon, Philippines, from stratigraphic evidence. In The Tectonic and Geologic Evolution of Southeast Asian Seas and Islands. Part 2. Edited by D. E. Hayes. Geophys. Mono. 27, 124-138 p.
- Seyfried, W. E. and Bischoff, J. L. (1977). Hydrothermal transport of heavy metals by seawater: the role of seawater/basalt ratio. Earth Planet. Sci. Lett. 34: 71-77.
- Seyfried, W. E. and Mottl, M. J. (1982). Hydrothermal alteration of basalt by seawater under seawater-dominated conditions. Geochem. Cosmochim. Acta 46: 985-1002.
- Seyfried, W. E. Jr. and Dibble, W. E. Jr. (1980). Seawater-peridotite interaction at 300°C and 500 bars: implications for the origin of oceanic serpentinites. Geochim. Cosmochim. Acta 44: 309-321.
- Shand, S. J. (1949). Rocks of the Mid-Atlantic Ridge. J. Geol. 57: 89-92.
- Sharp, W. E. (1962). The thermodynamic functions for water in the range -10 to 1000°C and 1 to 250,000 bars. Univ. of California, Lawrence Livermore Laboratory, Livermore, California, 50 p.
- Sissom, L. E. and Pitts, D. R. (1972). Elements of Transport Phenomena. McGraw-Hill Co., New York, 814 p.
- Steinmann, G. (1927). Die ophiolithischen zonen in den Mediterranean Fettengebirgen. 14th Internat. Geol. Congr., Madrid, C.R. 2: 638-667.
- Stoll, W. C. (1958). Geology and petrology of the Masinloc chromite deposit, Zambales, Luzon, Philippine Islands. Bull. Geol. Soc. Am. 69: 419-448.
- Straus, J. M. and Schubert, G. (1977). Thermal convection of water in a porous medium: effects of temperature- and pressure-dependent thermodynamic and transport properties. J. Geophys. Res. 82: 325-333.
- Stumm, W. and Morgan, J. (1981). Aquatic Chemistry: An Introduction Emphasizing Chemical Equilibria in Natural Waters. John Wiley and Sons, New York, 780 p.

Swartzendruber, D. (1961). Modification of Darcys law for the flow of water in soils. Soil Sci. Soc. Amer. Proc. 93: 22-29.

Swartzendruber, D. (1963). Non-Darcy behavior and the flow of water in unsaturated soils. Soil Sci. Soc. Amer. Proc.

Taylor, B. and Hayes, D. E. (1983). Origin and history of the South China Sea Basin. In The Tectonic and Geologic Evolution of Southeast Asia Seas and Islands. Part 2. Edited by D. E. Hayes. Geophys. Mono. 27, 23-56 p.

Thain, J. F. (1967). Principles Of Osmotic Phenomena. The Royal Institute of Chemistry, London, 68 p.

Thayer, T. P. (1960). Some critical differences between alpine-type and stratiform peridotite-gabbro complexes. Geol. Cong. 21(13) Copenhagen: 247-259.

Thayer, T. P. (1964). Principal features and origin of podiform chromite deposits, and some observations on the Guleman-Soridag district, Turkey. Econ. Geol. 59: 1497-1524.

Thayer, T. (1966). Serpentinization considered as a constant volume metasomatic process. Am. Mineral. 51: 685-710.

Thayer, T. P. (1967). Chemical and structural relations of ultramafic and feldspathic rocks in alpine intrusive complexes. In Ultramafic and Related Rocks. Edited by P. J. Wyllie. Wiley, N.Y., 222-239 p.

Thayer, T. P. (1969). Peridotite-gabbro complexes as key to the petrology of mid oceanic ridges. Bull. Geol. Soc. Am. 80: 1515.

Thompson, J. B. (1959). Local equilibrium in metasomatic processes. In Researches in Geochemistry 1. Edited by P. H. Abelson. John Wiley, 427-457 p.

Thompson, R. B. (1968). Serpentinization accompanied by volume changes. Pacific Geol. 1: 167-174.

Trommsdorff, V. and Evans, B. W. (1972). Progressive metamorphism of antigorite schist in the Bergell tonalite aureole (Italy). Am. J. Sci. 272: 423-437.

Trommsdorff, V. and Evans, B. W. (1974). Alpine metamorphism of peridotitic rocks. Schweiz. Min. Pet. Mitt. 54: 333-352.

Turner, J. F. and Verhoogen, J. (1960). Igneous and Metamorphic Petrology. McGraw-Hill, N.Y., 694 p.

Uyeda, S. (1979). Subduction zones: facts, ideas, and speculations. Oceanus. 22: 52-62.

Uyeda, S. and Kanamori, H. (1979). Back-arc opening and the mode of subduction. J. Geophys. Res. 84: 1049-61.

van Schaik, J. C. and Kemper, W. D. (1966). Chloride diffusion in clay-water systems. Soil Sci. Soc. Amer. Proc. 30: 22-25.

Vance, J. A. and Dungan, M. A. (1977). Formation of peridotites by deserpentinization in the Darrington and Sultan areas, Cascade Mountains, Washington. Geol. Soc. Am. Bull. 88: 1497-1508.

Vanko, D. A. and Batiza, R. (1982). Gabbroic rocks from the Mathematician Ridge failed rift. Nature 300: 742-744.

Verhoogen, J., Turner, F. J. and Fyfe, W. S. (1970). The Earth: An Introduction to Physical Geology. Holt, Rinehart and Winston, N.Y., 748 p.

Villones, D. R. (1980). The Askitero Formation - Its implication and relationship with respect to the Zambales ophiolite. Philipp. Bur. of Mines Techn. Inf. Series. Manila, Philippines.

Vine, F. J. and Mathews, D. H. (1963). Magnetic anomalies over oceanic ridges. Nature 199: 947-949.

Wadden, M. M. and Katsube, T. J. (1982). Radionuclide diffusion rates in igneous crystalline rocks. Chem. Geol. 36: 191-214.

Wares, R. P. and Martin, R. F. (1980). Rodigitization of granite and serpentine in the Jeffery Mine, Quebec. Can. Mineral. 18: 231-240.

Watkins, N. D. and Paster, T. P. (1971). The magnetic properties of igneous rocks from the ocean floor. Phil. Trans. Roy. Soc. A265: 507-550.

Weissel, J. K. (1980). Evidence for Eocene oceanic crust in the Celebes Basin. In: The Tectonic and Geophysical

- Evolution of Southeast Asian Seas and Islands. Ed. by D. E. Hayes. Geophys., Monog. 27, p. 37-47.
- Wenner, D. B. (1979). Hydrogen, oxygen and carbon isotopic evidence for the origin of rodingites in serpentized ultramafic rocks. *Geochim. Cosmochim. Acta* 43: 603-614.
- Wenner, D. B. and Taylor, Jr. H. P. (1971). Temperatures of serpentinization of ultramafic rocks based on $^{18}\text{O}/^{16}\text{O}$ fractionation between co-existing serpentine and magnetite. *Contrib. Mineral. Petrol.* 32: 165-185.
- Wenner, D. B. and Taylor, H. P. (1973). Oxygen and hydrogen isotope studies of the serpentinization of ultramafic rocks in oceanic environments and continental ophiolite complexes. *Am. J. Sci.* 273: 207-239.
- Wenner, D. B. and Taylor, H. P. (1974). D/H and $^{18}\text{O}/^{16}\text{O}$ studies of serpentinization of ultramafic rocks. *Geochim. Cosmochim. Acta* 38: 1255-1286.
- Whittaker, E.J.W. and Wicks, F. J. (1970). Chemical differences among the serpentine "polymorphs": a discussion. *Am. Mineral.* 55: 1025-1047.
- Whittaker, E.J.W. and Zussmann, J. (1956). The characterization of serpentine minerals by x-ray diffraction. *Mineral. Mag.* 31: 107-126.
- Wicks, F. J. (1979). Mineralogy, chemistry and crystallography of chrysotile asbestos. In *Short Course in Mineralogical Techniques of Asbestos Determination*. Edited by R. L. Ledoux. *Mineral. Assoc. Can. Short Course* 4: 35-78 p.
- Wicks, F. J. (1979). Mineralogy, chemistry, and crystallography of chrysotile asbestos. In *Short Course in Mineralogical Techniques of Asbestos Determination*. Edited by R. L. Ledoux. *Mineral. Assoc. Canada Short Course* 4: 35-78.
- Wicks, F. J. and Plant, A. G. (1979). Electron-microprobe and x-ray-microbeam studies of serpentine textures. *Can. Mineral.* 17: 785-830.
- Wicks, F. J. and Whittaker, E.J.W. (1975). A reappraisal of the structures of the serpentine minerals. *Can. Mineral.* 13: 227-243.
- Wicks, F. J. and Whittaker, E.J.W. (1975). A reappraisal of the structures of the serpentine minerals. *Can. Mineral.* 15: 459-488.

- Wicks, F. J. and Whittaker, E.J.W. (1977). Serpentine textures and serpentinization. Can. Mineral. 15: 459-488.
- Wicks, F. J. and Zussman, J. (1975). Microbeam X-ray diffraction patterns of the serpentine minerals. Can. Mineral. 13: 244-258.
- Wicks, F. J., Whittaker, J. W. and Zussman, J. (1977). An idealized model for serpentine textures after olivine. Can. Mineral. 15: 446-458.
- Wicks, F. J. (1984a). Deformation histories as recorded by serpentinites. I. Deformation prior to serpentinization. Can. Mineral. 22: 185-195.
- Wicks, F. J. (1984b). Deformation histories as recorded by serpentinites. II. Deformation during and after serpentinization. Can. Mineral. 22: 197-203.
- Wicks, F. J. (1984c). Deformation histories as recorded by serpentinites. III. Fracture patterns developed prior to serpentinization. Can. Mineral. 22: 205-209.
- Wiederhorn, S. M. (1967). Influence of water vapor on crack propagation in soda-lime glass. J. Amer. Ceram. Soc. 50: 407-414.
- Wiederhorn, S. M. (1972). A chemical interpretation of static fatigue. J. Amer. Ceram. Soc. 55: 81-85.
- Wilson, J. T. (1949). The origins of continents and Precambrian history. Roy. Soc. Canada, Trans., 43 ser. 3, sect. 4: 157-184.
- Wilson, L. (1972). Specific Gravity. In The Encyclopedia of Geochemistry and The Environmental Sciences. Edited by R. H. Fairbridge. Dowden, Hutchinson and Ross, Pennsylvania, p. 1110-1113.
- Wilson, R.A.M. (1959). The Geology of the Xerox-Troodos Area. Geological Survey Dept., Cyprus. Memoir No. 1, 184 p.
- Wyllie, P. J. (1971). The Dynamic Earth. Wiley, New York, 416 p.
- Yada, K. (1987). A study of chrysotile asbestos by a high resolution electron microscope. Acta Cryst. 29: 704-707.

Yoder, H. S. (1952). The MgO-Al₂O₃-SiO₂-H₂O system and the related metamorphic facies. Amer. J. Sci., Bowen Vol. 2: 569-627.

END

24H03|85

FIN